A low-cost, fluorescence-based amyloid fibrin(ogen) sensing device for systemic inflammation detection.

by

Este Marié Burger

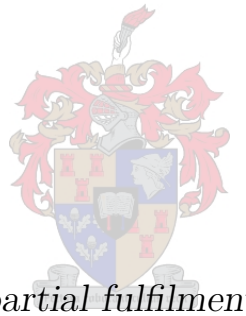

Thesis presented in partial fulfilment of the requirements for the degree of Master of Engineering in Electronic Engineering in the Faculty of Engineering at Stellenbosch University

Supervisor: Prof. WJ Perold
Co-supervisor: Prof. E Pretorius

December 2020

Declaration

By submitting this thesis electronically, I declare that the entirety of the work contained therein is my own, original work, that I am the sole author thereof (save to the extent explicitly otherwise stated), that reproduction and publication thereof by Stellenbosch University will not infringe any third party rights and that I have not previously in its entirety or in part submitted it for obtaining any qualification.

Date: 04/08/2020 .....

Acknowledgements

I would like to thank my parents for their endless support, wisdom and love. I would also like to thank Prof. Perold and Prof. Pretorius for their guidance and for giving me the opportunity to explore the fascinating intersection between engineering and physiology.

Abstract

A low-cost, fluorescence-based amyloid fibrin(ogen) sensing device for systemic inflammation detection.

EM Burger

Department of Electrical and Electronic Engineering,
University of Stellenbosch,
Private Bag X1, Matieland 7602, South Africa.

Thesis: MEng (Electronic)

December 2020

Noncommunicable diseases (NCDs) such as cancer, cardiovascular and neurodegenerative diseases are amongst the top leading causes of death globally. Chronic systemic inflammation is inextricably linked to the onset and development of NCDs. In light of this global disease burden, the need for affordable and portable inflammation screening and monitoring tests is evident.

This thesis reports on the development and evaluation of a low-cost fluorescence sensing device for the detection of the inflammatory marker, amyloid fibrin(ogen), in human platelet poor plasma (PPP). The prototype employs a spectrofluorometric-based design and raw smartphone imaging to quantify the fluorescence intensity emitted by samples of PPP to which the amyloid-staining fluorescent marker, Amytracker630, has been added. It has been shown that the prototype successfully excites bound Amytracker630, eliminates background light, detects fluorescence within the Amytracker630 emission spectrum, and quantifies the detected fluorescence intensity. The design is affordable, compact, lightweight and USB-powered.

The prototype was used to test Amytracker630-stained PPP samples from colorectal cancer (CRC), psoriasis (PSO), and control patients. On average, the fluorescence intensity measurements of the CRC and PSO samples were higher than that of the control samples. An analysis of variance and post-hoc test showed a significant difference between the control and CRC group means, and also between the control and PSO group means. However, the results from further tests, in which stained reconstituted fibrinogen samples were analysed, suggested that Amytracker630 molecules also interact with other non-amyloid plasma molecules and possibly experience aggregation-induced fluorescence. Therefore, it was concluded that the fluorescence emissions from the stained PPP samples could not be attributed solely to the presence of amyloid fibrin(ogen). Certain plasma molecules, like fibrinogen, are upregulated during inflammation. Therefore, the fluorescence-inducing interaction between the Amytracker630 and such plasma molecules may have contributed to the increased fluorescence emission in inflammatory disease samples.

Uittreksel

'n Lae-koste, fluoressensie-gebaseerde amiloïed fibrien(ogeen) opsporingstoestel vir sistemiese inflammasie diagnosering.

EM Burger

Departement Elektries en Elektroniese Ingenieurswese,
Universiteit van Stellenbosch,
Privaatsak X1, Matieland 7602, Suid-Afrika.

Tesis: MIng (Elektronies)

Desember 2020

Nie-aansteeklike siektes soos kanker, kardiovaskulêre, en neurodegeneratiewe siektes is van die hoofoorsake van sterftes wêreldwyd. Kroniese sistemiese inflammasie word geassosieer met die aanvang en onwikkeling van sulke nie-aansteeklike siektes. Dit is dus duidelik dat daar 'n behoefte vir die onwikkeling van bekostigbare inflammasie toets- en monitering-toestelle is.

Hierdie tesis lewer verslag op die ontwikkeling en evaluasie van 'n lae-koste, fluoressensiemetingstoestel vir die opsporing van amiloïed fibrien(ogeen) - 'n inflammatoriese merker in menslike plaatjie-vrye plasma (PVP). Die prototipe implementeer 'n fluorospektrometriese ontwerp en rou slimfoonafbeelding om die fluoressensie-intensiteit wat deur PVP monsters waarby die amiloïed-spesefieke fluoresserende merker, Amytracker630, bygevoeg is, te kwantifiseer. Dit is bevestig dat die prototipe in staat is om verbinde Amytracker630 op te wek, agtergrond lig uit te skakel, fluoressensie binne Amytracker630 se emissie-spektrum op te tel, en die fluoressensie te kwantifiseer. Die prototipe ontwerp is beskostigbaar, kompak en USB-aangedryf.

Die prototipe is gebruik om PVP monsters van kolorektale kanker (KRK), psoriase (PSO) en kontrole pasiënte te toets. Die gemiddelde fluoressensiemeting vir die KRK en PSO monsters was hoër as die gemiddelde fluoressensiemeting vir die kontrole monsters. 'n Variasie-ontleding en post-hoc-toets het gewys dat daar 'n beduidende verskil tussen die KRK en kontrole groepgemiddelde en ook tussen die PSO en kontrole groepgemiddelde was. Verdere toetse waartydens gerehidreerde fibrinogeen monsters geanaliseer is, het wel aangedui dat die Amytracker630 molekules ook met nie-amiloïede plasma-molekules reageer en moontlik aggregasie-geïnduseerde fluoressensie produseer. Daarom is die gevolgtrekking gemaak dat die die fluoressensie wat deur die PVP monsters geproduseer is, nie alleenlik as gevolg van die teenwoordigheid van amiloïed fibrien(ogeen) was nie. Gedurende inflammasie word sekere plasmamolekules, soos fibrinogeen, opgereguleer. Die interaksie tussen Amytracker630 en sulke plasmamolekules sou dus bydra tot die verhoogde fluoressensie emissie in die inflammatoriese siekte monsters.

Contents

List of Figures

List of Tables

Nomenclature

Abbreviations

NCD	Noncommunicable Disease
PPP	Platelet Poor Plasma
LPS	Lipopolysaccharide
LTA	Lipoteichoic Acids
CRP	C-reactive Protein
ESR	Erythrocyte Sedimentation Rate
TEG	Thromboelastography
PV	Plasma Viscosity
ThT	Thioflavin T
CR	Congo Red
LCO	Luminescent Conjugated Oligothiophenes
UV	Ultraviolet
IR	Infrared
LED	Light Emitting Diode
NA	Numerical Aperture
FOV	Field of View
CCD	Charged Coupled Device
CMOS	Complementary Metal Oxide Semiconductor
C.I.E	Commission Internationale de l'Elcairage
FID	Fluorescence-based Inflammation Detector
FPN	Fixed Pattern Noise
DSNU	Dark Signal Non-uniformity
ADU	Analogue Digital Unit
CRC	Colorectal Cancer
PSO	Psoriasis
HREC	Health Research Ethics Committee
ANOVA	Analysis of Variance
NMR	Nuclear Magnetic Resonance

Chapter 1

Introduction

1.1 Background

Between 1346 and 1350 the black plague wiped out a third of Europe's population [1]. The 1918 flu was responsible for at least 50 million casualties, and small pox took as many as 300 million lives in the 20th century, alone [2] . Technological and scientific advances have allowed us to gain the upper hand against history's leading causes of death by bacterial or viral infection. Ironically, it has also catapulted us into an age where modern lifestyle factors have become the root of a new global health burden - noncommunicable diseases (NDCs).

Noncommunicable diseases such as cancer, diabetes, cardiovascular, neurodegenerative and chronic respiratory diseases are amongst the top leading causes of death globally. In February 2020, the World Health Organisation published a report titled, *Noncommunicable Diseases Progress Monitor 2020* [3], in which they state that noncommunicable diseases are responsible for more than 70% of all deaths, worldwide. The report sheds light on the devastating economic impact of these statistics and points out that "taking action against NCDs is therefore not only a moral imperative, it's an economic imperative [3]".

It has been shown that NCDs share certain common pathophysiological mechanisms and molecular alterations. One such common mechanism is systemic inflammation. It is becoming increasingly evident that chronic systemic inflammation is inextricably linked to the onset and development of NCDs [4]. Since rapid globalization and urbanization has cultivated a modern lifestyle that is riddled with inflammatory risk-factors, it is no wonder we have an epidemic on our hands [5]. Pollution, abnormal dietary composition, sedentary behaviour and chronic stress are but a few of these factors that most people are subjected to on a daily basis [6]. Managing chronic inflammation and inflammatory risk factors is an important line of defence in the fight against non-communicable diseases.

As the global healthcare focus shifts towards preventative medicine, the demand for point-of-care diagnostic tools grows. In light of the current global disease burden, the need for point-of-care screening and monitoring tests for inflammatory markers is apparent. Although there are standardised tests for a variety of inflammatory markers and inflammation indicators, these tests are often expensive and time consuming. Such tests are typically performed in pathology labs, on expensive, non-portable equipment, and are

not suitable for large-scale, point-of-care population screening and monitoring. Therefore, the development of a point-of care inflammation-detection device will transform global healthcare. Such a device will not only play an imperative part in the early detection and treatment of NCDs, possibly even before the disease onset, but will also serve as a way to monitor a patient's recovery progress.

According to the WHO, over 85% of the global number of "premature" deaths caused by NCDs occur in middle to low-income countries [5]. This statistic calls attention to the fact that the development of such testing and screening solutions should be affordable and practical within both a rural and urban context.

The first step in developing such an inflammation-detection device is the identification of the inflammatory marker for which the device will be testing. Prof. E. Pretorius and her research group at the Stellenbosch University Department of Physiological Sciences, have focused their research on the discovery of new inflammatory markers. They have discovered a prevalence of anomalous amyloid fibrin(ogen) clot formation in the blood of individuals with inflammatory conditions [7] [8]. Fluorescent markers known to stain amyloid structures have been shown to stain these anomalous amyloid fibrin(ogen) clots. A protein is referred to as amyloid when it has undergone a specific process of misfolding. An in-depth discussion about amyloid fibrin(ogen) as an inflammatory marker is given in Section 2.1.2.

Based on the research done by Pretorius *et al.* these amyloid fibrin(ogen) structures are promising indicators of chronic systemic inflammation. Furthermore, the ability of these structures to bind to amyloid-staining fluorescent dyes make them detectable through the conduction of fluorescence assays.

This thesis discusses the development and testing of a compact, low-cost device that uses a fluorescence-detection system to detect the presence of amyloid fibrin(ogen) clots in samples of human platelet poor plasma (PPP). Furthermore, the thesis evaluates the device's effectiveness as a tool to discriminate between the PPP of healthy individuals and individuals with an inflammatory NCD.

1.2 Objectives

The objectives of this project are rooted in the research conducted by Pretorius *et al.* on the topic of anomalous amyloid fibrin(ogen) clot formation under inflammatory conditions [7] [8]. Since this research is ongoing, it is important to specify on which assumptions this project and it's objectives are based. These assumptions include:

1. Circulating inflammatory molecules interact with fibrinogen and induce the formation of anomalous amyloid fibrin(ogen) clots.

2. The presence of amyloid fibrin(ogen) clots in the blood is, therefore, indicative of an inflammatory condition.

3. Fluorescent dyes, commonly used to stain amyloid structures, stain these amyloid fibrin(ogen) clots and do not interact with other components of human platelet poor plasma.

The problem-statement given in the previous section and these fundamental assumptions inform the objectives of this project. The objectives are to:

1. develop a device that detects the presence of amyloid fibrin(ogen) in human platelet poor plasma by implementing an in vitro, fluorecence-based assay that utilises a fluorescent dye known for staining amyloid structures.
2. keep the design low cost, compact, modular and low-power so that it is suitable for use in mobile and rural clinic setups.
3. investigate the relationship between the measured fluorescence signal and the inflammatory status of the patient.
4. evaluate the device's effectiveness as a tool to discriminate between the PPP of healthy individuals and individuals with inflammatory NCDs.
5. report on possible improvements and recommendations for future development.

1.3 Thesis outline

Chapter 2 is the literature review. Firstly, this chapter discusses the physiology of inflammation, available standardised tests for inflammation and the role of amyloid fibrin(ogen) as an inflammatory marker. Since the device is required to perform fluorescence assay, the rest of the literature review discusses relevant biophotonic, optical design and imaging concepts.

Chapter 3 discusses the design and development of the device prototype. In this section the design requirements, system overview, component selection and evaluation, final prototype assembly and cost analysis are discussed.

Chapter 4 discusses the experimental methodology used to evaluate the prototype's performance as a tool to discriminate between control individuals and individuals with an inflammatory disease.

Chapter 5 concludes the thesis and provides recommendations for further work.

Chapter 2

Literature Review

2.1 Chronic inflammation

Inflammation is an essential part of the immune system. It is a complex and highly coordinated response to injury, infection and other harmful stimuli - a spectacular defence and repair system. During an acute inflammatory response, a cascade of microcirculatory events is set in motion. Vascular dilation and permeability increase, leukocytes (white blood cells) accumulate in the inflamed area, and a host of inflammatory mediating molecules is released into the circulatory system [9].

Different inflammatory stimuli activate different inflammatory pathways. Microbial products and cell-signalling proteins called cytokines act as inflammatory mediators by activating their corresponding receptors. This protein-ligand binding in turn activates intracellular signaling pathways that direct cellular response and the production of inflammatory molecules [9].

Acute inflammation is localized, short-term and vital to the body's healing process. However, when one or more of the inflammatory pathways are dysregulated, it can lead to a prolonged inflammatory response that is damaging to the body [9]. This type of persistent, low-grade inflammation has a whole-body effect and is called chronic inflammation. It can occur for a variety of reasons, such as long-term exposure to irritants, recurring acute inflammatory episodes, autoimmune disorders and oxidative stress [10].

Another relevant hallmark of chronic inflammation is the metabolic dysregulation of iron. Under non-pathogenic conditions, dietary iron in the ferric state (Fe^{3+}) is reduced to Fe^{2+} by intestinal absorptive cells, transported into the bloodstream and then oxidised to Fe^{3+}. Free ferric ions released in plasma are bound to the protein, transferrin, and transported throughout the body [11]. The dysregulation of iron homeostasis may lead to the accumulation of free ferric ions in the bloodstream, which in turn produce reactive oxygen species and oxidative stress.

Furthermore, research shows that intestinal permeability, also known as leaky gut, leads to bacterial translocation into extraintestinal sites such as the blood stream [12]. Dormant bacteria circulating in the blood may be awakened by free iron and start to shed inflammation inducing microbial products. Lipopolysaccharide (LPS) and lipoteichoic acids (LTA), bacterial cell wall components of gram-negative and gram-positive bacteria

respectively, are prominent examples of such microbial products [13].

Chronic inflammation has been linked to a variety of noncommunicable diseases that plague modern society - cancer, diabetes, cardiovascular diseases, obstructive pulmonary disease and neurodegenerative diseases such as Alzheimer's [10]. As mentioned in Chapter 1, noncommunicable diseases are the leading global cause of death, and it is becoming increasingly evident that chronic inflammation is a common underlying cause [3].

Unlike acute inflammation, chronic inflammation often goes undetected until it is too late. It can wage a slow and subtle war on the body for years before a person develops a detectable inflammatory disease [14]. Managing chronic inflammation and inflammatory risk factors is an important line of defence in the fight against noncommunicable diseases.

The ability to measure people's chronic inflammation levels opens doors to preventative care, treatment management, patient progress monitoring and further epidemiological research. The following section discusses existing tests for chronic inflammation.

2.1.1 Tests for chronic inflammation

Chronic inflammation is partly characterised by the up-regulation of various molecules. Some of these molecules are used as biomarkers in common inflammation tests. A biomarker is a molecule that is up-regulated or down-regulated during a pathogenic process and can therefore be used to identify a certain pathogenic state [15].

Standardised tests for chronic inflammation include the detection of biomarkers CRP, fibrinogen, tnf-α and interleuken 1-β, 6 and 8 [10]. Plasma viscocity (PV) and erythrocyte sedimentation rate (ESR) are also used as indicators of inflammation. These tests are not suitable for point-of-care testing and high-volume patient screening, since they require large and expensive equipment and technical expertise.

C-reactive protein

C-reactive protein (CRP) is an acute-phase protein produced in the liver. Acute-phase proteins are proteins that become up-regulated or down-regulated in response to inflammatory cytokines. Although the concentration of acute-phase proteins also changes during acute inflammation caused by injury or infection, it has been shown that CRP is also associated with chronic inflammation [16]. Therefore, the blood concentration of CRP is a widely used, relatively inexpensive measure of systemic inflammation.

Standardised CRP tests are done in pathology laboratories, which means that the blood samples have to be sent away and that the results are only made available after a few days. These test can therefore not be used as a quick screening tool for chronic inflammation and inflammatory disease risk cases. CRP test costs approximately R200 at Pathcare [17].

Fibrinogen

Fibrinogen is a plasma protein that plays an important role in blood-coagulation. In the event of an injury, fibrinogen is converted to fibrin by the enzyme thrombin. Fibrin is

a fibrous protein that aggregates into a polymerized mesh-like structure and joins forces with activated platelets to seal the injured area [18].

Fibrinogen is also an acute phase protein. It circulates in the bloodstream at concentrations between 2 and 5 mg/ml in healthy individuals. During an inflammatory response, the concentration of fibrinogen may exceed 7mg/ml [18]. Fibrinogen tests are also done at pathology laboratories and they cost approximately R600 [17].

ESR, TEG and VP

The increased concentration of fibrinogen and other factors during an inflammatory response, has an effect on the body's hemodynamics. Erythrocyte sedimentation rate (ESR), viscoelastic properties of blood clots, and the viscosity of blood are all examples of hemodynamic factors that can be tested to gain insight into a person's inflammatory profile.

Fibrinogen is a pro-sedimentation factor, and therefore causes the erythrocyte sedimentation rate to increase [19]. The ESR is measured as the rate at which red blood cells separate from the plasma and settle at the bottom of a standardised tube. ESR tests are also available at pathology laboratories. They are cheap, but very non-specific.

Thromboelastography (TEG) is a test that detects, quantifies and visualises the dynamic changes of the blood's viscoelastic properties during clotting [20]. Amongst others, proporties such as the rate of clot formation, clot strength and rate of fibrinolysis are measured and displayed on a graph called a thromboelastograph [21]. Figure 2.1 shows an example of an thromboelastograph. TEGs can be used to detect hypercoagulability and hypofibrinolysis, both of which have been shown to occur during chronic systemic inflammation [22]. However, in clinical settings, TEGs are more often used to inform haemostatic therapy in bleeding patients, and not to detect systemic inflammation.

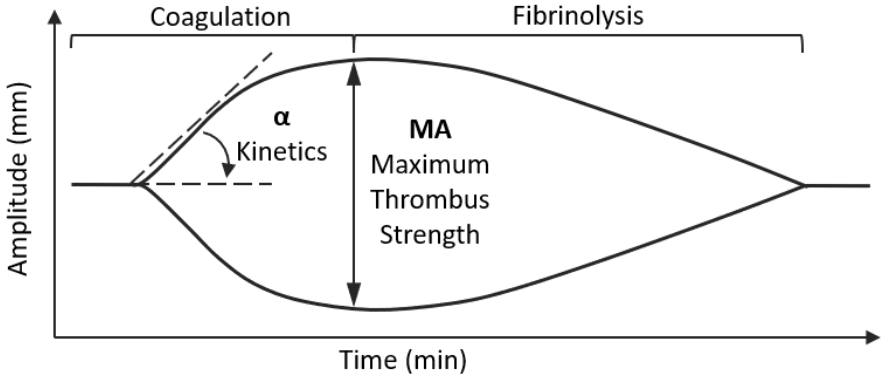

Figure 2.1: Thromboelastograph

Finally, an increase in fibrinogen also leads to an increase in plasma viscosity (PV) - a property that can be measured using a viscometer. Viscometer prices can range from R30 000 to more than R150 000.

TNF-α and Interleuken 1-β, 6 and 8

Tumor necrosis factor-alpha(NF-α) and Interleuken 1-β, 6 and 8 are inflammatory cytokines. As discussed earlier, inflammatory cytokines are proteins that regulate and mediate the inflammatory response.

Interleukin-1β (IL-1) and tumor necrosis factor- (TNF) play a significant role in the functional effects of Parkinson's disease [23], while Interleukin-6 has shown to be an important role-player in autoimmune diseases. It has been shown that people with obstructive pulmonary disease have elevated levels of Interleuken 8 [24].

Although these markers are more specific indicators, they are tested for with the use of expensive ELISA kits. ELISA kits cost between R4000 and R50000 and can only be used once.

2.1.2 Amyloid fibrin(ogen) as an inflammatory marker

It has recently been reported that many chronic inflammatory diseases, such as cancer, diabetes, psoriasis, rheumatoid arthritis and cardiovascular disease are accompanied, and possibly aggravated by the formation of anomalous amyloid fibrin(ogen) clots in the blood [7]. This discovery has brought these amyloid fibrin(ogen) clots into the spotlight as a potential inflammatory marker. The term fibrin(ogen) is used to simultaneously refer to both fibrinogen and fibrin, since the anomalous protein misfolding is observed both in circulating fibrinogen and the fibrin networks of clots.

This section discusses the mechanism of protein amyloid formation and the roll that certain microbial products and inflammatory markers play in the formation of anomalous amyloid fibrin(ogen) clots.

Protein amyloid formation

When proteins enter an amyloid state, they unfold into elongated fibrils that form dense, insoluble aggregates. These extracellular amyloid deposits build up in tissue and organs, causing a variety of diseases [25]. This section discusses the general structure of proteins and the mechanism of amyloid formation.

The functional properties of a protein is dependant on its three-dimensional structure [26]. A protein consists of multiple amino-acids that are linked together by peptide bonds to form a polypeptide. An amino acid consists of a central carbon atom that is linked to a amino group, a carboxyl group and a side chain. A peptide bond is formed when the carboxyl group of one amino acid links with the amino group of another in a dehydration synthesis reaction. There are twenty different types of amino acids, each with a different side chain chemistry [27]

.

The amino acid side chains are capable of forming intramolecular bonds with each other. Depending on the amino-acid sequence and the side-chain interactions, the polypeptide will fold into a specific structure. This is the protein's primary structure.

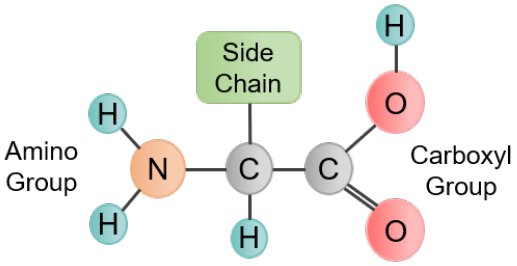

Figure 2.2: Amino acid

Furthermore, the formation of hydrogen bonds between amino and carboxyl groups causes the protein to fold and bend further. These folding patterns are known as alpha helices and beta strands. They make up the secondary structure of the protein. Figure 2.3 shows simplified illustrations of the side chain interactions as well as the alpha helix and beta strand folding patterns [27].

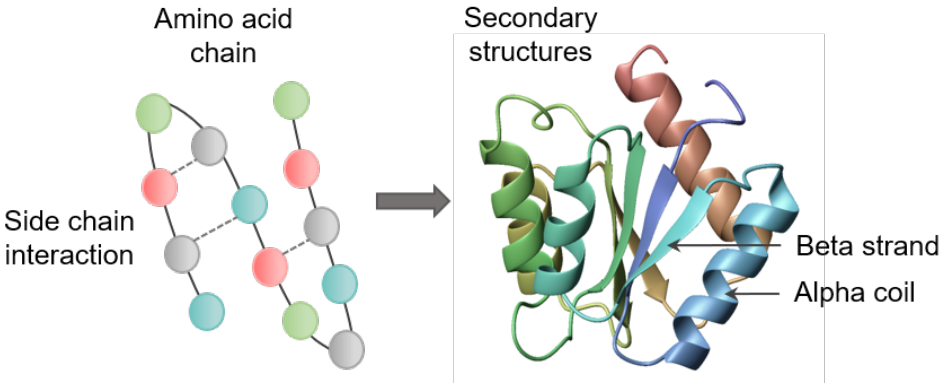

Figure 2.3: Primary and secondary protein structures

Amyloid protein aggregates are formed when sequential changes in the folding process lead to misfolded proteins [7]. These misfolded proteins settle into many-stranded beta sheet structures that stack on each other to form amyloid fibrils [25]. The amyloid fibrils are insoluble and aggregate to form matted deposits in tissue and organs. Figure 2.4 shows a simplified visualisation of the stacked beta-sheet amyloid structure.

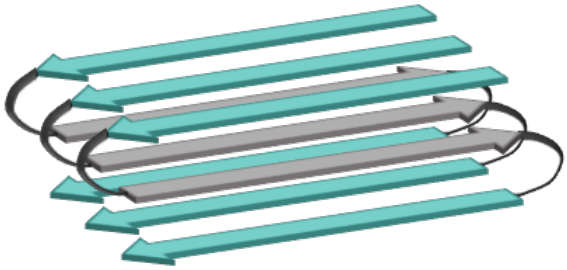

Figure 2.4: Amyloid protein structure

Amyloid fibrin(ogen) and inflammation

As discussed earlier in this section, fibrinogen and fibrin are key components of blood clots [18]. During thrombosis, the fibrinogen protein undergoes a process called proteolytic cleavage. The enzyme, thrombin, cleaves certain peptides from the fibrinogen proteins to form fibrin monomers that quickly polymerizes into a fibrin clot [18]. When a blood vessel wall is damaged, activated platelets and polymerized fibrin accumulate at the injured area, forming a clot that stops the bleeding.

Prof. E. Pretorius and her research group at the Stellenbosch University Department of Physiological Sciences have published numerous papers investigating and confirming the presence of anomalous amyloid fibrin(ogen) clots in the blood of patient with various types of inflammatory diseases. Figure 2.5 shows scanning electron microscope (SEM) images of fibrin networks in platelet poor plasma (PPP) from control, diabetes and Alzheimer's-type dementia patients [28] [29] [30].

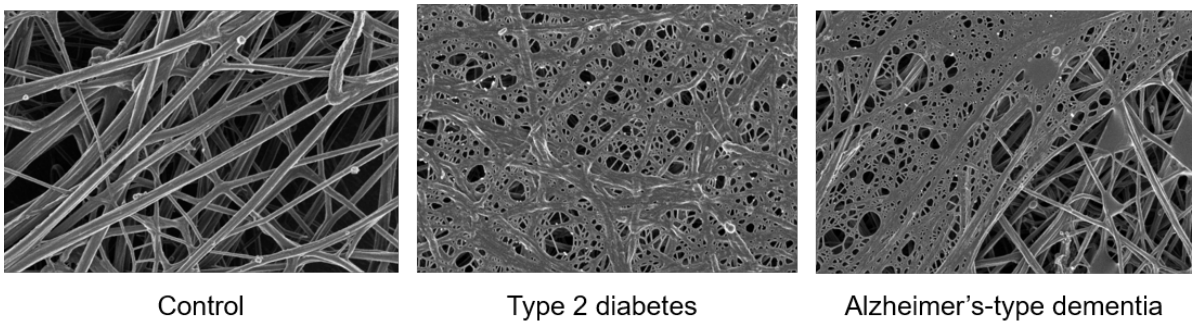

Figure 2.5: SEM images of control, diabetes and Alzheimer's-type dementia fibrin networks [from[28] [29] [30]]

The dense, matted deposits seen in the images of the diabetes and Alzheimer's-type dementia fibrin networks were also seen in other inflammatory diseases. Pretorius *et al.* also used confocal microscopy to show that the these matted deposits can be stained using fluorescent dyes known for staining amyloid structures, thereby confirming the amyloid-like nature of the deposits.

Pretorius *et al.* suggest that the presence of inflammogens and acute phase proteins interact with healthy fibrinogen and initiate protein misfolding that leads to the formation of anomalous amyloid fibrin(ogen) [28]. They have confirmed the role of LPS, LTA, SAA and free ferric iron in amyloid fibrin formation by comparing the amyloid content of fibrin clots formed in naive PPP with that in PPP which has been exposed to the mentioned inflammatory markers [28] [31].

Figure 2.6 shows confocal images of clots formed in control and LTA-exposed PPP. Both the control and LTA-exposed PPP were stained with three amyloid-staining dyes - Amytracker480, Amytracker680 and ThT.

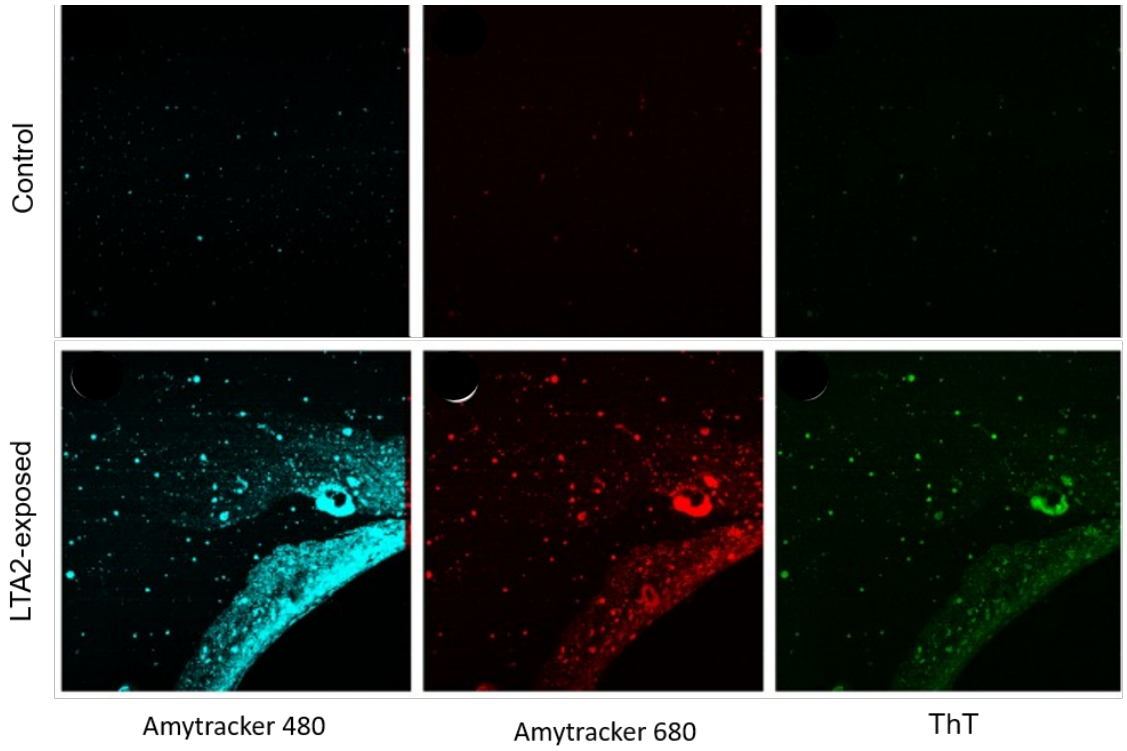

Figure 2.6: Confocal images of stained control and LTA-exposed clots

The use of amyloid-staining fluorescent dyes and confocal microscopy has been an imperative part of the research done by Pretorius *et al.* and has been invaluable in the detection, analysis and identification of amyloid fibrin(ogen). This is why the specified method of detection for this project is fluorescence-detection.

2.2 Biophotonics

Biophotonics is the science of the interaction between light and biological material. It is a multidisciplinary field that draws upon biological, chemical, optical, medical and engineering principles. Biophotonics has become an invaluable resource in medicine and medical research. Practical applications of biophotonic processes include noninvasive biometric measuring techniques, biological imaging and characterization, the detection of pathological structures and conditions, light therapies and laser-based surgical procedures [32].

The interaction between light and biological material manifests in a variety of optical phenomena. These include the reflection, refraction and scattering of the incident light, as well as the absorption of photon energy. The basic principles of light and general light-matter interactions are discussed in Section 2.2.1.

The absorption of light by target tissue is an important interaction utilised in many therapeutic and analytical processes. Techniques such as photoablation and the induction of thermal or photo-chemical effects are used to destroy unwanted tissue, while low light therapy is used to stimulate tissue healing[32]. Furthermore, a material's absorption cha-

racteristics may reveal information about its composition, structure and behaviour [33].

An important phenomenon in the world of biological imaging and analysis is a material's ability to re-emit absorbed light energy in the form of photons. This process is called fluorescence and is used in many microscopy and measurement tools.

Since this thesis reports the detection of anomalous amyloid fibrin(ogen) using a fluorescence-based assay, this section investigates the mechanisms of fluorescence, the utilization of fluorescence in the analysis of biological material, and finally, existing fluorometric techniques used to detect amyloid fibrin(ogen). But first, a firm grasp of the basic principles of light is required.

2.2.1 Basic principles of light

Light is electromagnetic radiation that can be perceived by the human eye. Electromagnetic radiation is the propagation of energy in the form of oscillating electric and magnetic fields [34]. It has a dual nature - in some instances electromagnetic radiation behaves as a wave, and in other instances as a particle that carries a discrete quantum of electromagnetic energy. This particle is called a photon [32].

An electromagnetic wave is described in terms of the amplitude and wavelength of its oscillating electric and magnetic fields. These fields oscillate in phase and perpendicular to each other and the direction of propagation [34]. Figure 2.7 shows a visual representation of an electromagnetic wave.

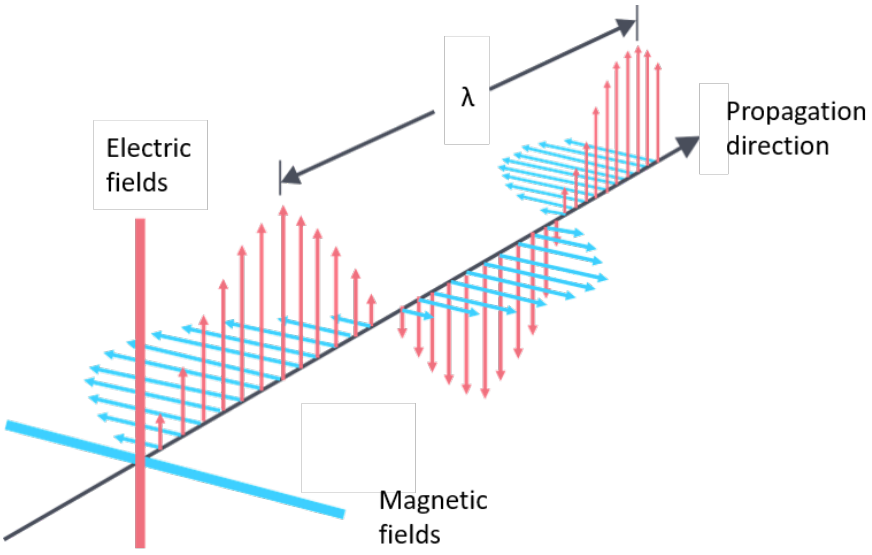

Figure 2.7: Electromagnetic wave

The energy carried by a photon is directly proportional to the frequency (f) and inversely proportional to the wavelength (λ) of the associated electromagnetic wave [35].

$$E = hf \tag{2.1}$$

$$E = \frac{hc}{\lambda} \tag{2.2}$$

where, h is Plank's constant (6.626×10^{-34} J.s) and c is the speed of light in a vacuum. The energy of a photon is measured in units of electron-volt (eV). An electron-volt is the kinetic energy gained by an electron after being accelerated by a potential difference of 1 volt (1 eV = 1.602×10^{-19} J) [34] [35].

The electromagnetic spectrum is the continuous distribution of electromagnetic radiation according to wavelength or frequency. Figure 2.8 shows the EM spectrum as well as the spectral ranges of the different classifications of EM radiation. The visible light spectrum exists between the UV and infrared (IR) spectral ranges. Biophotonics disciplines primarily involve EM radiation with wavelengths that range from mid-UV to mid IR - approximately 190nm to 10μm [32].

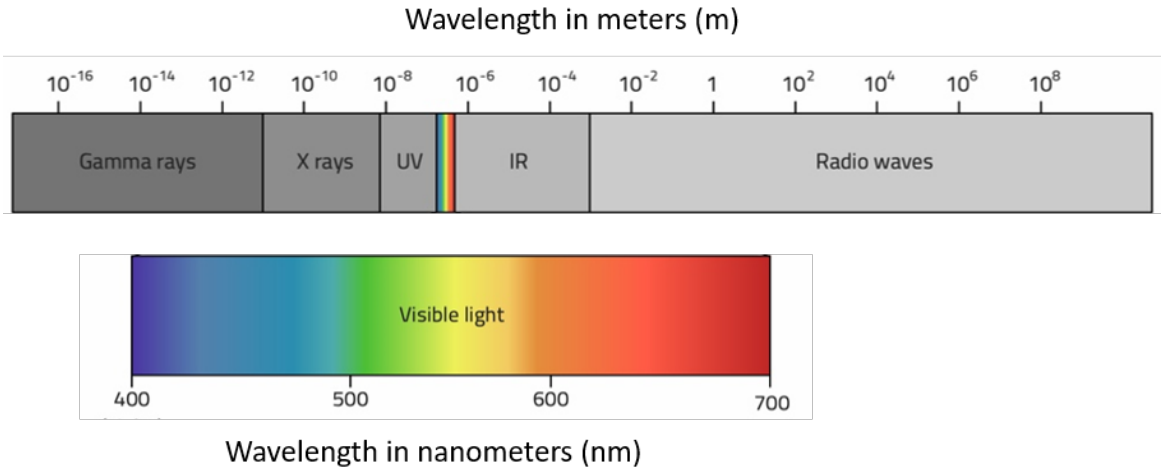

Figure 2.8: Electromagnetic spectrum

The scientific study of UV, visible and infrared light is called optics. The field of optics has three major branches. Each one uses a different model to describe the behaviour and nature of light [36].

- **Geometric optics** describes light as rays - hypothetical lines that illustrate the direction of light propagation.
- **Physical optics** describes light as electromagnetic waves.
- **Quantum optics** describes light as a stream of particles called photons - each carrying a quantum of electromagnetic energy.

These models are used to investigate the genesis, propagation and detection of light [32]. Geometric and physical optics are useful to investigate the interaction between light and matter in terms of transmission, reflection, refraction and diffraction [36]. An optical system utilises these interactions to direct and manipulate light through an optical path comprising a combination of elements such as lenses, filters, mirrors and prisms. These concepts are discussed further in the section on optical system components, Section 2.3.

Quantum optics allows us to model atomic-level interactions between light and matter, such as absorption and emission. This allows us to generate and detect light, and to understand phenomena like fluorescence.

2.2.2 Fluorescence

The internal energy content of atoms and molecules are quantized [37]. This means that they can only take on discrete values of energy. The energy state of an atom refers to the energy levels within which its electrons exist. The energy state of a molecule may additionally refer to the vibrational or rotational energy of the molecule [32] [37]. The discrete energy states available to atoms and molecules are specific to the type of molecular or atomic species.

Under normal circumstances, atoms and molecules mainly exist in the ground state, or the lowest energy state. They can, however, absorb energy and transition to an excited state, or a higher energy state. The absorbed energy can either be kinetic energy from a collision or photon energy from EM radiation [37]. A particle will typically only remain in an excited state for a few nanoseconds before it falls back to it's ground state. During this transition, energy is released in the form of heat or light.

Fluorescence occurs when a molecule absorbs light at a specific wavelength and then subsequently emits light at a longer wavelength. The Jablonski diagram (Figure 2.9) illustrates the three distinct events in a fluorescence process.

1. The molecule absorbs energy from a photon and transitions to an excited state. Since the molecule can only transition to specific discrete energy states, the absorbed energy must be equal to the difference between the ground state energy and the available excited state energy [37]. This explains why fluorophores can only be excited by certain wavelengths of light. The transition from the ground state to an excited state occurs in the order of 10^{-15} s [32].

2. The molecule loses some of the absorbed energy through internal conversion or vibrational relaxation, and relaxes to a slightly lower energy level. This is called a non-radiative transition and occurs in the order of 10^{-13} s [32].

3. The molecule transitions back to its ground state, emitting a photon with lower energy than the excitation energy. This means that the emitted light has a longer wavelength than the excitation light. The event occurs in the order of 10^{-9}s [32]. This time interval is known as the fluorescent lifetime [37].

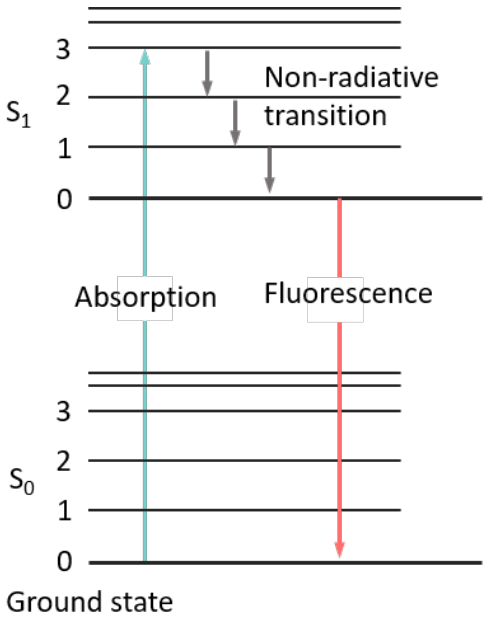

Figure 2.9: Jablonski diagram

Fluorescent molecules are called fluorophores. Some biological material have intrinsic fluorescent properties. The fluorescence produced by these kinds of biological materials is called autofluorescence. When a biological material has no intrinsic fluorescent properties, or a suboptimal autofluorecence spectral profile, external fluorophores can be bound to the molecule to facilitate a fluorescence-based molecular analysis. These external fluorophores are known as fluorescent dyes or probes.

Fluorophores are subject to photobleaching. Photobleaching occurs when a fluorophore undergoes photon-induced chemical and covalent alterations [38]. In the process, the fluorophore loses its ability to fluoresce permanently. Photobleaching can be minimized by reducing the intensity of the excitation light or minimizing the exposure time.

2.2.3 Fluorescence intensity sensing techniques

Fluorescence is a nondestructive, sensitive and versatile tool for detecting and analysing biological matter. Fluorescence emission has several measurable parameters. The parameters most commonly used in biological analysis are fluorescence intensity, fluorescence lifetime, and fluorescence anisotropy [37]. The implementation of fluorescence lifetime and anisotropy measurements is outside the scope of this project. Therefore, this section focuses on the mechanisms and existing implementations of fluorescence intensity sensing.

Fluorescence intensity sensing involves the excitation of a biological sample and the detection of the light emitted by the targeted fluorescent components in the sample. The intensity of the emitted light is proportional to the number op photons incident on the detector per unit time.

The fluorescence intensity of a fluorophore is dependent on the fluorescence quantum yield (ϕ) [39]. Fluorescence quantum yield is the ratio between the number of photons absorbed by a fluorophore and the number of photons emitted as fluorescence. In more accurate

terms, it is the ratio between the radiative rate constant (K_r) and the sum of all the non-radiative rate constants (K_{nr}) of an excited-state decay [37]. The quantum yield can therefore be described as the probability that the excitation energy will dissipate through non-radiative processes such as vibrational relaxation rather than photon emission.

$$\phi = \frac{K_r}{K_r + \sum K_{rn}} \tag{2.3}$$

Fluorescence intensity sensing is a popular way to detect specific biological structural components and dynamic chemical processes. The target-specific binding of fluorescent dyes and the unique spectral profile of tissue autofluorescence ensure high sensing specificity [32].

The most important parameters of a fluorescent assay are the absorption and emission spectra of the target fluoreophore. These spectra determine the selection of the excitation wavelengths and the spectral range of detection. Figure 2.10 shows an example of a typical absoption and emission spectra.

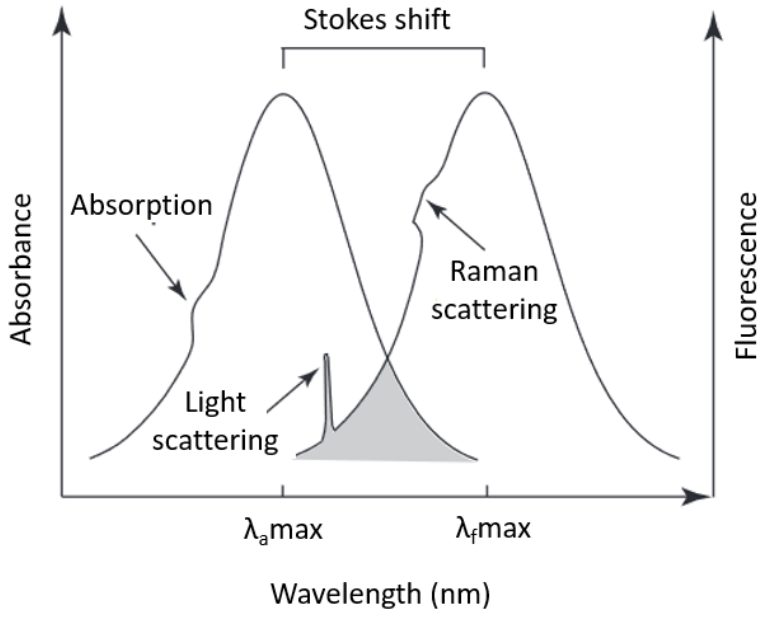

Figure 2.10: Absorption and emission spectra [from [37]]

The emission spectrum is typically a shifted copy of the absorption spectrum. The distance between the absorption and emission spectra peaks is called the Stokes shift [37]. It is preferable to select fluorophores with a large Stokes shift. If the Stokes shift is too small, the spectra will overlap, making it difficult to separate the emitted light from the excitation light.

A small Stokes shift may also lead to the superposition of Raman scattered light on the emission spectrum [37]. Raman scattering is an inelastic scattering phenomenon. An

incoming photon may either transfer a small amount of energy to a molecule, or gain a small amount of energy from a molecule before being scattered. The wavelength of the scattered light is therefore altered. The spectral shift may cause the scattered excitation light to overlap with the emission spectrum. This phenomenon is specifically noticeable in low light conditions.

There is a variety of commercially available microscopy and spectroscopy techniques that utilise fluorescence intensity sensing to analyse biological samples.

Fluorescence microscopy

Microscopy is the use of specialised optical systems and imaging techniques to view structures that cannot be seen by the naked eye. Fluorescent microscopy utilizes fluorescent probes to image and analyse molecular processes and structures at sub-cellular resolution.

There are multiple fluorescent microscopy techniques. The effectiveness of these techniques vary in terms of spatial and temporal resolution, as well as image depth and phototoxicity [40]. This section briefly discusses and compares the basic principles of wide-field fluorescence microscopy and laser scanning confocal microscopy. For a more detailed discussion on optical system components, refer to Section 2.3.

Wide-field fluorescence microscopy is a widely used fluorescence imaging technique. The basic optical setup for a wide-field fluorescence microscope includes an excitation light source, excitation and emission filters, an objective lens, and a detection component such as an eyepiece or camera [37] [40]. The relative simplicity of the optical system makes wide-field fluorescence microscopy affordable and user-friendly compared to other techniques. It also induces less photobleaching than methods that use focused laser light and have lower temporal resolution, such as laser scanning microscopy [37]. Wide-field fluorescent microscopy does, however, have very low axial resolution and imaging depth. In cases where high resolution 3D imaging is required, confocal microscopy is a more suited technique [41].

The laser scanning confocal microscope is a powerful piece of laboratory equipment. It not only has an advanced optical system with expensive beam steering and filtering optics, but often also provides software solutions for complex post-processing techniques. In its most basic form, laser scanning microscopy uses a combination of collimated laser light, dichroic filtering, scanning mirrors and an objective lens to focus the excitation beam onto the sample [42]. The emitted light is directed through various optical lenses and filters before it reaches the detector. A pinhole, placed in the conjugated image plane to a focus point on the sample, performs spatial filtering by removing light that originated from other sample focal planes [42]. This allows the microscope to perform optical sectioning which results in images with higher axial resolution. Since a confocal microscope does point-scanning signal collection, the temporal resolution is low and the photobleaching effects are more prominent.

Both wide-field fluorescent microscopes and confocal microscopes have diffraction-limited lateral resolution [32]. There are various super-resolution fluorescence microscopy techniques that achieve spatial resolutions that are not limited by light diffraction. These techniques are outside the scope of this project and are not be discussed.

Fluorescence spectroscopy

Fluorescence spectroscopy involves the detection and analysis of the fluorescence spectrum emitted by fluoreophores [43]. The emission spectrum of naturally fluorescing or dye-stained biological matter may reveal information about sample composition, molecular interactions and pathogenic conditions [44].

Two important observables in fluorecence spectroscopy is spectral intensity distribution and fluorescence lifetime [43]. The emitted radiant intensity per unit wavelength is dependent on the fluorophore concentration and the intensity of the excitation source. The fluorescence lifetime is independent of these parameters and is typically influenced by the local environment, such as the temperature, pH, refractive index and presence of fluorescence quenchers [32].

The spectrofluorometer is a key piece of lab equipment that detects the fluorescence signature of an analyte in a sample and correlates it to the analyte concentration. A basic spectrofluormeter design includes a light source that emits a wide, and typically continuous range of wavelengths [44]. Examples include high pressure xenon arch lamps or supercontinuum lasers. A monochromator is used both in the excitation channel to isolate a desired excitation wavelength, and in the detection channel to isolate a desired fluorescence emission wavelength [43]. The selected emitted light is finally measured using a detector such as a photomultiplier tube or photodiodes.

Spectrofluorometers may also contain other optical components such as fliters, mirrors and polarisers. The design depends on the types of measurements and features that the spectrophotometer offers. Some spectrophotometers are equipped to do more advanced measurements such as fluorescence lifetime and anisotropy detection.

2.2.4 Intrinsic fluorescence of amyloid proteins

The implementation of fluorescence sensing techniques to detect amyloid fibrin(ogen) in plasma, requires insight into the intrinsic fluorescence properties of amyloid fibrin(ogen) and amyloid specific stains. This section discusses the intrinsic fluorescent signature of aggregated amyloid proteins [45]. Section 2.2.5 explores the different commercially available amyloid-specific fluorescent stains.

Chan *et al.* [45] reported their findings on the development of intrinsic fluorescence during the aggregation of amyloid proteins. The fluorescent signature of the aggregates were determined with the use of confocal microscopy and fluorescence lifetime imaging. Confocal images were taken using a 405 nm laser and a detection range between 450 nm and 500 nm. The fluorescence lifetime images were taken using a 450 nm excitation source, while recording emission above 488 nm.

The study found that amyloid proteins have intrinsic fluorescence due to the electron levels that become available during the development of cross-beta sheet aggregates. Furthermore, it was concluded that the intrinsic fluorescence signature is independent of aromatic amino-acid residues [45]. Aromatic amino acids have aromatic side chains and are responsible for protein fluorescence [46]. The fact that the presence of aromatic residues is not

required to observe intrinsic fluorescence in amyloid aggregates, suggests that the fluorescence arises from energy states that are specific to cross β-sheet molecular arrangements [45]. Cross β-sheet aggregates are characteristic of all amyloid structures.

2.2.5 Fluorescent amyloid-binding ligands

The detection of extracellular amyloid deposits has been a topic of interest since the late 1800's. There are a variety of fluorescent molecules that bind to the generic fibrillar amyloid structure and are used to detect amyloidosis in histopathology sections [47]. Binding leads to conformational changes in the fluorescent molecule, which leads to alterations of the moelcule's optical and luminescent properties [48].

The most commonly used fluorescent amyloid-binding ligands are Congo red and Thioflavin T. Luminescent conjugated oligothiophene stains, trademarked under the name Amytracker, have recently been developed by the Swedish company, Ebba Tech, for amyloid-specific staining.

Thiovlavin T

Thioflavin T (ThT) is a benzothiazole fluroescent dye. It is widely used as an in vitro amyloid-binding ligand, since it fluoresces strongly when bound to amyloid cross β-sheet aggregates [49]. Unbound ThT in an aqueous environment has weak fluorescence with an excitation maxima of 350 nm and a emission maxima of 440 nm. When the molecules bind to amyloid structures, they experience conformational changes that cause them to fluoresce strongly at higher (red-shifed) excitation and emission maxima - 440 nm and 490 nm respectively. Figure 2.11 shows the chemical structure of a ThT molecule.

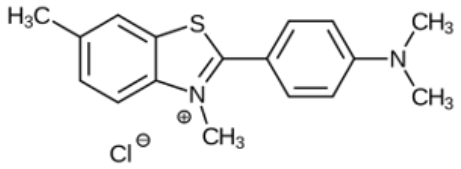

Figure 2.11: Thiovlavin T molecule

The interaction and binding mechanism between ThT and amyloid structures are not yet fully understood. However, the widely preferred theory is that ThT binds within the hydrophobic grooves between the solvent-exposed side-chains of the amyloid fibrils. This binding possibly provides rigidity that prevents the molecule to enter a less-radiative, twisted state [50] [51].

It has been reported that the relation between ThT binding and fluorescence intensity is non-linear, since the molecule is sensitive to self-quenching. Fluorescence quenching is a process where the interaction between molecules lowers or eliminates the fluorescence emission. In addition to its non-linear fluorescence emission, ThT also has the ability to induce fibril compaction [52].

Congo Red

Congo Red (CR) is a linear, amphiphilic molecule (Figure 2.12) [53]. It is a classic amyloid dye and was, in fact, the first dye used for the diagnosis of amyloidosis [54]. In aqueous solutions it absorbs blue and green light and has a peak absorption wavelength of 490 nm. This property gives the dye solution a bright red colour [53].

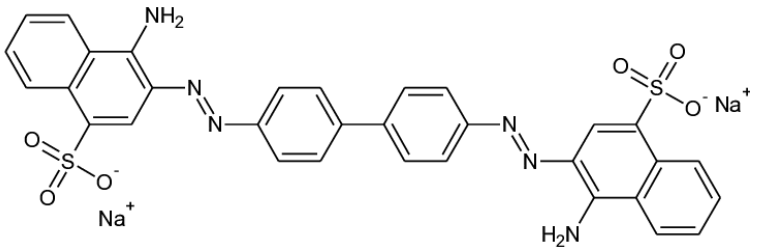

Figure 2.12: Congo Red molecule

When CR binds to β-sheet rich amyloid fibrils, the molecules become rigid and orient themselves parallel to the fibril axis. The conformational change causes the molecules' peak absorbance wavelength to shift from 490 nm to 512 nm, with a shoulder peak at 540 nm. The binding also increases the optical anisotropy of the CR, which allows the detection of apple-green birefringence under crossed polarisers [54] [53]. Birefringence is an optical property of a substance where the refractive index of substance changes as with the polarization and propagation direction of the light.

Although CR is a classic amyloid dye, research over the years has shown that the binding of CR is very non-specific for amyloid identification. The binding mechanism depend on a number of conditions including solvent type, solution composition, pH etc [54]. CR is also very toxic.

Amytrackers

Amytrackers are trademarked luminescent conjugated oligothiophenes (LCOs) manufactured by the Swedish company Ebba Biotech. In recent years LCOs have garnered attention as amyloid-binding ligands. They have proven to be useful for the identification of a broader variety of disease-associated protein aggregates than the classic amyloid stains such as Thioflavin T and Congo Red [55] [56].

LCOs have flexible thiophene backbones that change conformation and lose rotational freedom depending on the structures they bind to [48]. The absorption and emission spectra of an LCO depends on the conformation of this backbone. The performance of LCO as amyloid-specific ligands is dependent on the length of the backbone and location of the anionic side chains along this backbone [56]. Ebba Biotech has developed a range of LOCs that are specifically manufactured for amyloid-specificity. Since the molecules are trademarked, the molecular structures have not been disclosed. However, Figure 2.13 shows the pentameric thiophene-based ligands from which one of the Amytracker products, Amytracker680, was derived [28].

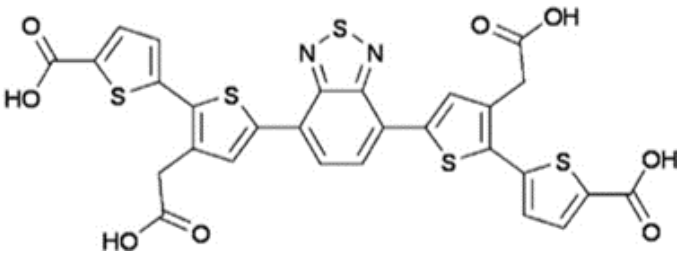

Figure 2.13: Pentameric thiophene-based ligands for amyloid binding

Ebba Biotech manufactures a range of Amytracker products with varying excitation and emission spectra. The emission spectra of the Amytracker 480, 520, 630 and 680 are shown in Figure 2.14. The fluorescent properties of the different Amytrackers are discussed and compared in Section 3.3.1, where the selection of a fluorescent amyloid-binding ligand is discussed.

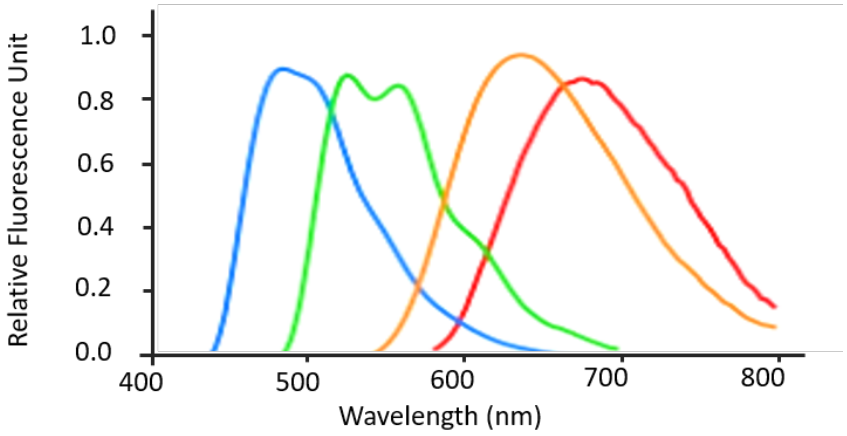

Figure 2.14: Amytracker emission spectra [from Ebba website [57]]

2.3 Optical system components

In Section 2.2, the basic principles of light, and the three major branches of optics were discussed. All three branches are applicable when investigating the components of a fluorescent-based biosensor. Where physical and quantum optics are used to describe the mechanisms behind biophotonics and photo-detection, geometric optics is useful to describe the propagation of light through the optical train.

In this section the optical components of a fluorescent-based sensor are grouped and discussed according to three different stages in the optical system. These stages are:

1. Sample excitation
2. Light propagation and manipulation between sample and detector, also referred to as the optical assembly.

3. Detection

The aim is to investigate existing optical setups for fluorescent detection and to identify critical components. Furthermore, the components are evaluated in terms of their affordability and practicality within a low-cost, portable device.

2.3.1 Excitation source

Section 2.2.2 described how the process of fluorescence is initiated when a fluorophore absorbs light energy. There is a broad selection of excitation sources to choose from when designing a biophotonics application. These include lamps, light emitting diodes and various types of lasers [58]. Since the construction and mechanisms of photon emission differ between these sources, so does the optical radiation output characteristics [59].

Radiometry is the science of measuring the power and geometric nature of electromagnetic radiation [60]. In order to understand the power output characteristics of the various commercially available excitation sources, it is important to understand basic radiometric principles and terminology, which are given in Table 2.1.

Table 2.1: Radiometric quantities

Quantity	Symbol	Description	Unit
Radiant flux	Φ	The energy radiated per unit time.	W
Radiant intensity	I	Radiant flux per unit solid angle.	W/sr
Irradiance	E	Radiant flux incident on a surface.	W/m^2
Radiance	L	The radiant flux emitted or reflected by a unit surface area (ds) into a unit solid angle in a given direction.	W/sr.m^2

A light source can be viewed as a surface area (ds) that emits or reflects radiant power with a certain degree of directivity. Directivity is the degree to which the emitted radiation is concentrated in a specific direction. The observed power density varies according to the distance between the observer and the source, as well as the direction from which the source is observed.

Radiant flux (Φ) is the amount of light energy radiated per unit time. This quantity only describes the radiant power, but not the directivity of the radiation. In order to account for the directivity, the quantity *radiant intensity* is used. Radiant intensity (I) is the radiant flux density per unit solid angle that is emerging from a point in space and propagating in a specified direction [60]. Figure 2.15 shows the geometry of a differential solid angle ($d\omega$). The radiant intensity is expressed as

$$I = \frac{d\Phi}{d\omega}. \tag{2.4}$$

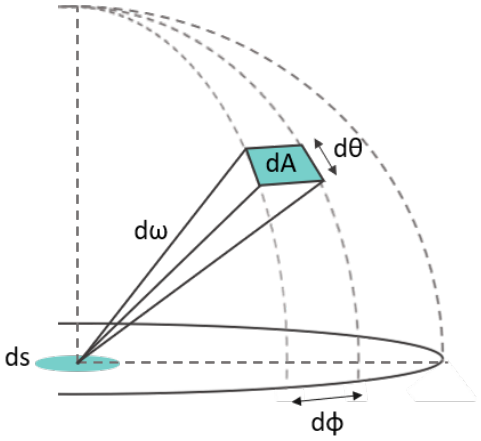

Figure 2.15: Differential solid angle

For biophotonics applications it is also important to be able to quantify the radiant power incident on the excited sample. This measurement is called irradiance (E), and is defined as the radiant flux density received by a surface (dA), as expressed by

$$E = \frac{d\Phi}{dA}. \tag{2.5}$$

The output-characteristics of light sources are sometimes expressed in terms of photometric quantities. Where radiometric quantities measure absolute power, photometric quantities are weighted according to the wavelength-dependent sensitivity of the human eye. The spectral sensitivity distribution of the human eye is shown in Figure 2.16 [60]. The photometric equivalent of radiant flux is luminous flux, which is measured in lumens (lm). Similarly, the photometric equivalent of radiant intensity and irradiance is luminous intensity and illuminance. The luminous intensity is measured in candela (cd) with one candela being equal to one lumen per unit solid angle.

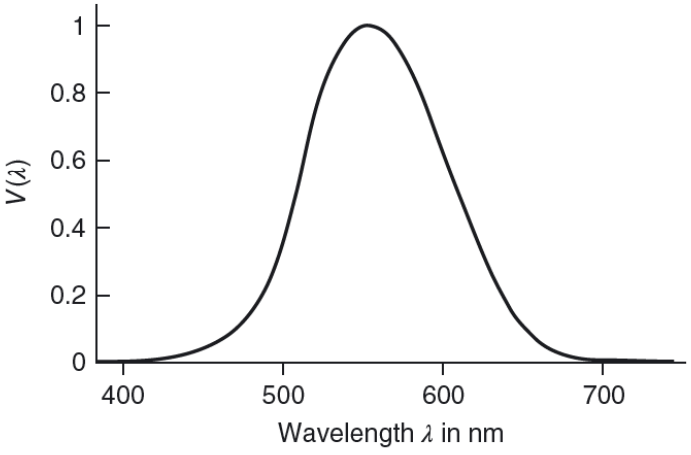

Figure 2.16: Spectral sensitivity of the human eye [from [60]]

For optical systems that deal with a range of wavelengths, it is often necessary to describe the above radiometric quantities as functions of wavelength. In such a case, the terms spectral flux, spectral radiance, spectral radiant intensity and spectral irradiance are used.

The radiometric properties of a light source determine for which biophotonic applications it is best suited. The choice of excitation source depends on the sample parameters, the illumination strategy and microscope configuration, and the detector sensitivity [59]. The most common light sources for widefield fluorescence microscopy include mercury and xenon arc lamps, metal halide lamps and LEDs. Lasers are also used in a variety of applications, such as laser scanning confocal microscopy, superresolution microscopy and certain fluorospectrometer designs.

Zeiss, a leading optical systems and optoelectronics company, provides the optical output power (presented in mW/cm^2) of the light sources most commonly used in widefield fluorescence microscopy [59]. They list the irradiance of these sources at a specified focal plane for a variety of common fluorophore filter sets. Table 2.2 shows the values provided by Zeiss and is included here to provide a reference for typical source power outputs. Next in this section, the most common light sources for fluorescence applications are discussed in order to evaluate their practicality in a low-cost, low-power, compact design.

Table 2.2: Light source irradiance outputs

Filter set	**Mercury Arc (mW/cm^2)**	**Xenon Arc (mW/cm^2)**	**Metal halide (mW/cm^2)**	**LED (mW/cm^2)**
DAPI	23.0	5.6	14.5	0.70 (365nm)
CFP	79.8	25.0	76.0	26.5 (445nm)
GFP/FITC	32.8	52.8	57.5	39.2 (465nm)
TRITC	43.1	12.2	33.5	2.7 (535nm)
Texas Red	153.7	54.4	119.5	7.9 (585nm)

Arc discharge lamps

Arc discharge lamps produce light through electric discharge in ionised gas or metal vapor. These lamps produce high radiant outputs and have broad spectral distributions that stretch over the entire visible spectrum [61]. The most popular arc lamps for fluorescence detection are mercury, xenon and metal halide lamps.

Mercury arc lamps have high intensity peaks over selected wavelength ranges, which make them versatile excitation sources when used with optical filters [62]. The xenon arc lamp has a more continuous and uniform spectral intensity distribution and is often used for quantitative fluorescence detection [63]. Metal halide lamps have a similar spectral intensity distribution as mercury arc lamps, save for pressure broadening of the spectral lines and the higher radiation levels between spectral lines [64]. The spectral intensity

distributions of the the popular HBO 100 mercury arc lamp and XBO75 xenon arc lamp are given in Figure 2.17 as an example of the continuous spectrum produced by arc lamps.

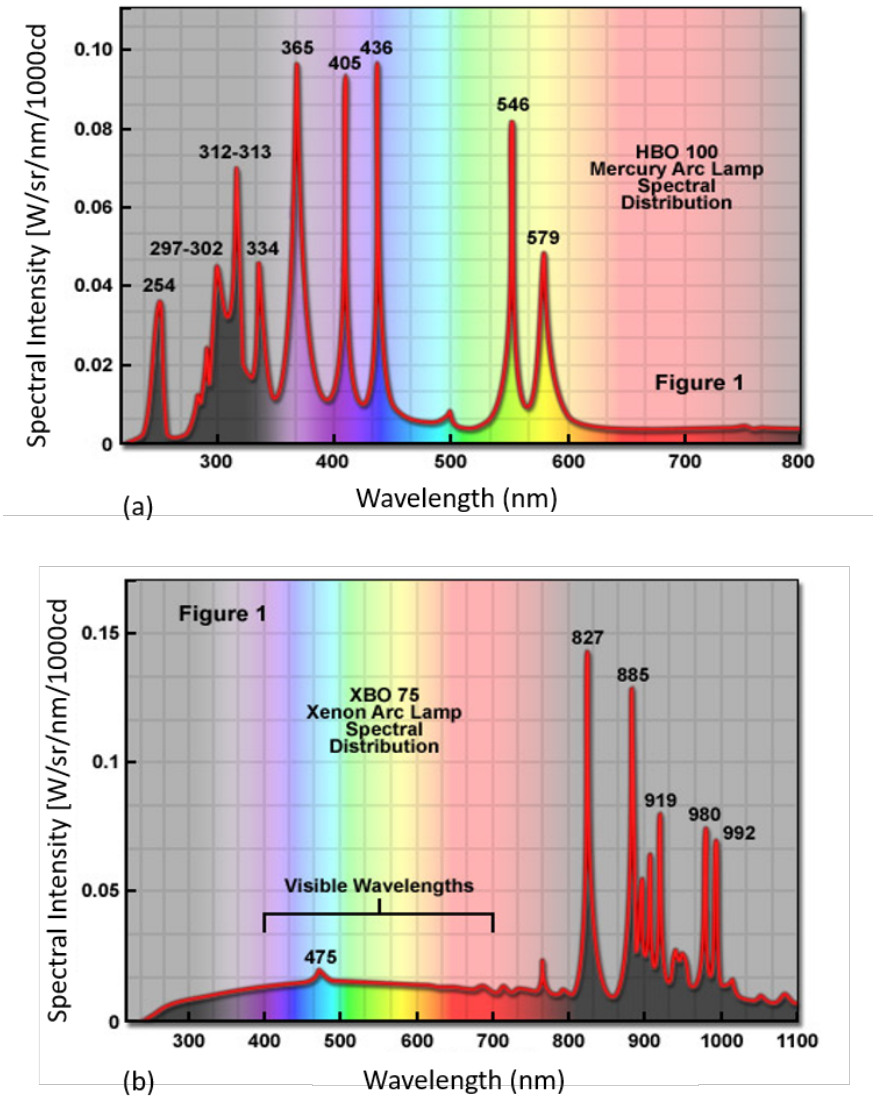

Figure 2.17: Spectral intensity distribution of the HBO 100 and XBO 75 [from [62] [63]]

The disadvantages of these lamps, in the context of a low-cost portable device, include the decay of intensity across the source lifetime and the production of excess heat. Arc discharge lamps are also relatively unstable light sources and can be affected by electromagnetic fields and unstable power supplies. They are also more expensive, more energy consuming, and typically larger than light emitting diodes.

LEDs

Light emitting diodes are solid-state semiconductor components that emit light through the recombining of electron-hole pairs in doped semiconductors. LEDs typically have narrow emission bandwidths, and are defined by their peak wavelength. They are available in an assortment of colours - or emission spectra - that vary across the visible light range

as shown in Figure 2.18.

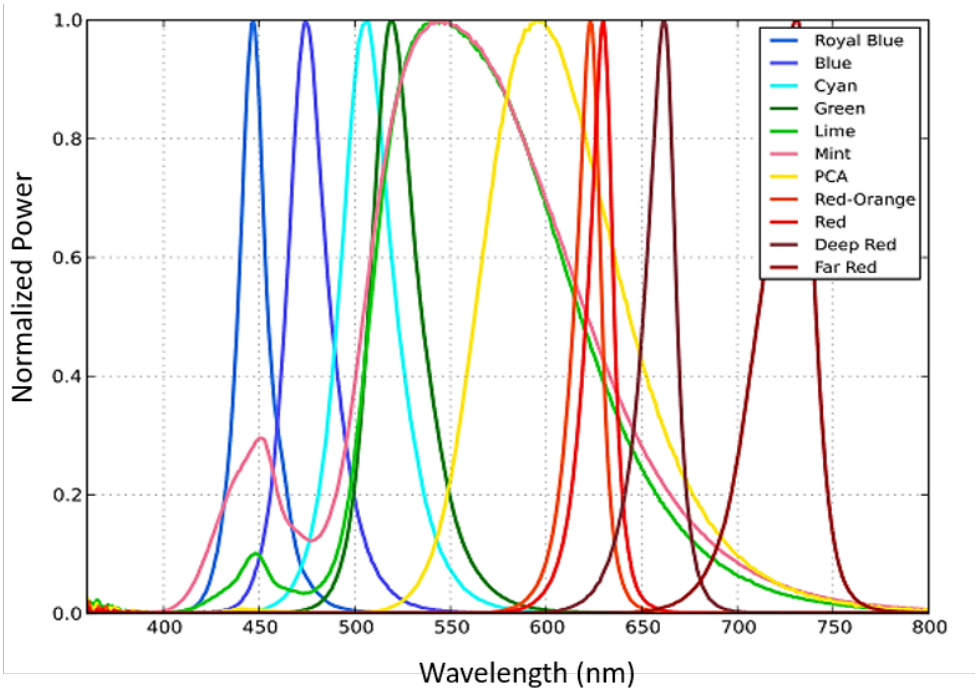

Figure 2.18: Spectral distribution for LUXEON 2835 Color LEDs [from datasheet]

In the last decade, LED technology has advanced tremendously. In the past, LEDs could not compete with arc discharge lamps in terms of intensity, and were impractical for microscopy applications. Today, individual high-power LEDs are bright enough to be used as effective monochromatic or polychromatic excitation sources in wide-field microscopy applications [61]. LEDs also have superior temporal and spacial stability compared to the arc discharge lamps, and their intensity can be controlled electronically and with precision [65]. In the context of a low-cost portable device, LEDs are also promising in terms of their compactness, affordability, long lifetimes and low energy consumption.

Lasers

Lasers are coherent, monochromatic light sources with highly collimated, gaussian output beams. There are a variety of laser types, such as gas lasers, solid state lasers, optical fiber laser and laser diodes. While the lasing mediums of these laser types differ, the basic principle of light production is the same and results in emission spectra with one or a few well-defined peaks [32]. Lasers are useful for high resolution imaging and are used in applications like confocal laser scanning microscopy and super resolution fluorescent microscopy.

Although the monochromatic laser beams can effectively and selectively excite single flurophores, the high-power output can cause rapid photo bleaching. Furthermore, high quality lasers are significantly more expensive, power-hungry and space-consuming than LEDs.

2.3.2 Optical assembly

The purpose of the optical assembly in a fluorescence detection device is to collect the emitted fluorescence signal and guide it towards a detector while filtering out unwanted wavelengths. As discussed in Section 2.2.3, there is a variety of fluorescence detecting techniques and tools. The optical assemblies of these tools differ in design and complexity. Section 2.2.3 briefly outlined the basic light path designs for widefield fluorescence microscopy, confocal microscopy, and spectrofluorometry.

Keeping in mind that the objective of this project is to design an affordable and compact device, it is important to identify the essential optical components required to collect, guide and filter the sample fluorescence. Therefore, the basic fluorescence microscope design in Figure 2.19 is used as a reference for an optical assembly that contains the fundamental components for fluorescence detection.

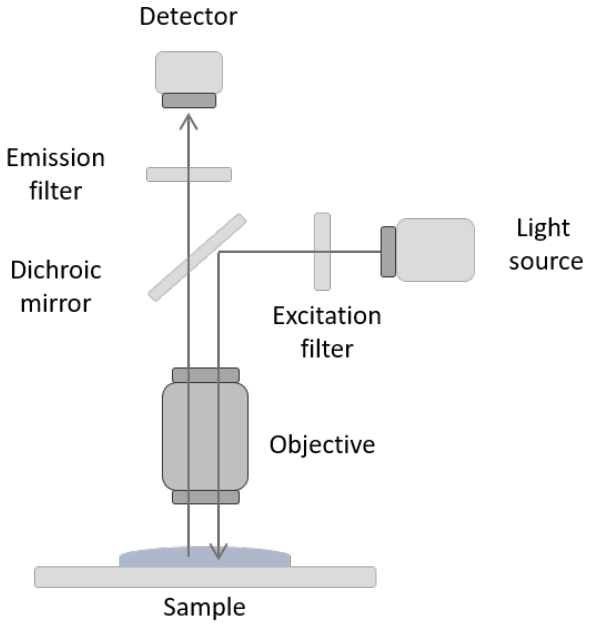

Figure 2.19: Basic fluorescent microscope design

In Figure 2.19, light from a light source passes through a filter that only transmits wavelengths in the required excitation range. A dichroic filter - designed to transmit certain wavelengths and reflect others - reflects the filtered excitation light towards the objective. The objective guides the excitation light towards the sample, where the sample area that falls within the objective field of view is illuminated. The objective collects the sample fluorescence emission and focuses it on the detector. Before the emitted light reaches the detector, it passes through the dichroic filter and an emission filter, so that only the desired emission wavelengths are detected. The rest of this section explores the relevant characteristics and parameters of objectives and optical filters.

Objectives

The role of an objective is to magnify the sample area under inspection by collecting the light from a focal plane in this area and focusing it at an image plane as shown in Figure 2.20 [66]. Objectives consist of muli-lens assemblies that direct light propagation through the process of refraction. The complexity of objective lens assemblies vary according to their ability to correct optical aberrations. Important objective specifications, other than the magnification, are the numerical aperture (NA), working distance and field of view.

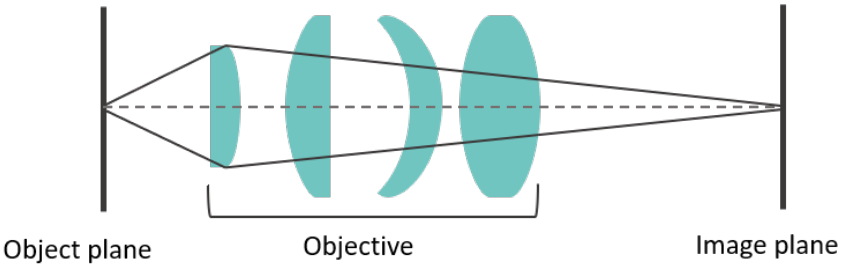

Figure 2.20: Example of an objective lens assembly

The numerical aperture specifies the objective's ability to collect light and resolve fine details in the object plane. The NA is a function of the half-angle (α) of the light cone collected by the objective, which means that it is a function of the entrance lens diameter (D) and the focal length or working distance (f) of the objective [66]. The working distance is the distance required between the front lens of the objective and the sample plane for the magnified sample image to be in focus. The equation for the NA is given by

$$\text{NA} = n\sin\alpha \approx D/2f \tag{2.6}$$

where n is the refractive index of the medium between the sample and the objective. Immersion oils are often used to increase the NA of an objective, since they have a higher refractive index than air. Where air has a refractive index of 1, immersion oils typically have a refractive index of 1.51 [66]. Figure 2.21 illustrates how a decrease in the focal distance results in a greater NA, which in turn yields a finer image resolution.

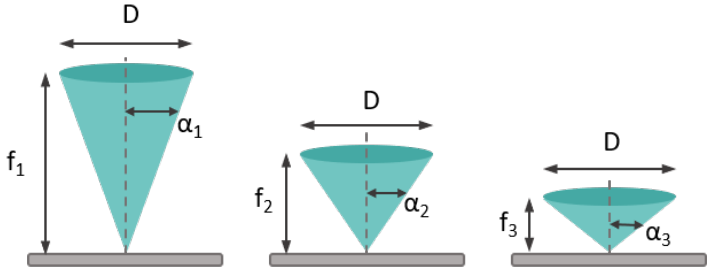

Figure 2.21: Numerical aperture as a function of lens diameter and focal length

The resolution of the magnified image is diffraction limited. The light collected from the sample can be seen as having its origin in multiple point sources of light [67]. As the light travels from the sample, through the objective, towards the detector, it is subject to diffraction and scattering. Therefore, when the light reaches the detector, it no longer consists of perfect point sources, but rather of broadened diffraction patterns called Airy disks [68]. The size of the Airy disk depends on the wavelength of the imaged light, the NA of the objective, and optical aberrations. The larger the NA of the objective, the smaller the Airy disk. Figure 2.22 illustrates how two point source diffraction patterns approach a diffraction limit.

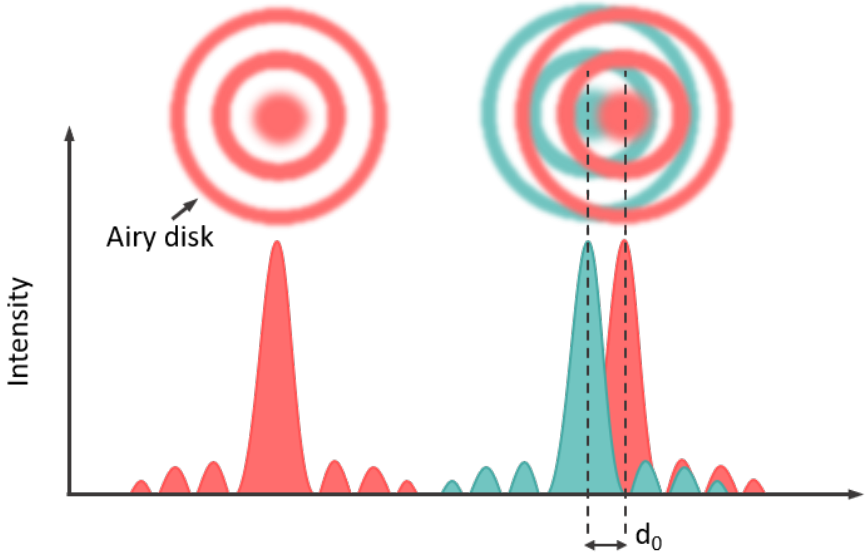

Figure 2.22: Point sources approaching diffraction limit.

The limit of resolution is the smallest distance between the peaks of two Airy disks for which the individual Airy disc patterns can still be resolved. According to the Abbe diffraction criterion, the the minimum distance that can be resolved in the lateral plane is represented by

$$r = \gamma/2\text{NA} \tag{2.7}$$

where γ is the wavelength of the light that is being detected. An objective's field of view (FOV) refers to the area that is being magnified and imaged. The field of view's size is dependent on the objective magnification [66]. When an objective is used in conjunction with an image sensor, the field of view can be described as

$$\text{FOV} = \frac{\text{Sensor imaging area}}{\text{Objective magnification}}. \tag{2.8}$$

Optical fiters

The role of the optical assembly is not only to guide light towards the detector, but also to isolate the fluorescence emission by eliminating the excitation light and other unwanted wavelengths. This is achieved with the use of optical filters. The two types of optical filters most commonly used for fluorescence detection are absorptive and dichroic filters.

Both absorptive and dichroic filters selectively transmit certain portions of the optical spectrum. The distinction between these two types of filters lies in the way they reject unwanted light. While absorptive filters absorb unwanted wavelengths, dichroic filters reflect them. Absorptive filters are typically placed perpendicular to the incident beam, however, their absorption and emission properties are maintained over a wide range of angles of incidence [69]. Conversely, dichroic filters are highly angle-sensitive and are placed at a 45 degree angle relative to the incident light beam. Figure 2.23 illustrates how a longpass absorptive and a longpass dichroic filter reject and transmit light.

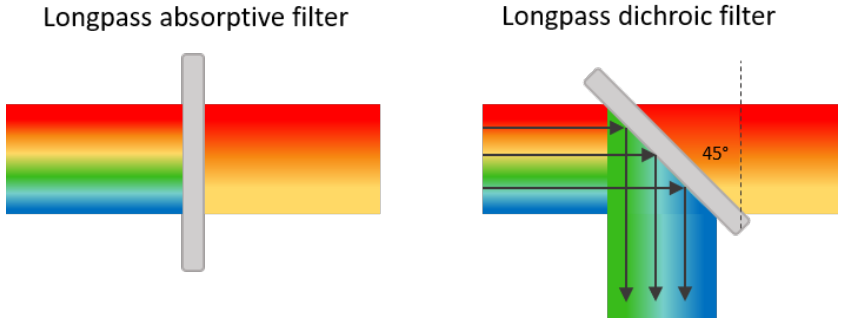

Figure 2.23: Absorptive and dichroic filter transmission and rejection

Absorptive and dichroic filters can be divided into three categories according their transmission and rejection band profiles. Longpass filters only transmit light above a certain wavelength, while shortpass filters only transmit light below a certain wavelength [70]. Bandpass filters transmit certain spectral bands while rejecting the rest. Some of the key filter specifications include cut-on and cut-off frequencies, slope and optical density.

The cut-on or cut-off wavelength of a filter defines the wavelength where the filter transmission is 50% of its maximum. The position of the cut-on and cut-off wavelengths for a shortpass, bandpass and longpass filter are shown in Figure 2.24. The slope of a filter describes the bandwidth over which the transmission shifts from a low transmission (typically 10%) to a high transmission (typically 80%) [69]. Bandpass filters are also defined by their center wavelength (CWL) and full-width-half-maximum (FWHM) parameters. The FWHM is the spectral bandwidth between the cut-on and cut-off wavelengths, and the CWL denotes the midpoint of the filter's transmission bandwidth [70].

Another important filter parameter is the optical density (OD). The optical density describes the filter's ability to reject wavelengths outside the passband of the filter [69]. The OD is related to the percentage transmission of wavelengths outside the passband via

$$\text{OD} = -\log(\frac{\text{Transmission}}{100\%}). \tag{2.9}$$

The required optical density of a filter depends on the filtering application. For fluorescence detection applications it is important that the filter rejects all of the unwanted light, and therefore ODs greater that 5 are typically recommended [70].

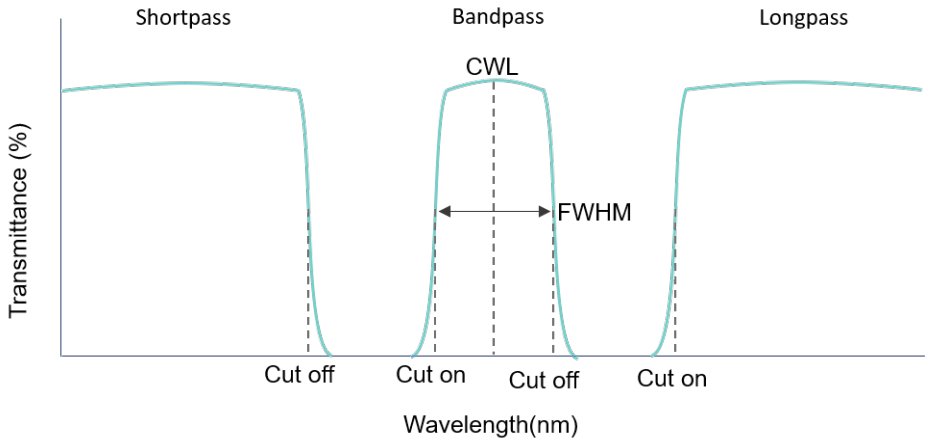

Figure 2.24: Filter pass bandwidths

Optical filters are fabricated in a variety of ways. The most affordable and least effective types of filters are coloured glass or plastic filters. For applications that require superior optical performance, hard coated and traditional coated filters are more suitable. A hard coated filter consists of a single substrate, such as fused silica, with dense coatings that optimise the transmission shape and performance [69]. These filters are very durable and ideal for precision applications. Traditional coated filters consist of stacked absorbing, interference and metallic layers. Although these filters are more affordable than hard coated filters, their optical performance are limited in comparison.

2.3.3 Optical sensing

There are a variety of electronic components that utilise the photo-electric effect to convert incident light to current. These include photodiodes, phototransistors, photomultiplier tubes and optical detector arrays, such as charged coupled devices (CCD) and complementary metal-oxide-semiconductor devices (CMOS) .

Single-channel detectors, such as photodiodes and phototransistors can only detect a single spectral channel at any given time. Multi-channel devices consist of two or three dimensional arrays of single-channel detectors (pixels) and are used to detect multiple spectral channels or multiple spatial channels for a given time sequence [32]. CCD and CMOS sensors are examples of multi-channel devices. These sensors are widely used for imaging, spectrophotometry and scientific measurements and are therefore the focus of this discussion.

Each pixel in a CCD sensor is a metal-oxide-semiconductor capacitor that builds up charge by collecting the electrons released by the semiconductor layer as the light impinges on the pixel [71]. After a specified illumination time, the pixel charges are shifted row by row to the output register array where they are processed sequentially.

Where CCD sensors perform the charge to voltage conversion sequentially by an external circuit, CMOS sensors do the conversion within each pixel. A CMOS pixel consists of a photodiode, CMOS conversion and amplification circuitry, and a capacitor which voltage is proportional to the incident light intensity [71]. Each pixel can be selected and read individually via a read-out switch.

When a magnified image is digitally sampled by a pixel array, the resolution of the image is once again limited. This resolution limit depends on the pixel size and can be calculated using the Nyquist-Shannon sampling theorem [72]. This theorem states that the minimum sampling frequency that will preserve the underlying information of a signal, must be double the frequency of the signal's highest frequency component. As discussed previously, the resolution of a magnified image is $\gamma/2\text{NA}$ and therefore, the highest spatial frequency component is $2\text{NA}/\gamma$. To maintain the resolution of the image light incident on the sensor, the spacial sampling frequency must be $4\text{NA}/\gamma$, which means that the pixel size must be less than or equal to $\gamma/4\text{NA}$.

In the past, CCD sensors have been the popular choice for high resolution imaging, since the absence of complex pixel circuity allowed for small pixels and close pixel proximity. CMOS sensors were preferred for rapid imaging applications, since the charge to pixel conversion is performed in parallel [73]. Both technologies, especially CMOS sensors, have undergone refinements aimed at minimizing limiting characteristics. Therefore, the choice between CCD and CMOS is less apparent today.

The technological advances in CCD and CMOS imaging technology have led to the increasing use of consumer cameras, and specifically smartphones, in low cost, portable scientific applications [74]. Today's smartphones offer high resolution and raw imaging capabilities with wireless connectivity and versatile processing abilities. Therefore, one of the first design decisions for this project was to use a smartphone camera as the image detector. Section 2.4 discusses smartphone image capturing, image file formats, and colour vision.

2.4 Smartphone imaging

The use of smartphones cameras as scientific tools has become an increasingly popular topic. Over the last decade, smartphone camera technology has improved at an impressive rate and today this technology is being recruited for applications like environmental monitoring, colour science, biomedical applications, etc. [74]. Since smartphones are widely used, compact and technologically versatile in relation to cost, the employment of smartphones for healthcare applications may help democratise healthcare services [75].

Smartphone cameras are inherently designed to capture images that are aesthetically pleasing to the human eye. From the spectral transmission of the image sensor, to preprocessing and image compression algorithms, smartphone camera technology is designed

to model the human visual experience - not to capture and present absolute spectral and radiometric information. In order to use a smartphone camera for scientific imaging purposes, it is important to understand how the light information is captured, how spectral information is converted to colour data and how post-processing alters the image information.

2.4.1 Image capturing and colour vision

A basic smartphone camera module consists of two major components - the camera lens assembly and the image sensor. The lens assembly consists of multiple micro-lens elements and has a fixed focal-length and aperture [76]. The lens is fixed to the image sensor to form a compact digital camera module as shown in Figure 2.25. Smartphone cameras almost universally have CMOS image sensors, since CCD technology is too expensive and power-consuming.

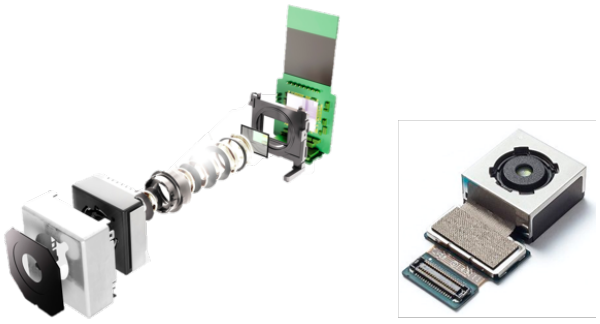

Figure 2.25: Smartphone camera module

Small lens movements driven by auto-focusing algorithms enable smartphone cameras to vary their focus distance. This allows smartphone cameras to take infinity-focused landscape shots as well as macro shots [76]. Infinity-focus refers to the ability to focus parallel light rays that originate from an object far away. For a macro shot, the imaged object is close, and the focus distance is finite. Figure 2.26 illustrates an infinity focus mode, and how varying finite object distances require lens-movement.

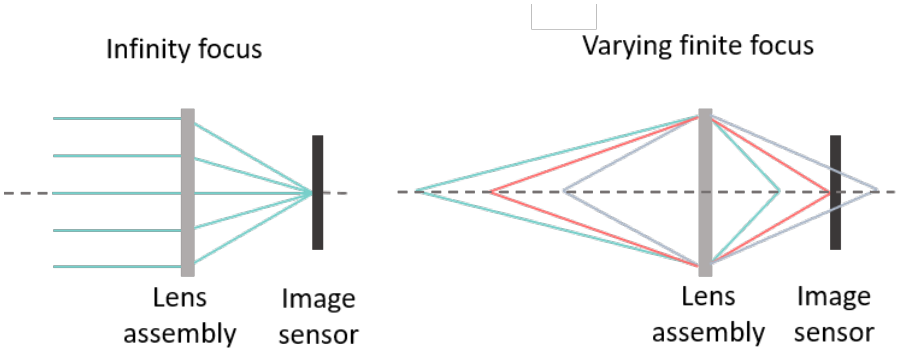

Figure 2.26: Smartphone focus modes

In order to interpret the information captured by a smartphone camera as radiometric and spectral measurements, it is important to understand how the incident light is processed. A CMOS sensor on its own can only detect the intensity of the light incident on each pixel, but not the spectral distribution, and therefore not the colour. The colour detection is facilitated by a colour filter array (CFA) and demosaicing algorithms. A CFA is a filter grid with alternating red, green and blue pixel-sized filters [77]. A CFA is placed over the CMOS sensor to create a pixel-grid with alternating red-, green- and blue- detecting pixels. During post-processing, a demosaicing algorithm constructs a full-colour image through interpolation [78]. Figure 2.27 shows a CFA filter in the Bayer configuration - the most popular configuration for consumer cameras.

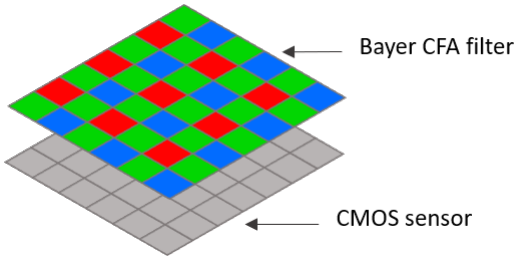

Figure 2.27: Bayer colour filter array

The spectral transmittance of the red, green and blue CFA filters is based on human colour vision. The human eye responds to electromagnetic radiation with wavelengths between 380 and 740 nanometers, but even though our colour perception is related to wavelength, our eyes cannot actually detect the exact wavelengths of the incident light [79]. Our colour perception relies on special photoreceptor cells in the retina, called cone cells. There are three types of cone cells that each respond to a specific range of wavelengths. They are often referred to as L (long), M (medium) and S (short) cones. Figure 2.28 shows the spectral response curves of the L, M and S receptors.

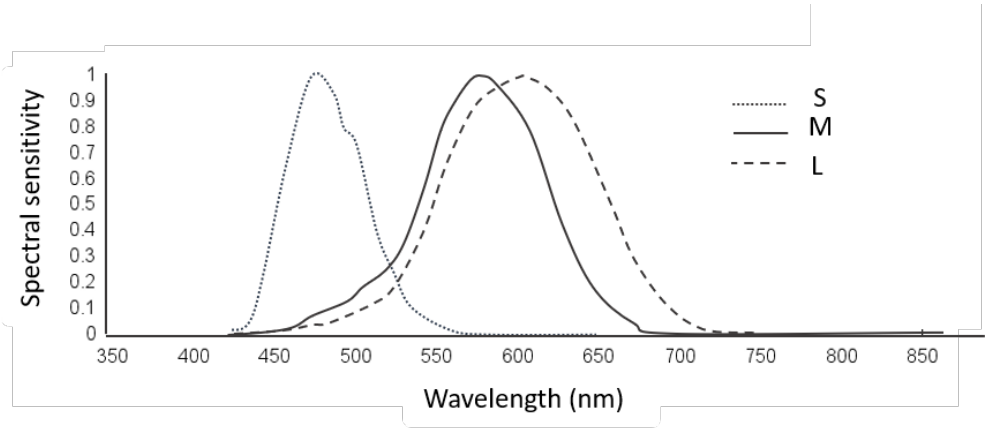

Figure 2.28: Spectral response of short, medium and long receptors

When light is incident on the retina, each cone cell responds to the wavelengths that falls within its spectral response bandwidth. The brain then forms a perception of colour

according to the degree to which the L, M and S cones were stimulated respectively. This mechanism of perceiving colour is called trichromacy and it allows us to describe colour as the combination of three primary colour values, or tristimulus values [80]. The distributions of the three primaries are called colour matching functions. The C.I.E. 1931 XYZ colour matching functions shown in Figure 2.29 give an example of how red, green and blue primaries can be combined to produce our perception of the visual spectrum.

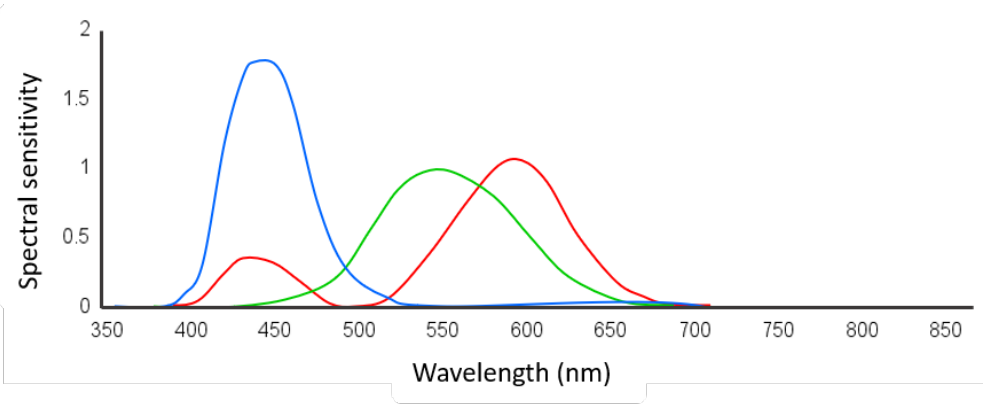

Figure 2.29: C.I.E. 1931 XYZ colour matching functions

The colour filter arrays used in smartphone cameras and other consumer cameras are based on the trichromacy and the spectral sensitivity of human vision. The spectral response of the alternating Bayer colour pixels facilitates the detection of red, green and blue tristimulus values. Furthermore, there are twice as many green pixels as there are red and blue pixels in order to compensate for the spectral sensitivity of the human eye as discussed in Section 2.3.1. Burggraaff *et.al.* [74] characterized the spectral response of a variety of smartphone and consumer cameras as part of a study aimed at standardizing spectral and radiometric calibration of consumer cameras. Although there are variations between camera models, and manufacturers keep the specific filter designs under wraps, Figure 2.30 shows what the typical spectral responses of a smartphone camera are.

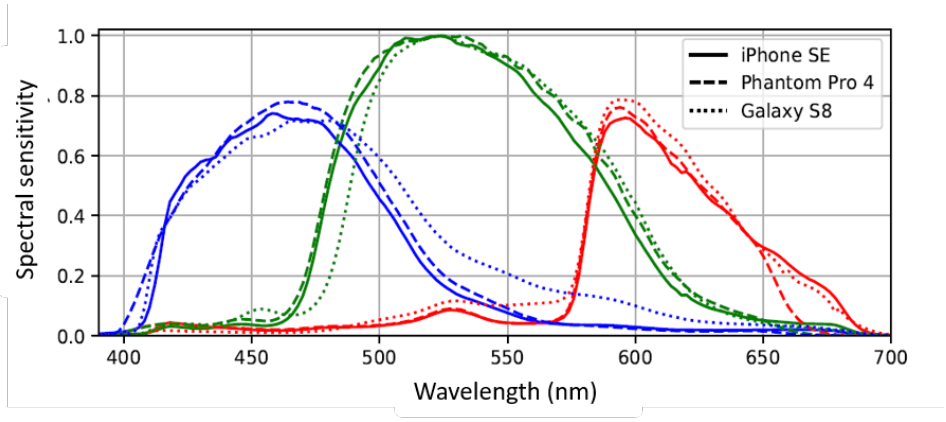

Figure 2.30: Spectral response of iPhone SE, Phantom Pro4 and Samsung Galaxy S8 [from [74]].

The conversion from detected spectra to numerical colour-coordinates is irreversible, since a single colour-coordinate can map to an infinite number of wavelength-combinations. However, the spectral response curves given in Figure 2.30 gives insight into the spectral content of the light that is detected by red, green and blue channels of the camera sensor.

2.4.2 RAW vs JPEG image format

Once the image is captured by the CMOS sensor, the raw sensor data is processed and saved in an image file format. The raw sensor data consists of the grayscale pixel values which represent the intensity of the light incident on each pixel. The red-, green- and blue-filtered pixels have grayscale values proportional to the respective amount of red, green and blue light reaching the sensor. In order to construct a detailed colour image from the raw data, a series of processing steps are performed.

As discussed in the previous section, the raw data undergoes demosaicing where the colour information for each pixel is interpolated from neighboring grayscale pixel values. Furthermore, colour processing steps such as white balancing, gamma-correction and tone-mapping are performed to ensure that the image is an acceptable representation of the captured scene as a human would see it [81]. The camera software also performs noise-reduction and sharpening to improve the perceived image quality. Once the image is processed, its is typically compressed into a JPEG image format [82]. Figure 2.31 shows a basic image processing pipeline. The processing order and algorithms may differ between smartphone cameras.

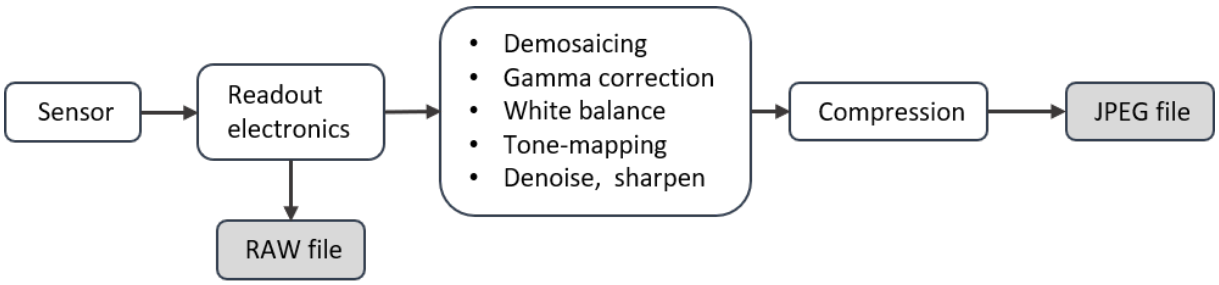

Figure 2.31: Image pre-processing pipeline

JPEG compression is lossy, since the process discards image data to which the human eye is not sensitive. Where most smartphone RAW images have 10- or 12-bit pixel-depths, JPEG image have 8-bit pixel-depths [82]. Due to the image pre-processing and the JPEG compression, much of the original RAW information is lost. Furthermore, where RAW image pixel values have a linear response to varying light intensities, JPEG images do not. Therefore, the use of JPEG-images for quantitative radiometric and spectral analyses is not recommended [74]. RAW image format are more suitable for such applications.

There are many types of RAW image file formats, since most consumer camera brands have their own RAW formats. However, Adobe developed a universal RAW image format that is supported across platforms, called the Digital Negative (DNG) format. Smartphones that have the ability to shoot RAW typically use the DNG file format.

A complication associated with using RAW images for scientific analysis is the mosaiced nature of the image. Since demosiacing results in the loss of information, RAW images can rather be treated as three independent images - each representing a red, green or blue colour channel [74]. Figure 2.32 shows how a RAW image can be divided into the red, green and blue colour channel images.

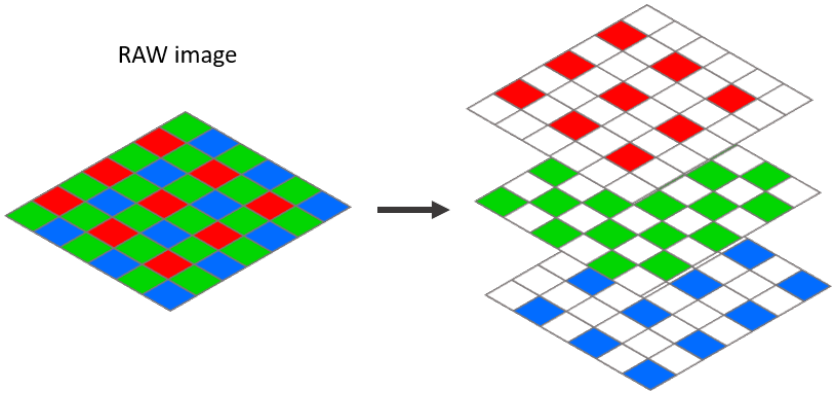

Figure 2.32: RAW image colour channels

2.5 Summary

The purpose of this literature review was to gain appropriate and sufficient insight into the various fields of knowledge related to the development of a low-cost, fluorescence-based amyloid fibrin(ogen) sensing device for systemic inflammation detection.

1. The mechanisms and consequences of systemic inflammation were discussed and an overview of standardised inflammation biomarkers and tests was provided. Thereafter, the mechanisms of amyloid formation and the role of amyloid fibrin(ogen) in the inflammatory response were discussed. Note that the research on amyloid fibrin(ogen) and its utility as a novel indicator of inflammation is still new and ongoing. The use of amyloid-staining fluorescent dyes and confocal microscopy has been the preferred method of detection in the existing studies on amyloid fibrin(ogen). Therefore, the specified method of detection for this project is fluorescence-detection.

2. The fields of knowledge related to fluorescence-detection were discussed next. Biophotonics, the basic principles of light and the process of fluorescence were reviewed. Traditional fluorescence microscopy and spectroscopy techniques where discussed in order to gain insights into the various mechanisms of fluorescence detection. These insights will inform a simplified optical design for the detection of amyloid fibrin(ogen). The intrinsic fluorescent properties of amyloid proteins and fluorescent amyloid-binding ligands were discussed in order to gain insight into the variety of fluorescence probes available for the detection of amyloid structures.

3. The investigation of the various fluorescence microscopy and spectroscopy techniques provided insight into the essential stages and components of fluorescence detection. Excitation sources, optical assembly components and optical sensing components were discussed to determine which components will be suitable for a low-cost, low-power, compact device.

4. After reviewing the various optical sensing components, smartphone imaging was chosen for the detection stage. Therefore, the image capturing mechanisms and spectral response of smartphones, as well as the various image file formats were discussed.

The literature review will inform the design and the evaluation of the low-cost, fluorescence-based amyloid fibrin(ogen) sensing device.

Chapter 3

Design and Development of the FID Prototype

In order to set the context for this chapter, the project objectives pertaining to the design and development stage are revisited. As specified in Chapter 1, the objective of this project is to:

1. develop a device that detects the presence of amyloid fibrin(ogen) in human platelet poor plasma by implementing an in vitro, fluorescence-based assay that utilises a fluorescent dye known for staining amyloid structures.

2. keep the design low cost, compact, modular and low power so that it is suitable for use in mobile and rural clinic setups.

This chapter discusses the design and development methodology, which includes the identification of the design requirements, a high level system overview and, finally, the low level design and component selection. For the sake of practicality, the device will henceforth be referred to as an FID (fluorescence-based inflammation detector).

3.1 Design requirements

The design requirements are informed by project objectives as well as the target market, target environment and the prospective use-cases for a FID prototype. The typical target market for the FID includes medical practitioners, nurses and lab technicians working in mobile care-units or rural clinics. The prospective use-cases for the FID are listed in Table 3.1.

Table 3.1: Prospective use-cases for a FID

Preventative care	Inflammatory diseases are typically preceded by undiagnosed long-term chronic inflammation. The FID can be used as a point-of-care screening tool in mobile clinics and medical consulting rooms. Risk cases can be referred for further tests and treatment to prevent disease development or progression.

Reactive care	The FID may serve as an affordable point-of-care tool to monitor response to treatment and recovery progress of patients with chronic inflammation and/or inflammatory diseases.
Research	The FID may be used as an affordable tool to test and analyse large sample sizes in a lab environment.

In these settings, medical and lab equipment must offer simple, quick and point of care based solutions. The high level design requirements must take into consideration the practical needs of the above-mentioned target market, target environment and use-cases. The high-level design requirements are listed in Table 3.2.

Table 3.2: High level design requirements

Physical Characteristics	• Compact and stable. • Easy to move and transport. • Modular design for easy maintenance and component replacement.
Samples	• Sample size must be small enough for point of care testing. • Accurate and repeatable sample preparation and placement. • Disposable sample holders.
Outputs	• Quantification of sample fluorescence via image processing. • Processing software must facilitate multiple sample testing and statistical analysis.
Power Consumption	• Low power • Battery- or USB-powered
Cost	• Low cost both in terms of cost to manufacture and cost to use. • Affordable to maintain and repair.

3.2 System overview

The development of a fluorescence-based inflammation detecting device requires the application of multi-disciplinary concepts and the synergistic integration of various hardware and software components. As a first step, the main high-level system components of an in vitro fluorescence-based assay and the requirements for successful integration are identified.

A fluorescence-based assay can be divided into four main processes - excitation, light manipulation, detection and quantification. During excitation, target fluorophores in the sample absorb incident light from an excitation source and then emit fluorescent light. Secondly, a combination of filters and lenses guide the emitted fluorescent light toward the detector, while filtering out the excitation light. Lastly, photo-detecting electronics convert the incident light to an electronic signal which is analysed to quantify the fluorescence intensity.

The absorption spectrum of the target fluorophore determines the emission spectrum of the excitation source. The fluorophore emission spectrum determines the spectral transmission of the optical assembly, and the spectral sensitivity of the photo-detecting electronics. Finally, the nature of the detected signal determines how the signal is analysed. The design methodology is directed by the interdependence between the sample composition, sample excitation, optical assembly components, and detection mechanism.

Figure 3.1 illustrates the high level system components of a fluorecence-based assay as well as the dependencies between the spectral properties of these components. In order to ensure the effective integration between the system components, system-level technical requirements are defined in Table 3.3.

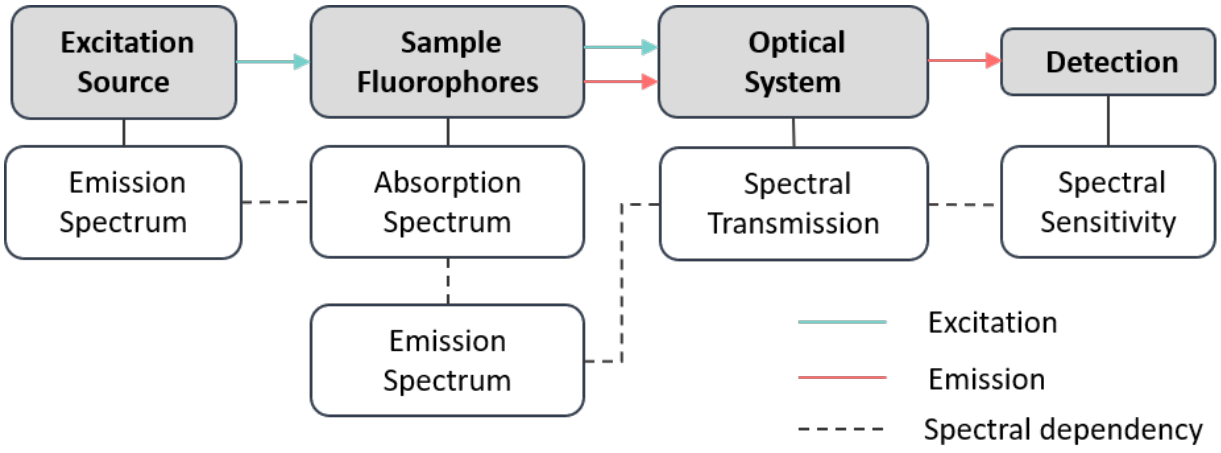

Figure 3.1: High level system components

Table 3.3: System-level technical requirements

Fluorescent marker	• The Stokes shift of the fluorescent marker must be large enough so that the absorption and emission spectra do not overlap. This ensures that the excitation light can be rejected without attenuating the fluorescence emission. • If other components in the sample have auto-fluorescence properties, the emission spectrum of the fluorophore must be distinguishable from the surrounding auto-fluorescence emissions.
Excitation	• The peak emission wavelengths must match the peak absorption wavelengths of the fluorescent probe. • The excitation source should be configured in a way that maximises irradiance and irradiant uniformity.
Optical assembly	• The optical axis of the assembly components should be aligned. The components must be positioned such that the sample is situated at the assembly's working distance. • Optical filters should ideally have rejection optical densities greater than 4.0, and high (>90%) pass band transmissions.
Detection	• The red, blue or green spectral response peaks of the sensor colour filter array must ideally match the spectral peak of the detected fluorescence. • Pixel and sensor size should correspond to the desired field of vision and image resolution. • The camera module should provide access to raw image data.
Analysis	• Image processing software and data organisation must allow for the automatic quantification of sample fluorescence for varying sample and sub-sample sizes, as well as varying numbers of technical repeats per sub-sample. • A statistical analysis must be performed to determine the significance of the results.

The system-level technical requirements specify the general criteria according to which the components of the FID must be selected. These requirements address typical challenges associated with fluorescence detection such as the reduction of background noise, optical aberrations, signal attenuation and artifacts. The low-level technical requirements are further determined by the type of information that the FID must extract from the fluorescence signal.

In Section 2.2.3 the two major types of fluorescence intensity sensing techniques were discussed - fluorescence microscopy and fluorescence spectroscopy. Where fluorescence microscopy aims to capture in-focus, high-resolution images of microscopic fluorescent structures, fluorescence spectroscopy captures the spectral distribution of the detected fluorescence.

In terms of a low-cost, compact, smartphone-based fluorescence detection device, a microscopy-based solution poses a series of challenges. These include:

- The image resolution is limited by the smartphone pixel-size. Furthermore, the sensor is divided into three colour channels, which means the resolution per colour channel is reduced further.
- The quality and resolution of the image is highly influenced by optical aberrations. Optical components that correct aberrations are typically more complex and expensive.
- In order to achieve adequate magnification the field of view must be very small. This limits the sample-volume and therefore the amount of fluorescence signal that can be detected.
- The sample-thickness must be close to zero as to avoid out-of-focus light from other focal planes. Not only does this reduce the number of detectable fluorophores per area, but it also creates challenges regarding repeatable sample placement.

While fluorescence microscopy images may provide valuable insight into molecular structures and binding mechanisms, it may not be the most practical solution for point-of-care fluorescence quantification. A spectroscopy-based solution does not aim to maximize resolution, magnification and focus, but rather to maximize the amount of sample fluorescence within a specific bandwidth that reaches the detector.

The implementation of a spectroscopy-based solution is more affordable, allows for larger sample sizes and sample depths, and is more practical for a point-of-care application. Therefore, it was decided that the FID should implement a spectroscopy-based solution by detecting the intensity of the sample fluorescence within the emission bandwidth of the chosen amyloid-staining fluorophore.

Figure 3.2 is a conceptual representation of the selected high-level design and component assembly. Section 3.3 discusses each of the components shown in the high-level design, as well as the rationale behind the design, component selection and device assembly.

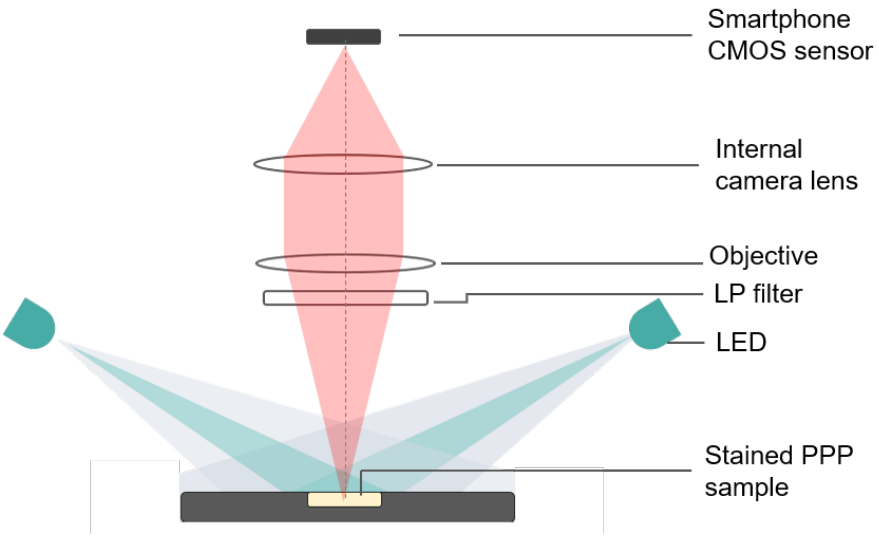

Figure 3.2: High level design

3.3 System components selection

In Section 2.3, the typical components used in fluorescence intensity sensing devices were evaluated in terms of their affordability and practicality within a low-cost, portable device. In this section, knowledge gained in Section 2.3 is applied and the component selection and design rationale are discussed. The discussion includes:

1. Fluorescent marker selection
2. Sample holder design
3. Excitation module design
4. Magnification and filtering
5. Detection and image processing
6. Device assembly

3.3.1 Fluorescent marker

This section discusses the selection of the fluorescent marker to be be used for the identification of amyloid fibrinogen structures. The fluorescent markers under consideration include:

- Amyloid fibrin(ogen) autofluorescence
- ThT
- Congo Red
- Amytrackers

As discussed in Section 2.2.4, amyloid structures have intrinsic fluorescent properties. Therefore, it was considered to detect and quantify the amyloid fibrinogen autofluorescence, without adding and external fluorescent marker. A spectral analysis of amyloid fibrin(ogen) clots, using confocal microscopy, showed that the amyloid fibrin(ogen) autofluorescence over a wide spectrum that overlaps with that of blood plasma. Furthermore, the exact spectral difference between normal fibrinogen and anomalous amyloid fibrin(ogen) could not be confirmed. Therefore, it was decided that a fluorescent marker with a narrower, more distinguishable emission spectrum should be used.

The more traditional amyloid-stains, ThT and Congo Red, were also considered as possible candidates. However, the ThT absorption and emsission spectra have a narrow Stokes shift of about 40nm and the light used to excite bound Congo Red must be polarized to observe the apple-green birefringence. Furthermore, neither of these stains are very amyloid-specific.

Eventually, it was decided to use Amytracker as the fluoroescent marker for this application. Amytracker products consist of fluorescent conjugated oligothiophene molecules, manufactured by Ebba Tech. They are advertised as being photo- and thermo-stable and ideal for "reliable fluorescent staining of early, pre-fibrillar states of amyloids arising from a variety of amyloidogenic proteins or peptides in tissues from a wide range of species [57]." As discussed in Section 2.2.5, there are four Amytracker products. The absorption and emission specifications for these products are given in Table 3.4

Table 3.4: Fluorescent marker absorption and emission spectra in nm

Fluorecent Marker	Bound Absorption	Bound Emission
Amy480	405-458	470-550
Amy520	405-488	500-600
Amy630	460-514	600-650
Amy680	530-565	600-800

Amytracker630, henceforth referred to as Amy630, was chosen for the reasons listed below.

1. The Amy630 emission spectrum is distinguishable from that of plasma and other biological autofluorescence. Biological autofluorescence typically peaks between 480nm and 580nm. Therefore, Amy480 and Amy520 were disqualified.

2. Amy630 has virtually no unbound fluorescence, which facilitates a high signal to noise ratio.

3. The Stokes shift between the Amy630 emission and absorption spectra is large enough to filter out the emission spectra comfortably.

4. The Amy630 peak emission band falls within the the peak spectral transmittance band of the red filter in a typical colour filter array. This is not the case with Amy680.

Figure 3.3 shows how the peak emission of the Amy630 almost matches the peak spectral sensitivity of a typical CFA red filter and how it is distinguishable from the peak auto-fluorescence spectrum of PPP.

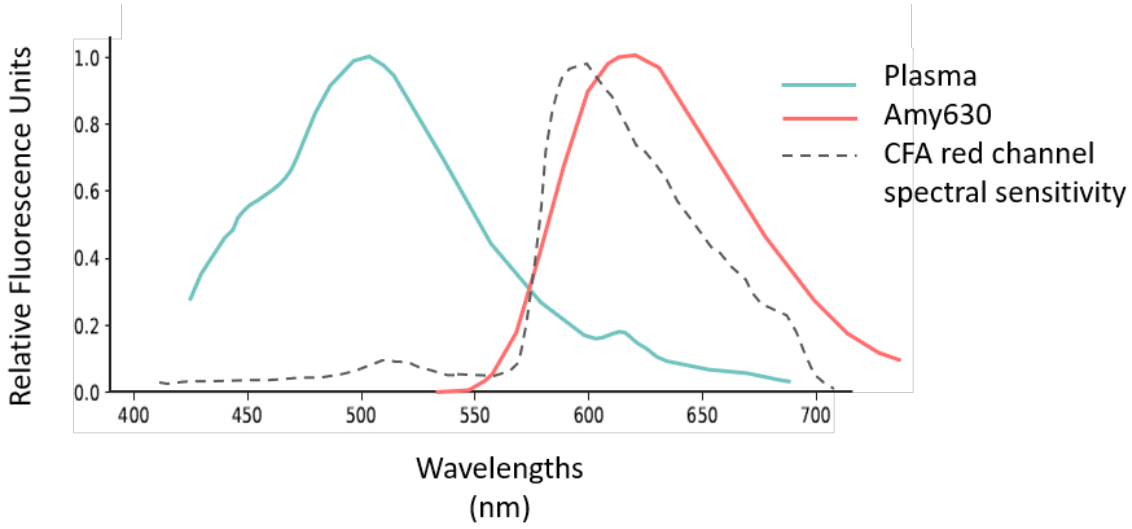

Figure 3.3: Emission spectra of plasma and Amy630

3.3.2 Sample holder

The sample holder is responsible for containing the sample and ensuring that the sample placement is accurate and repeatable. The aim of the FID design is not to capture high-resolution, structural fluorescent images, but rather to collect the maximum amount of fluorescent light from a relatively small sample volume. This means that the sample depth is not limited to the optical assembly's depth of field, and that the detection is not limited to a singe focal plane. The sample holder must keep the sample in a fixed position within the field of view. Two options were considered for sample-containment: qualitative filter paper and a disposable 3D-printed sample holder with a sample well.

The qualitative filter paper was considered for its ability to contain the sample even when the sample holder is not positioned horizontally. The proposed design for the filter-paper sample holder is shown in Figure 3.4. However, after experimenting with this design, the following issues were identified and the design was rejected.

- Sample placement is inconsistent and non-uniform
- The filter paper has high auto-fluorescence.
- Since the paper is white, it is very reflective and reflects the excitation light back to the detector. As discussed in Section 3.3.4, a high-perfomance emission filter is used to filter out the excitation light. However, the filter has an optical density of 4, which is not high enough to filter out direct, high-power light incidence.

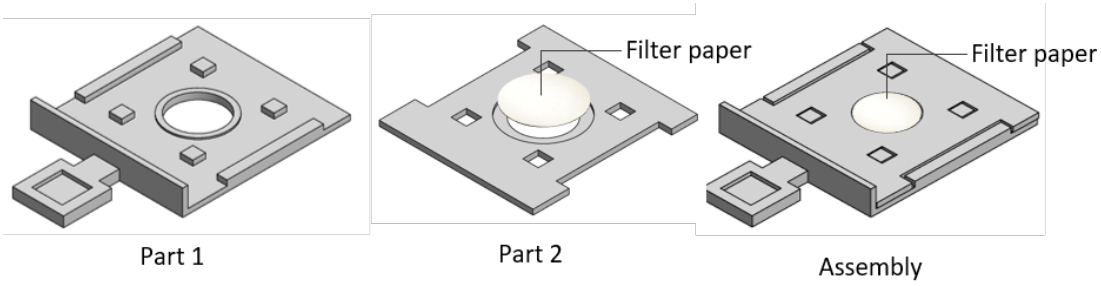

Figure 3.4: Sample holder with filter paper

Therefore, it was decided to use the 3D-printed sample-well design shown in Figure 3.5. The rectangular, plastic sample holder fits into a slider that slides into the FID and positions the sample well in the optical assembly's field of view. The benefits of this design include:

- Sample placement is repeatable.
- Sample area can be controlled and optimised for maximum fluorescence detection.
- The sample holder can be printed using black filament to maximise absorption and minimise reflection.
- The sample holder is low-cost and disposable.

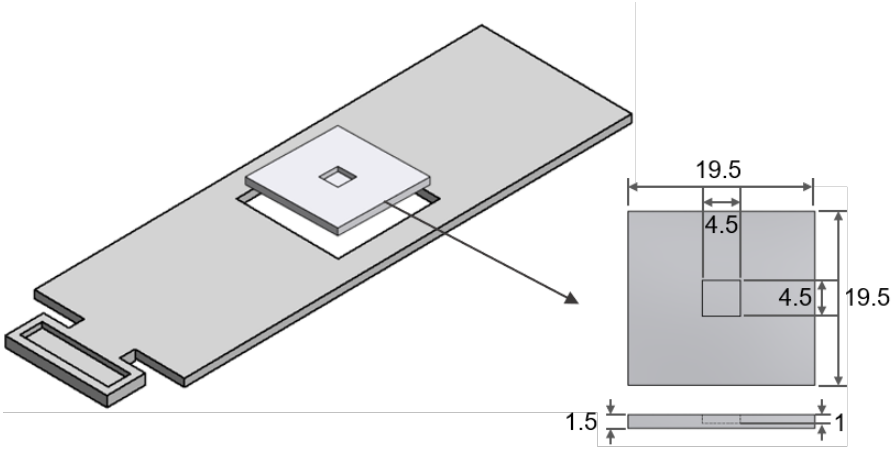

Figure 3.5: Sample slider and sample holder with well

Figure 3.5 shows the dimensions of the sample holder. The sample well can contain a sample volume of 20 μl. The sample preparation and testing protocols are described in Chapter 4. Furthermore, it was decided to make the sample-area slightly larger than the optical assembly's field of view to avoid the detection of edge effects at the sample edges. Details regarding the field of view are discussed in Section 3.3.4.

3.3.3 Excitation source

In Section 2.3.1 the most popular excitation sources for fluorescence detection applications were discussed. From this discussion it became apparent that modern LED technology offers various desirable features. LEDs are popular and versatile low cost lighting solution. They are ideal for compact, low-energy, low cost applications that do not require highly collimated, spectrally coherent or monochromatic light. Since these criteria match those of the FID, it was decided to use LEDs for this application.

After considering multiple commercially availabe LEDs, the HLMP-CE34-Y1CDD LED by Avago Technologies was selected. The HLMP-CE34 is a high-intensity cyan InGaN (indium gallium nitride) LED. InGaN is known for having higher luminescence efficiency than many other semiconductor materials used for green and blue LEDs. The HLMP-CE34 LEDs also have well-defined spacial radiation patterns, clear caps for non-diffuse radiation and good moisture and temperature resistance. The LED is available in a round through hole package with a 5mm cap-diameter. Table 3.5 lists the electrical and radiometric characteristics as found in the HLMP-CE34 data sheet.

Table 3.5: HLMP-CE34 electrical and radiometric characteristics

Parameter	Typ	Units	Test Conditions
Forward Voltage	3.2	V	I = 20mA
Dominant Wavelength	505	nm	I = 20mA
Peak Wavelength	501	nm	Peak Wavelength of Spectral Distribution at I=20mA
Luminous Efficacy	326	lm/W	Emitted Luminous Power/Emitted Radiant Power
Luminous Flux	2.1	lm	I = 20mA
Max Luminous Intensity	21	cd	I = 20mA

This section first discusses the spectral and radiometric properties of the HLMP-CE34. Thereafter, the geometric design of the FID excitation module is discussed, and finally the LED circuitry design is given.

Spectral and radiometric characteristics

The most important requirement for the selected LED is that its emission spectra should match the absorption spectrum of the chosen fluorescent marker. Furthermore, the LED emission bandwidth should be narrow enough that the excitation light can be filtered out without attenuating the fluorescent emission too much.

As discussed in Section 3.3.1, the recommended excitation range of Amy630 is 460-514 nm. The HLMP-CE34 has a peak wavelength of 501 nm and a spectral halfwidth of 30 nm. The LED emission spectrum therefore matches the absorption spectrum of the Amy630 well, and has a narrow enough bandwidth to avoid an overlap with the Amy630 emission spectrum. The spectral profile of the HLMP-CE34 is shown in Figure 3.6 and the Amy630 absorption spectrum is shown for reference.

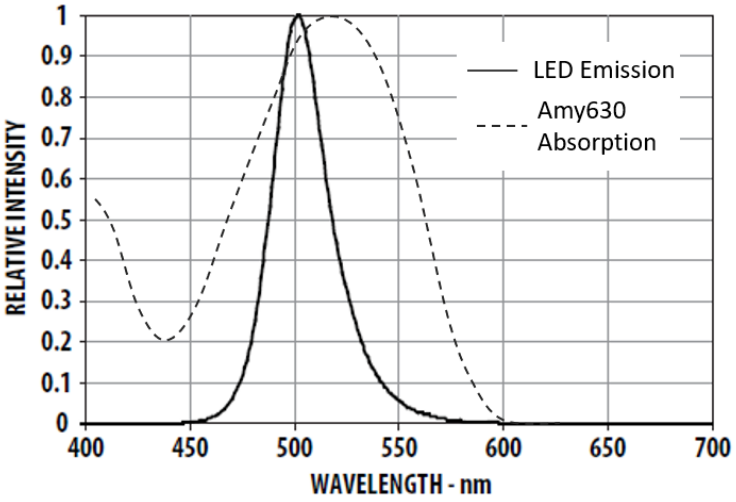

Figure 3.6: LED emission spectrum vs Amy630 absorption

Next, the radiometric characteristics of the HLMP-CE34 LED are discussed. The LED module design relies greatly on the optical power output and the spacial intensity distribution of the HLMP-CE34. The spatial intensity distribution is provided in the data sheet and is shown in Figure 3.7. This pattern shows the normalised radiant intensity of the LED with regards to the angular displacement. The angular displacement is the angle from the LED surface normal at which the light is being viewed.

From the intensity distribution, it can be seen that the LED is an imperfect Lambertian source with a viewing angle of 30°. The intensity distribution of an imperfect Lambertian source can be approximated by

$$I(\theta) = I_{(0)}\cos^{m}(\theta) \tag{3.1}$$

where, $I_{(0)}$ is the radiant intensity normal the source surface, which is also the maximum radiant intensity. The value of m depends on the viewing angle of the LED as shown in

$$m = \frac{-\ln(2)}{\ln(\cos(\theta_{(1/2)}))} \tag{3.2}$$

where the value of $\theta_{(1/2)}$ is half the viewing angle of the LED. The value of m is calculated as $m = 19.99$.

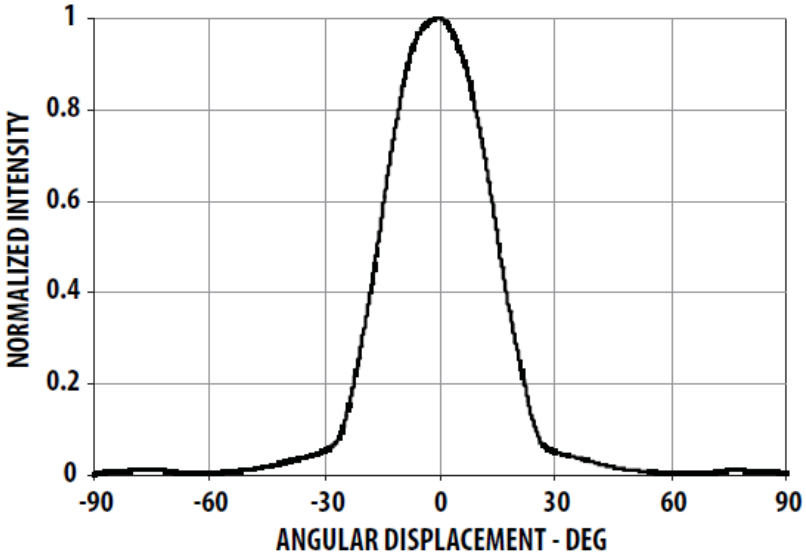

Figure 3.7: Spatial radiation pattern

The quantity of interest is the optical power incident on the sample area. This quantity is referred to as irradiance and is measured in W/m^2. The irradiance at a specific point can be calculated using

$$E(\phi) = \frac{I\cos(\phi)}{d^2} \tag{3.3}$$

where ϕ is the angle of incidence and d is the distance from the source to the irradiated surface. The angle of incidence is measured between the incident ray and the surface normal at the point of incidence. Substituting (3.1) into (3.3) yields

$$E(\phi) = \frac{I_{(0)}\cos^m(\theta)\cos(\phi)}{d^2} \tag{3.4}$$

which will be used in Section 2.1.2 to model the sample irradiance distribution. In order to calculate the value of $I_{(0)}$, the maximum luminous intensity given in Table 3.5 must be converted to radiant intensity, using the luminous efficacy. The luminous efficacy is

given in lm/W, while the maximum luminous intensity is given in candela (cd). Since one candela equals one lumen per unit solid angle, the conversion between luminous intensity and radiant intensity is calculated as shown by

$$I_e = \frac{I_v}{V}.\frac{\text{lm/sr}}{\text{lm/W}} = \frac{I_v}{V}.\frac{\text{W}}{\text{sr}} \tag{3.5}$$

where, I_e is the radiant intensity, I_v is the luminous intensity and V is the luminous efficacy. Using the maximum luminous intensity and the luminous efficacy given in Table 3.5, $I_{(0)}$ can now be calculated as

$$I_0 = \frac{21}{326} = 64.4 \text{ mW/sr}. \tag{3.6}$$

Geometric design

The geometric design of the excitation module refers to the placement and orientation of the LEDs. The design must provide efficient radiation without relying on expensive and space-consuming optics to guide and filter the excitation light. Therefore, preliminary requirements for the geometric design of the excitation module are defined as follows:

- The sample must be irradiated from above so that the excitation light is not directed towards the image sensor. In order to keep the design compact and affordable, it is necessary to do as much excitation elimination through geometric design before adding additional filtering components.
- The LED placement must maximise irradiance and irradiance uniformity over the sample area within the constraints of the design.

The optical assembly components and the imaging sensor must be placed directly above the sample with the optical axis originating at the center of the sample area. To make place for these components, the LEDs have to irradiate the sample at an angle as shown in Figure 3.8. This causes the irradiation-pattern to have rotational non-uniformity and reduces the irradiance according to the Lambert's cosine law as shown in (3.3).

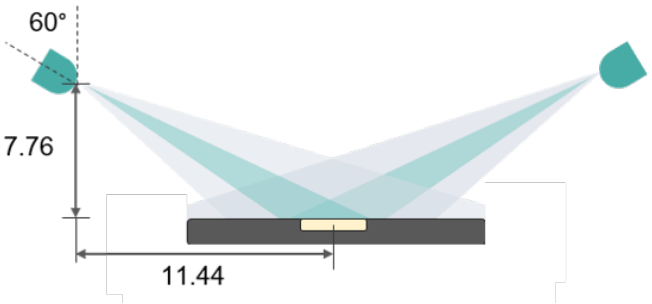

Figure 3.8: Cross section of the excitation geometry

Therefore, in the chosen design, two LEDs are placed opposite each other in order to improve the irradiance uniformity and increase the radiant power incident on the sample area. The chosen geometric design for the excitation source is shown in Figure 3.8. The LEDs are angled such that the sample area receives the portion of the light that is contained within approximately a 10 degree viewing angle.

When a surface is irradiated directly from above - when the LED surface and the irradiated surface are parallel - the viewing angle (θ) and the angle of incidence (ϕ) are the same and the irradiation pattern has rotational symmetry. This is not the case for this design where the LEDs are fixed at an angle (β) . The irradiation pattern for an angled LED has longitudinal axis symmetry as shown in Figure 3.9, but not rotational symmetry.

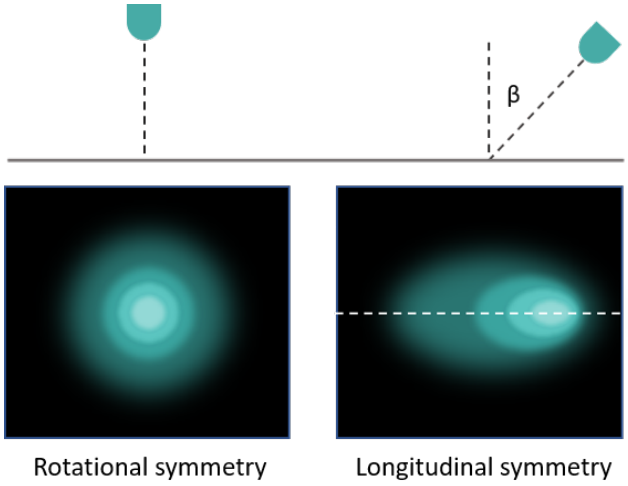

Figure 3.9: LED irradiation distributions

In order to visualise of the irradiation distribution on the symmetry axis, (3.4) is used. Figure 3.10 shows the theoretical irradiance distribution across the length of the sample area when a single LED, on the left, is switched on. Figure 3.11 shows the theoretical distribution when both LEDs are switched on.

When both LEDs are switched on, the irradiance reaches a theoretical maximum of 27.6 mW/cm^2 and a minimum of 27.3 mW/cm^2 along the symmetry axis. There is an increase in uniformity when two LEDs are used in the given configuration compared to when a single LED is used. Furthermore, the irradiance produced by the two LEDs falls within an acceptable range when compared to the most popular light sources used in fluorescence microscopy. Table 2.1 contains the irradiance levels of these light sources and is given in Section 2.3.1.

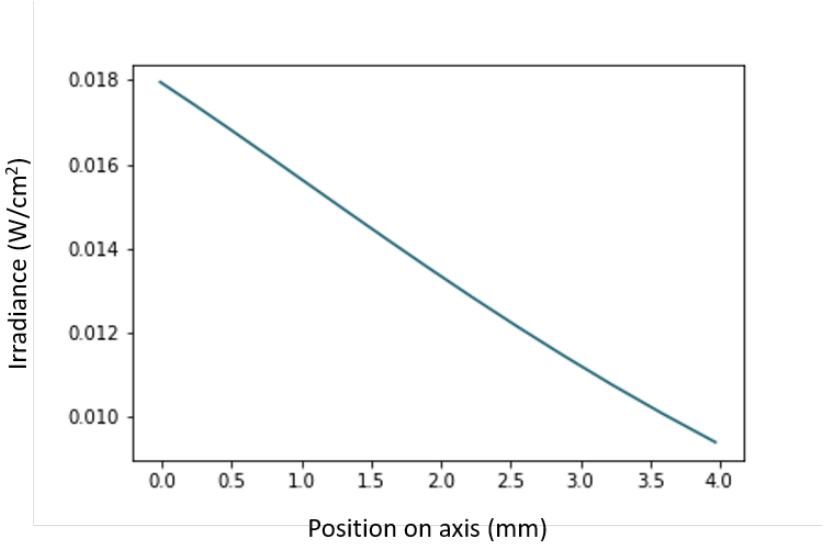

Figure 3.10: Distribution for the left side LED

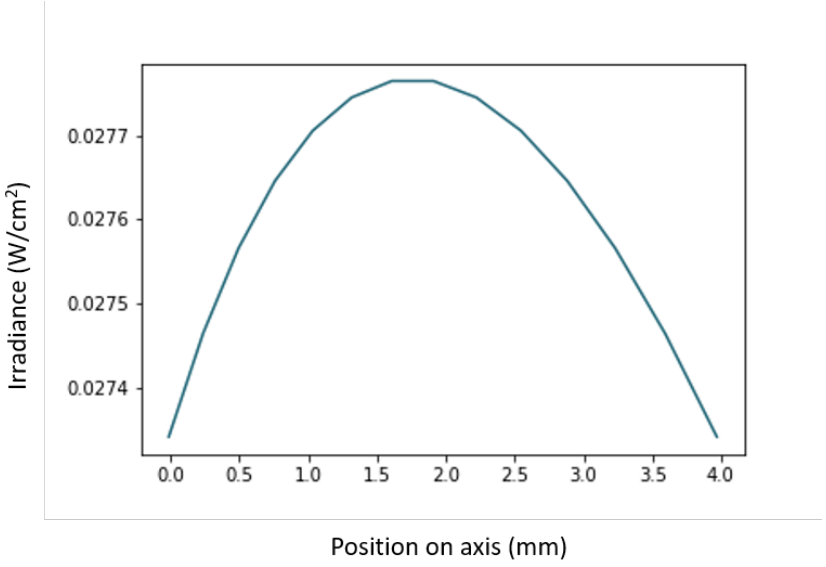

Figure 3.11: Accumulative distribution of both LEDs

LED circuitry

The LEDs are powered using a transistor switching circuit and an Arduino Nano. Although a battery would have been a sufficient power-source, the Arduino provides the ability to modulate the LED outputs, which keeps the door open for future experimentation with fluorescence lifetime-imaging.

The transistor switching circuit causes the LED to draw current from VCC instead of the Arduino output pin. Although the Arduino Nano will be able to provide enough current for two LEDs, using the switching circuit is good practice and allows for practical scaling. The transistor and resistor values were chosen such that the LED draws 20 mA, since this

is the test condition given in the data sheet. The circuit diagram for the LED circuit and the PCB design for the final excitation module is shown in Figure 3.12. The KTC9014S surface mount NPN transistor for general purpose switching applications was selected. Both the 47 Ω and 47 kΩ resistors are 1206 SMD resistors.

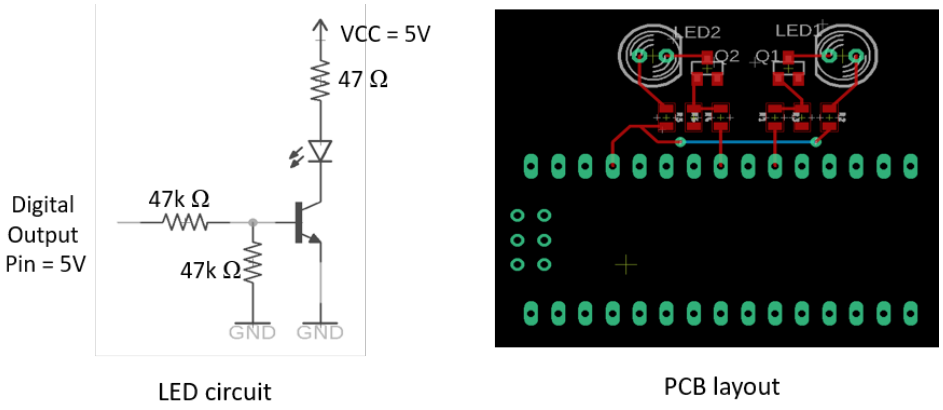

Figure 3.12: LED circuit and PCB Layout

3.3.4 Magnification and filtering

The optical assembly consists of magnification and emission filtering components. The goal of the magnification component is to relay an image of the viewing area on the camera sensor such that the image fills most of the sensor. The goal of the filtering component is to reject the excitation light, while passing the fluorescence emission from the Amy630. This section discusses the selection of these magnification and filtering components.

Magnification

When a smartphone is set to infinity-focus, the internal camera lens converges parallel light rays at the lens focal point, which is where the image sensor is positioned. A basic smartphone microscope consists of an external lens component that collects light from the viewing area and converts the diverging light to parallel light, and the internal camera lens that converges the parallel light at the image sensor. The most basic external lens that can be used to create a smartphone microscope is an aspheric lens. Figure 3.13 shows the lightpath through a smartphone microscope with a single aspheric lens.

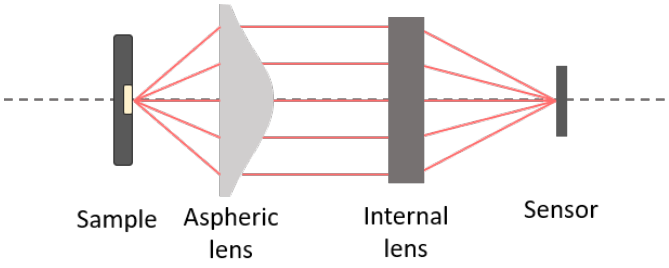

Figure 3.13: Smartphone microscope using a single aspheric lens

Although using a single aspheric lens is certainly desirable for a compact design, the fixed working distance makes it impossible to adjust the focus if need be. Being able to adjust working distance and focus is useful for prototyping. Furthermore, a single aspheric lens introduces spherical aberrations that can be reduced with a more complex design. Therefore, an affordable two-lens smartphone microscope with an adjustable working-distance and field of view was selected for this design. The microscope also has a mechanical clamp that helps to hold the smartphone in place. The clamp was incorporated in the design as shown later in Figure 3.19. The microscope is shown in Figure 3.14.

The working distance of the microscope is set to 19.5mm, which results in a 3mm diameter field of view. For these settings, the microscope creates a 1:1 magnification of the viewing area on the image sensor. A 1:1 magnification implies that the image of the viewing area spans a 3mm diameter area on the image sensor, which equates to a diameter of approximately 2600 pixels. This information is used when determining the region of interest in terms of pixel count during image processing.

Figure 3.14: Smartphone microscope

Filtering

Since the emission spectrum of the excitation source does not overlap the emission spectrum of Amy630, there is no need for an excitation filter. Therefore, this design only uses a single emission filter to pass the fluorescence emission and reject the excitation light. Since a single fluorophore is being detected, only one emission spectrum is of interest, which means there is no concern for overlapping fluorophore signals. Therefore, a long pass optical filter that passes all wavelengths above the highest excitation wavelength is adequate for this application.

For this application, a high performance, 600 nm cut-on long-pass filter from Edmund optics was selected. The filter is made from UV grade fused silica and is hard-coated to prevent scratching. It has a cut-on slope of less than 1%, a minimum optical density of

4 and 91% pass-band transmission. The filter is contained within a 3D printed holder that is mounted on the smartphone microscope as shown in Figure 3.19. A visual representation of the filter range as well as the chosen filter dimensions are given in Figure 3.15.

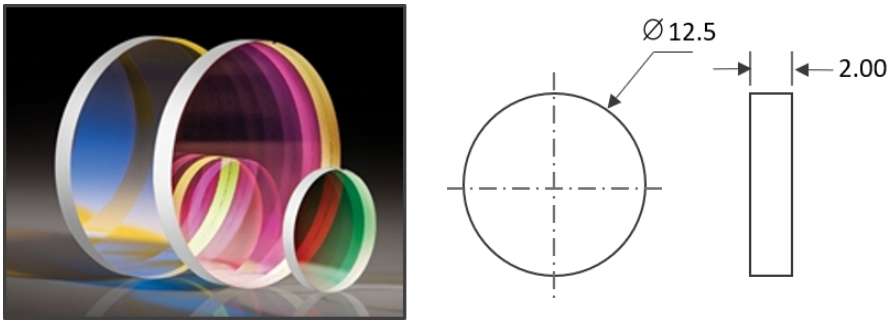

Figure 3.15: Optical filter dimensions

3.3.5 Detection

The accurate quantification of fluorescence intensity relies on the linearity of the sensor output with regards to the intensity of the incident light. As discussed in Section 2.4.2, raw image pixel values have a much better linear response to varying light intensities compared to JPEG pixel values. The resolution of the fluorescent intensity measurement is dependant on the sensor temporal noise, while the image quality at low light conditions is influenced by the fixed pattern spatial noise.

For this design, a Samsung Galaxy S6 was chosen to detect and image the fluorescence signal. The Samsung Galaxy S6 has raw-imaging capabilities and a back-illuminated CMOS image sensor that allows for better low-light performance. The image sensor used in the Galaxy S6 is the IMX240 from Sony. The sensor specs are listed in the Table 3.6.

Table 3.6: Samsung Galaxy S6 camera specifications

Sensor type	IMX240 Sony CMOS
Effective Megapixels:	16.0
Sensor size	5312 x 2988 pixels
Approximate Pixel Pitch	1.12 microns
Color Filter Type	RGB
Lens	Fixed focal length and aperture
RAW imaging capabilities	Yes

Raw images are captured using the Android Camera2Raw sample app that utilizes the Android Camera2 API. The app uses the camera's auto-focus, auto-exposure and auto-white balance controls, but does no further image processing or compression. When an image is captured, the app saves a raw DNG image with a 10-bit pixel depth, as well as a JPEG version of the image. Raw image outputs from CMOS sensors have pixel-to-pixel variability in terms of dark current, read-out noise, shot noise, pixel bias and gain. This variability leads to spatial and temporal image noise.

Fixed pattern noise (FPN) refers to the spatial variability in pixel outputs under uniform illumination conditions. FPN is fixed between images taken at the same illumination intensity and exposure-time. Under low illumination the dominant type of FPN is dark signal non-uniformity (DSNU) which is mainly a result of dark-current variations.

The fixed pattern noise and average dark signal for the Samsung Galaxy6 camera sensor was determined. Eighty dark exposures were taken and then averaged on a pixel-level to eliminate the temporal noise. The average pixel value and standard deviation of the resulting average dark image was then calculated to obtain the average dark signal and the rms fixed pattern noise. The average dark image was used as a master-dark frame and subtracted from the sample fluorescence images to correct the DSNU. Figure 3.16 shows the dark signal distribution of the master-dark frame. The rms FPN of the sensor under dark conditions is 7.21 ADU (analogue to digital units).

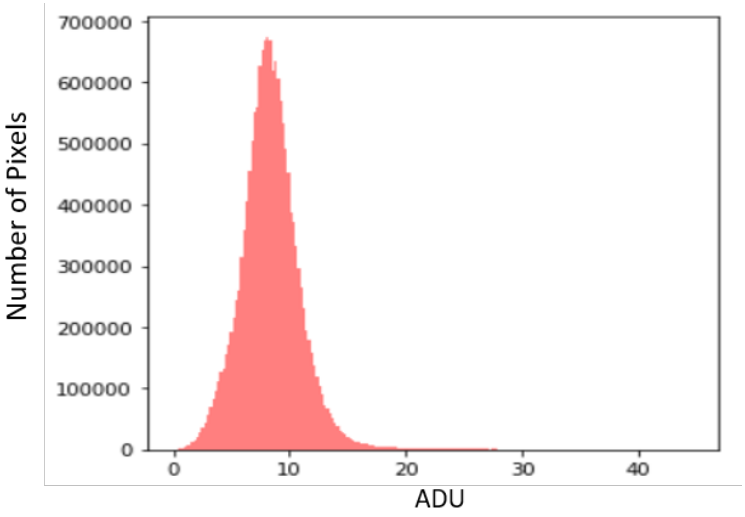

Figure 3.16: Dark-signal distribution

When the pixel values are averaged to calculate the average incident fluorescence intensity, the spatial noise is mostly averaged out. The noise that determines the measurement resolution is the variation in the pixel average between dark images - the temporal noise. Temporal sensor output variation under low light conditions is mainly due to read-out noise. The measurement resolution was approximated by calculating the standard deviation of the averaged pixel output per dark image. A standard deviation of 0.15 ADU was calculated.

3.3.6 Fluorescence intensity quantification

Once the raw image of the sample area is captured, the sample fluorescence intensity must be quantified. For the evaluation phase of the FID, multiple control and inflammatory-diseases samples have to be tested and statistical analyses have to be performed on the results. The image processing software and data organisation must allow for the automatic quantification of sample fluorescence for varying sample and sub-sample sizes, as well as varying numbers of technical repeats per sub-sample. The raw DNG images are saved according to the following naming convention:

S_SS_I.dng

where S is the sample name, comprising the population identifier and the patient number. The population identifier specifies a group of people with a specific medical condition and the patient number identifies the person from whom the blood sample was taken. SS identifies the sub-sample number, since more than one sub-sample is tested per sample. Each sub-sample is imaged multiple times to reduce the effect of image noise through averaging. I refers to the image number. Figure 3.17 shows the testing pipeline for clarity. The testing protocols are discussed further in Chapter 4.

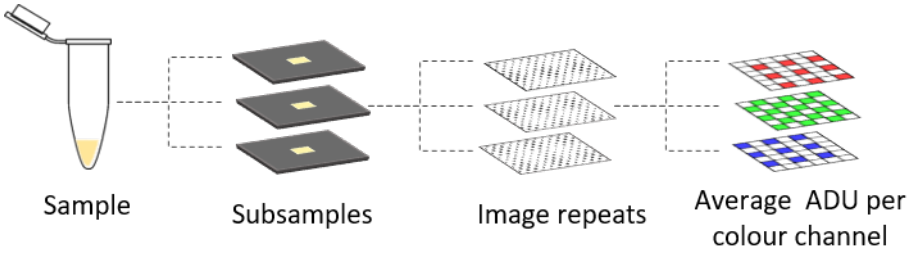

Figure 3.17: Sample testing pipeline

A Python script was developed to process the raw images and store the fluorescence measurements in a database format that allows for data analysis per image, per subsample, per sample, and per condition. The script reads the raw image files in a specified directory, converts the images to 2D numpy arrays using the rawpy library - a Python wrapper for the C++ imraw library - and then processes the images. The following processing steps are executed for each image:

- A master-dark image, created by averaging 80 dark exposures, is subtracted from the image to eliminate the dark signal.
- The image is split into its red, green and blue channels according to the sensor CFA pattern.
- The average intensity for each colour channel is calculated by averaging the pixel values within the circular region of interest. The red colour channel is the channel of interest, but the blue and green channel intensities are still calculated for reference.

The repeat images of each sub-sample are averaged to quantify the sub-sample's fluorescence intensity. The unit used to describe pixel values, ADU (analogue to digital units),

is also used here to describe the calculated fluorescence intensity. The sub-sample colour channel values, as well as the sample and disease identifiers are saved in a Python Pandas DataFrame data structure. Pandas DataFrames are two-dimensional, size mutable tabular data structures that provide a variety of data manipulation operations. An example of a Pandas DataFrame containing the sample fluorescence results is given in Figure 3.18.

disease	sample	subsample	red	green	blue
CRC	CRC1	1	27.847616	11.273099	3.257008
CRC	CRC1	2	26.775994	10.902255	3.073666
CRC	CRC1	3	27.121901	10.758581	2.930427
CRC	CRC2	1	29.627079	11.468942	3.146770
CRC	CRC2	2	28.653746	11.359596	3.191404
CRC	CRC2	3	30.630049	11.550151	3.063458

Figure 3.18: Pandas DataFrame containing sample fluorescence results

Pandas DataFrames, used in conjunction with the pingouin library, are powerful data-analysis tools. As a last processing step, descriptive statistics, analysis of variance and post hoc tests are calculated for the data. The statistic analysis results are discussed further in Chapter 4.

3.4 Prototype assembly

In order to assemble the FID prototype, multiple mounting and housing components were designed in Autodesk Inventor and 3D printed using a Makerbot Z18. The assembly was designed to be modular and easily disassembled, yet stable and sturdy. Black PLA filament was used to 3D print the components. The black filament was chosen for its ability to absorb stray light and for the fact that it does not autofluoresce. The assembly mounting and housing components, as well as their descriptions are listed in Table 3.7. Figure 3.19 shows how all the components are assembled, while Figure 3.20 show the real completed prototype.

Table 3.7: Assembly components

Main casing	The main casing holds the lighting rig, the microscope and the LED electronics. It has a slot on the side where the sample slider holding the sample holder is inserted. A sliding groove guides the sample slider so that when the sample slider is fully inserted, the sample is positioned within the field of view. The casing was designed to have an L-shape for improved stability. The foot of the casing contains the LED electronics and has a slot for the USB power cable.

Light Rig	The light rig mounts the LEDs at the correct angle. It is designed to fit perfectly into the main casing so that no adhesives or screws are necessary. This makes it easier to remove and replace components.
LED holders	The LED holders fit into the light-rig as shown in Figure 3.19. The LED holders are separate from the light rig so that different sizes LEDs can be used interchangeably.
Filter holder	The filter holder is designed so that it can be adhered to the bottom of the microscope using an easily removable adhesive polymer.
Smartphone mount	The smartphone mount fits onto the main casing. It has a platform on which the smartphone rests and that positions the smartphone while it is being held in place by the microscope clip.

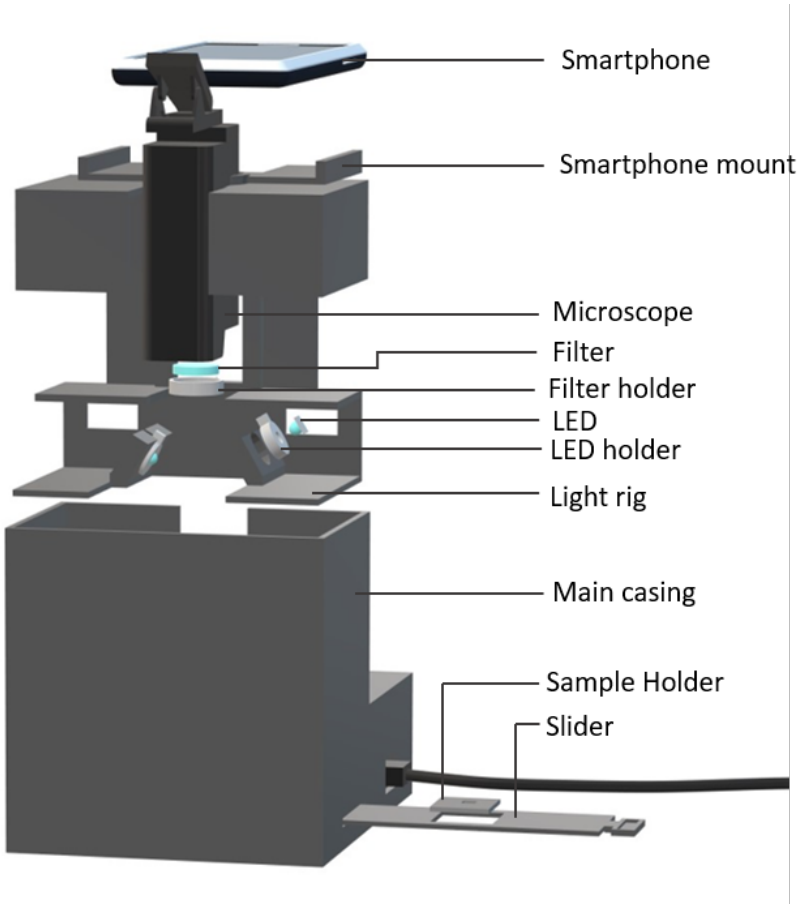

Figure 3.19: FID Assembly

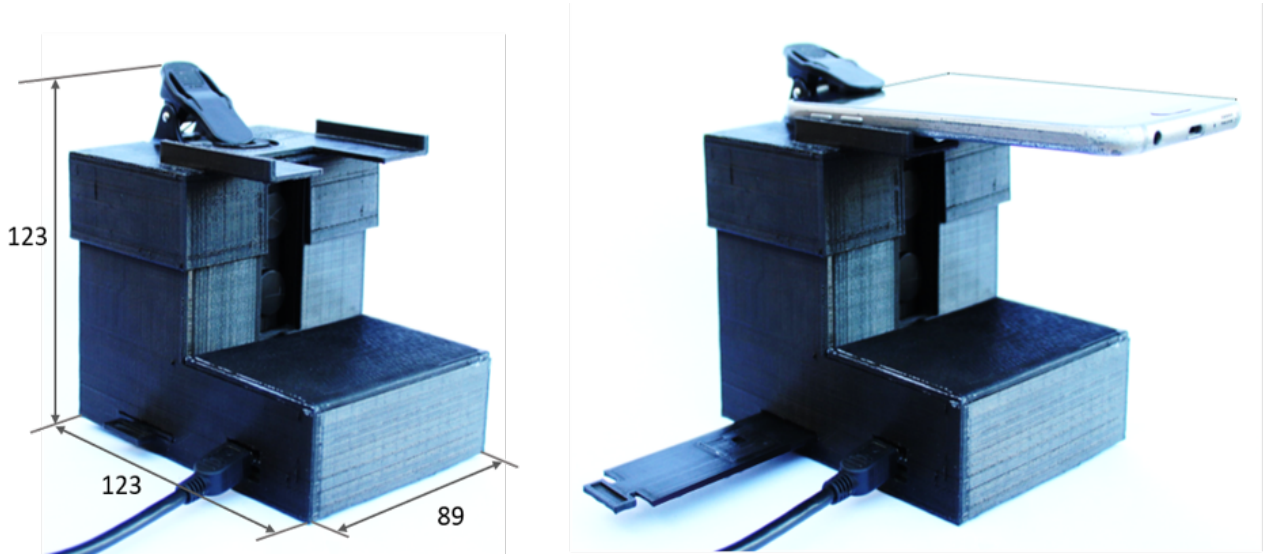

Figure 3.20: Final prototype

The final prototype is compact, light-weight and modular as required in the project objectives. The prototype, excluding the smartphone, weighs approximately 250g and has the dimensions shown Figure 3.20. Table 3.8 gives the bill of materials for the FID prototype and Table 3.9 gives the cost per sub-sample. Sub-sample refers to a single sample holder containing an aliquot of the sample under test.

In comparison to typical fluorescence intensity sensing and imaging equipment, the FID prototype is affordable in terms of the cost to manufacture, as well as the cost to use. The cost of the smartphone is excluded from the bill of materials, since the design can be used with a variety of smartphone models - from high quality mid-range to high-end. Most individuals or institutions already own smartphones that can be used with the FID prototype. Further work will focus on the standardisation of smartphone requirements and system calibration for various smartphone models.

Table 3.8: Bill of materials

Part Name	Units	Unit Cost (R)	Total Cost (R)
Optical Filter	1	2330	2330
Microscope	1	150	150
LED	2	8.50	17
Arduino Nano	1	150	150
Resistor	6	0.30	1.80
Transistor	2	0.60	1.20
3D-printing	150g	1/g	150
TOTAL			**2800**

Table 3.9: Cost per sub-sample

Part Name	**Units**	**Unit Cost (R)**	**Total Cost (R)**
Amy630	0.05μl	150/μl	8.50
Sample Holder	0.4g	1/g	0.40
TOTAL			**8.90**

Chapter 4

Evaluation of the FID Prototype

In order to set the context for this chapter, the project objectives pertaining to the evaluation of the FID are revisited. As specified in Chapter 1, the objectives of this project include to:

- investigate the relationship between the measured fluorescence signal and the inflammatory status of the patient.
- evaluate the device's effectiveness as a tool to discriminate between the PPP of healthy individuals and individuals with inflammatory NCDs.
- report on possible improvements and recommendations for future development.

During the evaluation phase, three main investigations were conducted in order to meet the project objectives. Each of these investigations is discussed separately in this chapter. The aim of these investigations, respectively, is to:

1. identify potential light sources that may cause background noise and evaluate the FID design's effectiveness in minimising such background noise.
2. use the FID to detect the fluorescent signal emitted by bound Amy630 in PPP from control individuals and individuals with inflammatory conditions. Evaluate the relationship between the measured fluorescence signal and the inflammatory status of the patient and determine whether the device can differentiate between healthy and diseased individuals.
3. determine whether the detected fluorescence originates exclusively from Amy630 bound to amyloid structures.

The evaluation of the FID prototype was conducted in a histology lab at Stellenbosch Department of Physiological Sciences. Ethical clearance was obtained for this project from the Health Research Ethics Committee (HREC) of Stellenbosch University and a written form of informed consent was obtained from all blood donors. The ethical clearance documentation is given in Appendix A.

4.1 The elimination of background light

The specificity and sensitivity of the FID depends on its ability to eliminate noise from background light sources and to isolate the Amy630 fluorescence signal. Potential sources of background light and the design choices aimed at minimising these sources are given in Table 4.1. In this section the effectiveness of the measures taken to minimise noise due to background light is evaluated.

Table 4.1: Background light sources and the minimisation thereof

Excitation Light	The chosen fluorescent marker has a large Stokes shift and the selected excitation source has a narrow bandwidth. Therefore, the excitation spectrum does not overlap the Amy630 emission spectrum, and a single high-performance longpass optical filter is used to reject the excitation light.
PPP autofluorescence	The fluorescent marker emission, excitation source, and filtering components were specifically chosen to operate outside the absorption and emission spectrum of PPP autofluorescence.
Unbound fluorescence	The manufacturers of Amy680 claim that the fluorescent marker has no unbound fluorescence.

First, the long-pass filter's ability to reject the excitation light is evaluated. An empty sample holder was placed in the FID and the light intensity was measured with and without the optical filter. Figure 4.1 shows the comparison. The measured average light intensity when the filter is removed was approximately 313 ADU. The vertical sections in the image is the sample holder's 3D-printed grooves. When the filter is added to the optical train, the measured intensity drops to the sensor's dark-signal value. From the images and numeric intensity measurements, it is clear that the filter does effectively minimise the amount of excitation light that reaches the sensor.

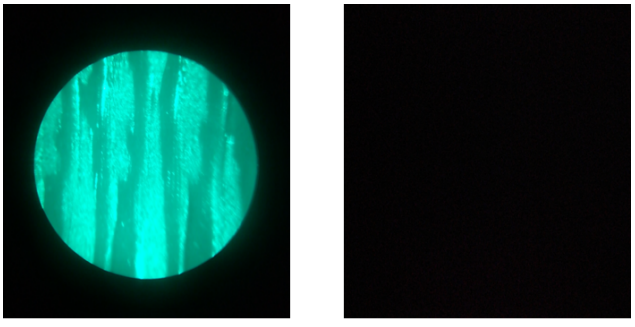

Figure 4.1: Empty sample holder imaged with and without filter

The next part evaluates whether the chosen excitation and detection spectra truly do eliminate the effect of PPP autofluorescence. In order to create a reference, the setup was temporarily modified so that the excitation and detection spectra fall within the absorption and emission spectra of PPP. The LEDs and long-pass filter were temporarily replaced with counterparts that have the same specifications except for the LED emission spectra and the longpass filter cut-on frequency. The 501 nm LEDs and 600 nm long-pass filter from the original FID design were temporarily replaced with 405 nm LEDs and a 450 nm long-pass filter.

The same 20 μl unstained PPP from a control individual was tested with both the original and temporary excitation and filter setups. Figure 4.2 shows a comparison between the fluorescence detected by the two. The image on the left illustrates how important it is to operate outside the absorption and emission spectra of PPP. The PPP autofluorescence is very prominent when a 405 nm excitation source and 450 nm cut-on LP filter is used. Other amyloid-staining fluorescent tags like the Amy680, Amy520 and ThT would have been very difficult to detect amongst the autofluorescent background noise. The image on the right shows that the official FID design does indeed minimise the influence of PPP autofluorescence. The measured intensity is, once again, approximately equal to the sensor dark-signal.

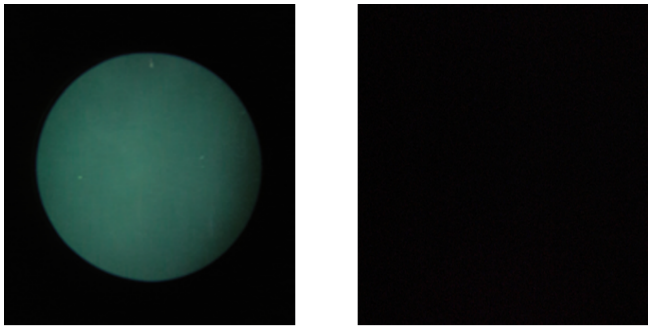

Figure 4.2: PPP autofluorescence for 405 nm and 501 nm excitation

Lastly, the unbound fluorescence of the Amy630 was evaluated. Some fluorophores do fluoresce when they are unbound, albeit to a lesser degree than when they are bound. This is a potential source of background noise. Therefore, a sample of an unbound Amy630 dilution was tested with the FID to confirm whether Amy630 truly has no unbound fluorescence.

First an Amy630 working solution was prepared by diluting 4 μl Amy360 stock solution with 76 μl PBS. An Amy630 dilution was then prepared by adding 6 μl Amy630 working solution in 89 μl PBS. The concentration of Amy630 in PBS was made the same as the concentration of Amy630 in the stained PPP samples as discussed in Section 4.2. Finally, 20 μl of the unbound Amy630 dilution was tested using the FID. No fluorescent signal was detected, which confirmed that unbound Amy630 has no unbound fluorescence under the FID's excitation and filtering conditions.

4.2 PPP sample tests

In this section the FID is used to detect the fluorescence signal emitted by bound Amy630 in PPP from control individuals and individuals with inflammatory conditions. The results are evaluated to determine whether there is a significant difference between the signal detected from these two test groups and whether the FID has the potential to differentiate between healthy and inflamed individuals. This investigation was limited by the following factors:

- The limited availability of blood and patient data
- Variance in the severity of patient inflammatory status within diseased groups.
- The uncertain effect of plasma molecules in the Amy630 binding process.

Firstly, the procurement and preparation of the PPP is discussed. Secondly, the protocol for the sample preparation and testing is discussed. Lastly, the measured results are presented and evaluated.

4.2.1 PPP procurement and preparation

Platelet poor plasma from six patients with colorectal cancer (CRC) and three individuals with psoriasis (PSO) were obtained. Both these conditions are associated with elevated systemic inflammation. These samples had been collected by Pretorius *et* al. for various ongoing studies on fibrin(ogen) amyloidogenesis. The following patient information was obtained for reference:

- TEG results
- CRP levels
- Other chronic conditions
- Chronic medication
- Cancer stage for CRC patients
- Psoriasis severity for PSO patients

Platelet poor plasma from six healthy individuals were used as controls. Whole blood from each control individual was collected in citrate tubes by a registered phlebotomist. Each citrate tube was centrifuged at 3000 g for 15 min to separate the platelet poor plasma. Aliquots of the PPP were prepared and stored at -80 degrees for future analysis. TEG and CRP tests were performed on the control blood to verify that the individuals were, in fact, suitable controls.

The control samples were labeled C1 to C6, the colorectal cancer samples were labeled CRC1 to CRC6, and the psoriasis samples were labeled PSO1 to PSO3.

4.2.2 Protocol

The PPP sample tests were performed according to the steps listed below. Research-grade measuring pipettes were used to dispense the various quantities described in the protocol.

1. First, the Amy630 working solution was prepared by diluting 4 μl Amy630 stock solution in 76 μl PBS. The Amy630 stock solution contains 1mg fluorescent conjugated oligothophene molecules per ml.

2. Amy630-stained PPP samples were prepared by adding 6 μl of the Amy630 working solution to 89 μl PPP from each CRC, PSO and control individual.

3. From each PPP-Amy630 sample, three sub-samples of 20 μl each were placed in three separate sample holders. Each sample holder was inserted into the device where the sample was excited and the sample emission light was imaged three times.

4. The images were then processed as discussed in Section 3.3.6. The fluorescence intensity of each sub-sample was quantified by calculating the red channel measurement of the triplicate images. The fluorescence intensity for each sample was then obtained by averaging the red channel measurements of the three sub-samples.

4.2.3 Results and discussion

The PPP from the six control, six CRC and three PSO individuals were analysed according to the protocol described previously. While it has previously been shown that the unstained PPP produced no fluorescence, the PPP samples with added Amy630 did. This indicates that the Amy630 molecules bind to molecular structures in the PPP and undergo conformational changes that enable them to fluoresce. Figure 4.3 shows the fluorescence detected for C3 and CRC3 as a visual example.

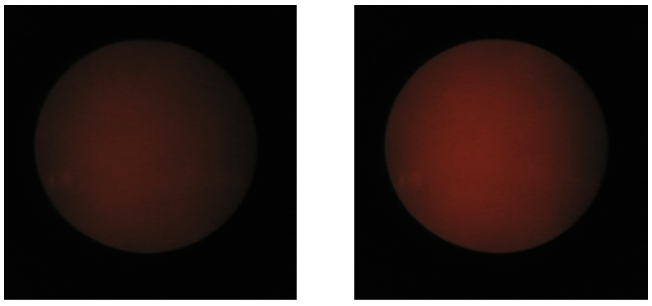

Figure 4.3: Fluorescence detected for C3 and CRC3 samples

The fluorescence measurement for each sample is plotted in Figure 4.4. Since these measurements are the average of three sub-sample measurements, error bars were added to illustrate the standard deviation within each averaged sample measurement. The bar graph shows that the fluorescence measurements of the CRC and PSO samples were, on average, higher than that of the control samples. The average fluorescence measurements

for the C, CRC and PSO groups were 22.80 ADU, 28.67 ADU and 26.3 ADU respectively.

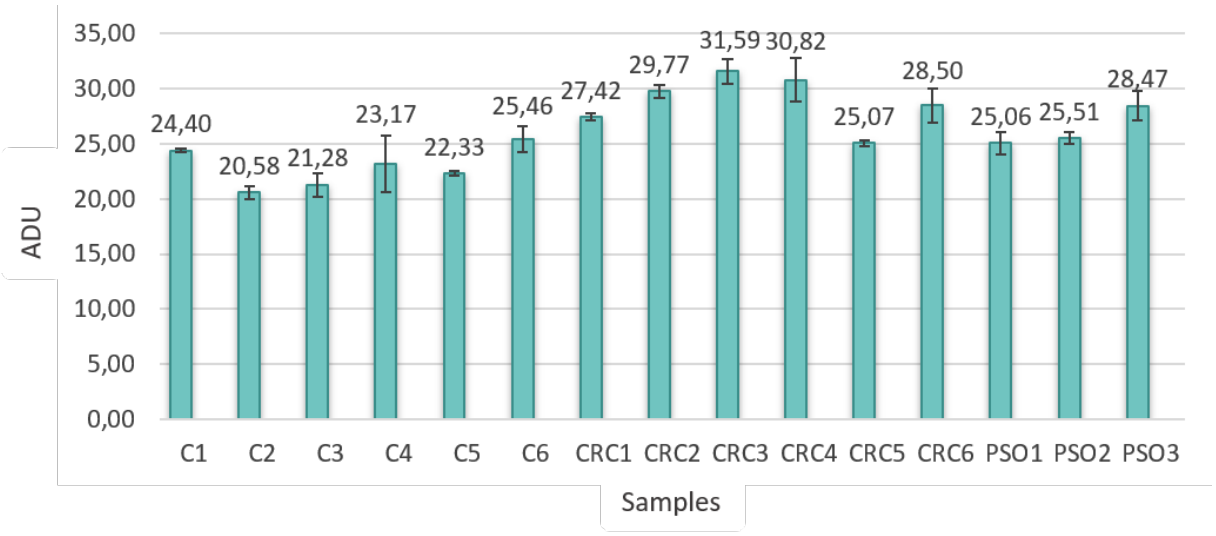

Figure 4.4: Average fluorescence intensity per sample

An Analysis of variance (ANOVA) was conducted to determine whether the variance between the C, CRC and PSO groups is smaller than the variances within the groups and whether the differences between the group means are statistically significant. A significance level of 0.05 was chosen and a Welch ANOVA was used, since it accounts for unequal variances and sample sizes. A p-value of $0.01 < 0.05$ was calculated, which indicates that at least one of of the group means differ significantly. A pairwise Games-Howell post hoc test was conducted to determine which means differ significantly. Table 4.2 lists the calculated p-values.

Table 4.2: Pairwise Games-Howell post hoc test p-values

A	B	p-value
C	CRC	0.001
C	PSO	0.03
CRC	PSO	0.25

The p-values show that there is a significant difference between the control and CRC group means, and also between the control and PSO group means. There is, however, no significant difference between the CRC and PSO group means, which is expected since they both fall under the diseased population.

Although these results are promising, one must keep in mind that the sample sizes are small due to limited PPP supplies. A more extensive study with larger sample sizes must be conducted for more reliable results. Furthermore, the following concerns have to be addressed:

1. The variation in sample measurements within each of the three groups, as well as the variation in sub-sample measurements for a specific sample.

2. The unexpectedly high amount of fluorescence in control samples.

Group and sub-sample variation

It is to be expected that the measurements for individuals within a population will differ, since there are many factors that influence a person's blood profile. These factors include genetics, age, lifestyle, medication, etc.

Within a population of colorectal cancer patients, the individuals' inflammatory profiles vary according to the cancer stage, the patients' response to treatment and other complex factors. The inflammatory profile of blood taken from psoriasis patients depend on the disease severity, disease activity, whether the patient is experiencing an inflammatory flare at the time when the blood is drawn and whether the patient is taking any anti-rheumatic medication. Furthermore, patients form a specific diseased population may also have other types of medical conditions, which complicate their inflammatory profiles even further.

The variation in sub-sample measurements for a specific sample can possibly be ascribed to the following factors:

- The bound Amy630 may be non-uniformly distributed throughout the sample volume.

- The Amy630 might be interacting with other plasma molecules. The conformational changes that the Amy360 molecules undergo when they bind might be inconsistent throughout the sample.

- Variability in sample meniscus shape may cause variability in emission light refraction.

Control fluorescence

Although the control fluorescence measurements were lower than the CRC and PSO measurements, the control fluorescence measurements were much higher than expected. The project objectives and device design was based on the assumptions that Amy630 is amyloid-specific and that the formation of amyloid firbin(ogen) clots is an indication of an inflammatory condition.

According to the results reported by Pretorius *et al.* [8][14][28], the presence of amyloid fibrin(ogen) clots in the PPP of healthy individuals is virtually non-existent compared to PPP from individuals with inflammatory conditions. The fact that control measurement were only marginally less than that of the CRC and PSO samples, raises the following questions:

- Does Amy630 truly only bind to amyloid structures?

- If not, what type of alternative binding or conformational change is taking place?

- Can the fluorescence detected from this alternative binding still be related to a person's inflammatory profile?

In an attempt to gain more insight into the structural binding of the Amy630, the sub-samples were allowed to evaporate so that the settled particles could be observed on a single focal plane. Figure 4.5 shows the fluorescence images of three CRC and three control samples. The vertical lines may be a result of particles settling in and the light reflecting off the grooves created by the 3D-printing process.

There is a significant difference between the CRC and control images. Although the control images show less fluorescence than the CRC images, the fluorescence is still too uniformly distributed to conclude that it exclusively originates from the anomalous and sporadic amyloid fibrin(ogen) clots described by Pretorius *et al.* [8][14][28]. In order to gain further insight into the amyloid-specificity of the detected signal, the interaction between Amy630 and pure fibrinogen was conducted. This investigation is discussed next.

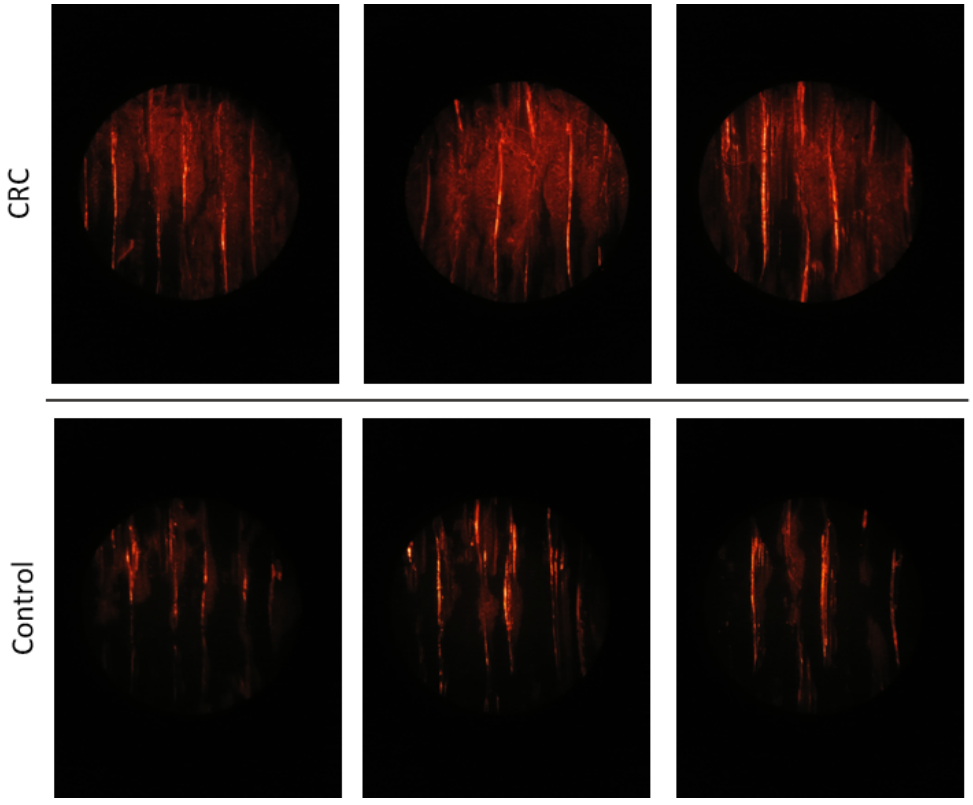

Figure 4.5: Fluorescence images of evaporated CRC and control samples

4.3 Amyloid-specificity of Amy630

The goal of this investigation was to draw more informed conclusions about the amyloid-specificity of Amy630 by observing and comparing its interaction with normal and amyloid fibrinogen without the presence of other plasma molecules. The investigation was conducted in an attempt to answer the following questions:

1. Does Amy630 fluoresce in the presence of normal fibrinogen?
2. Is there a significant difference between the normal and amyloid fibrinogen sample fluorescence when Amy630 is added?
3. What is the relationship between the sample fluorescence intensity and the Amy630 concentration?
4. How do the results relate to the PPP results of the previous section?

In order to conduct this investigation, increasing volumes of Amy630 working solution was added to samples of reconstituted normal fibrinogen as well as LTA-exposed fibrinogen, which were then tested using the FID. The aim of the LTA-exposure is to induce amyloid formation in the fibrinogen molecules. According to Pretorius *et al.*, substoichiometric concentrations of LTA causes anomalous amyloid fibrin clots [28]. The sample preparation and testing protocol as well as the results are discussed next.

4.3.1 Protocol

The following steps were executed for this investigation:

1. Reconstituted fibrinogen was sampled from a 2 mg/ml stock solution. The stock solution had previously been prepared by reconstituting dehydrated fibrinogen with phosphate-buffered saline.
2. An LTA-exposed fibrinogen sample was prepared by adding 10 μl LTA to 90 μl of the 2 mg/ml fibrinogen stock solution. The exposed fibrinogen was allowed to incubate for 30 min.
3. The Amy630 working solution was prepared by diluting 4 μl Amy630 stock solution in 76 μl PBS.
4. Exposed and normal fibrinogen samples with increasing concentrations of Amy630 working solution were prepared. For both the exposed and normal fibrinogen, four samples of 49 ul were stained with 1 μl, 3 μl, 9 μl and 27 μl Amy630 respectively.
5. Thereafter, the same testing procedures used to analyse the PPP samples were followed. Three sub-samples for each of the four LTA-exposed fibrinogen samples, and each of the four normal fibrinogen samples were tested.

4.3.2 Results and discussion

Figure 4.6 shows the fluorescent measurements of both the normal and LTA-exposed fibrinogen for the increasing concentrations of Amy630. Figure 4.7 shows images of normal fibrinogen with increasing concentrations of Amy630.

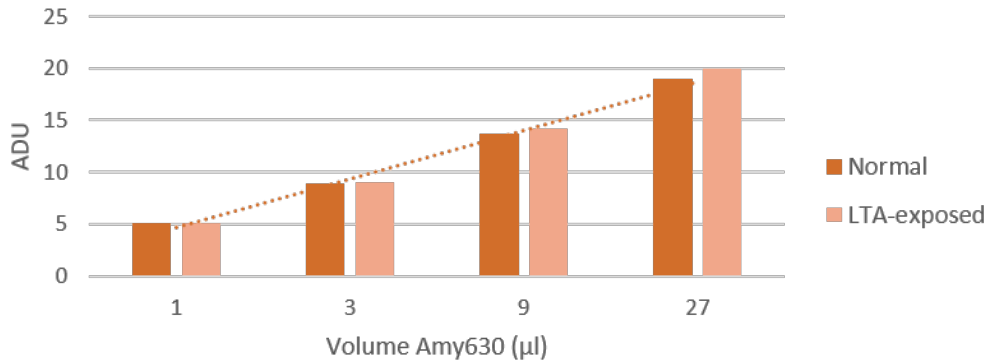

Figure 4.6: Fluorescence measurements of normal and LTA-exposed fibrinogen for increasing Amy630 concentrations

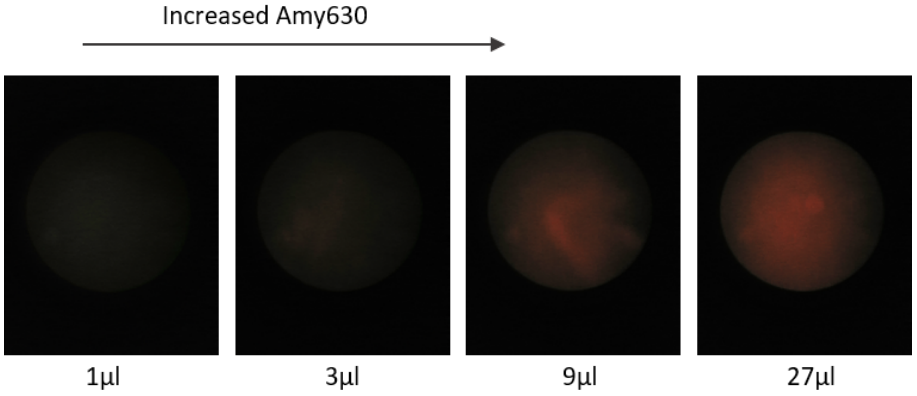

Figure 4.7: Normal fibrinogen with increasing Amy630 concentrations

Firstly, it is clear that the normal fibrinogen with added Amy630 does emit fluorescence. This means that the conformational changes that the Amy630 molecules undergo in order to fluoresce are not exclusively due to amyloid-binding. There is also no significant difference between the normal and LTA-exposed fibrinogen. This could be due to the fact that any change in fluorescence due to amyloid-bound Amy630 is inundated by the background fluorescence.

Furthermore, the fluorescence produced by the fibrinogen sample is still significantly less than that of PPP samples with the same Amy630 concentration. A fibrinogen concentration of 2 mg/ml falls within the range for a healthy individual, and therefore the fibrinogen fluorescence results are comparable to the control PPP fluorescence results. The average measurement for the control samples was 22.87 ADU, while the average measurement for normal fibrinogen samples with the same Amy630 concentration was 8.87 ADU. Therefore, it can be argued that the binding mechanism and emission of Amy630 is influenced by the presence of other plasma molecules as well.

The graph shows that an exponential increase of Amy630 leads to linear increase in the fluorescence measurement. Since the binding sites should become less as the Amy360

increases it would be expected for the fluorescence to plateau. This raises the question whether the increasing fluorescence is due to increased binding, or due to another type of interaction.

This question led to the conduction of further research on the matter. Through the research it was discovered that, while most fluorophores experience aggregation induced quenching, some organic fluorophores experience aggregation-induced emission. Aggregation-induced emission is a phenomenon where the fluorescent efficiency of a fluorophore increases when the molecules aggregate [83] [84].

The manufacturers of the Amytracker630, Ebba Tech, where contacted directly to confirm whether aggregation-induced emission could occur. The manufacturers said that, while they have no experience when it comes to blood and plasma (only tissue), they suspect that it is possible that the emission could be increased through aggregation. The linearisation of the molecule when it binds to amyloid structures induces the fluorescence. The same linearisation might occur when the molecules aggregate.

If this is the case, the question remains why the Amy630 molecules aggregate when they are added to PPP and not when they are diluted in PBS. This suggests that there is an interaction between the plasma molecules and the Amy630 molecules. It could be argued that an increase in certain plasma molecules, such as fibrinogen, causes an increase in Amy630 interaction, aggregation and emission. And since the upregulation of certain plasma molecules, like fibrinogen, are indicative of inflammation, the inflammatory disease samples would therefore be expected to emit more fluorescence. This could explain why the CRC and PSO samples had higher fluorescence intensity measurements on average than the control samples.

This theory does not exclude the effect of Amy630 bound to amyloid fibrin(ogen), since any amyloid-bound Amy630 fluorescence would just have added to the overall fluorescence. The contribution of amyloid-bound Amy630 fluorescence to the total fluorescence intensity could not be determined, since the signal would have been indistinguishable from the rest of the fluorescence.

The theories presented in this section can only truly be tested and proven by doing extensive nuclear magnetic resonance (NMR) and affinity studies. This is outside the scope of this project.

Chapter 5

Conclusions and Recommendations

5.1 Conclusions

Following the objectives, a prototype was developed that aims to detect the presence of the novel inflammation marker, amyloid fibrin(ogen), in human platelet poor plasma by implementing an in vitro, fluorescence-based assay. The final prototype is capable of detecting the fluorescence intensity emitted by samples of platelet poor plasma (PPP) to which the amyloid-staining fluorescent marker, Amy630, has been added. The final prototype has been shown to successfully:

- excite bound Amytracker630 molecules in 2 0μl platelet poor plasma samples, using two high intensity 501 nm LEDs.
- filter out the excitation light with a 600 nm cut-on high-pass filter.
- magnify the sample area and relay an image of the sample light to the camera sensor of a Samsung Galaxy S6 that is mounted on the device.
- capture raw images of the detected light using the Samsung Galaxy S6 smartphone camera and a raw camera app that uses the Android Camera2 API.
- quantify the captured sample fluorescence intensity with a Python image processing script.

The project objectives state that the device should be low-cost, compact, modular and low-power, and suitable for use in mobile and rural clinic setups. The final prototype only weighs 250 g and occupies a 123 mm×123 mm×89 mm space. In order to meet the aforementioned objectives the following design decisions were made:

- The selected fluorescent marker has a large Stokes shift as well as absorption and emissions spectra that are distinguishable from PPP autofluorescence. This eliminates the need for multiple expensive and space-consuming optical filtering components.
- LEDs are used for the excitation source. They are compact, affordable and low-power in comparison to other traditional excitation sources. The excitation is USB powered, but can easily be battery-powered as well.
- The LEDs, optical filter and microscope are easily replaceable due to modular mounting components.

- The design is smartphone-based. Smartphones are widely used, compact and technologically versatile in relation to cost. They are becoming popular tools for mobile scientific applications.

The project objectives also require that the relationship between the measured fluorescence signal and the inflammatory status of the patient should be evaluated. Furthermore, the effectiveness of the device should be evaluated in terms of it's ability to discriminate between the PPP of healthy individuals and individuals with inflammatory NCDs.

In order to reach these objectives, the prototype was used to test the PPP of six control, six colorectal cancer (CRC) and three psoriasis (PSO) patients. The fluorescence intensity measurements of the CRC and PSO sample were, on average, higher than that of the control samples. An analysis of variance showed a significant difference between the control and CRC group means, and also between the control and PSO group means. The evaluation was, however limited by the number of available PPP samples. For more accurate results, a larger sample size is required.

Even though the results are promising, the control samples had more bound Amy630 than expected and the difference between the control and inflammatory group means were not as large as expected. During the evaluation, the presence of background noise due the excitation source, unbound Amy630 fluorescence and PPP autofluroescence was ruled out. Therefore, the excessive control sample fluorescence brought the amyloid-specificity of the detected signal into question. It was hypothesised that the Amy630 molecules interact with other plasma molecules, such as fibrinogen, and undergo conformational changes that cause them to fluoresce. To test this hypothesis, increasing concentrations of Amy630 was added to samples of reconstituted normal fibrinogen and LTA-exposed fibrinogen. The LTA-exposure induces amyloid-formation. The following observations and corresponding conclusions were made during this investigation:

- Amy630 does fluoresce in the presence of normal fibrinogen. Therefore, the detected fluorescence signal does not exclusively originate form Amy630 bound to amyloid fibrin(ogen) structures.
- The fibrinogen concentration in the samples was comparable to that in healthy PPP, yet the fluorescence was still significantly less than the fluorescence emitted by the control PPP samples containing the same concentration of Amy630. Therefore, it was concluded that Amy630 not only interacts with fibrinogen, but with other plasma molecules as well.
- The fluorescence intensity emitted by the normal fibrinogen samples increased linearly with a exponential increase in added Amy630. Although the mechanism of interaction is unknown, it is suggested that the emission is most likely aggregation-induced. If the emission was due to binding between the Amy630 and plasma molecules, one would expect to see a plateau in fluorescence intensity as the Amy630 concentration is increased, due to the decrease in available binding sites.
- The difference between the normal and LTA-exposed sample fluorescence was insignificant. Although some of the detected fluorescence may still be a results of the binding between Amy630 and amyloid fibrin(ogen), this fluorescence could not be

extracted from the background noise and its contribution to the total fluorescence could not be determined.

- If it is the case that an interaction between the Amy630 and plasma molecules causes Amy630 aggregation and aggregation-induced fluorescence, an upregulation in certain plasma-molecules may result in increased fluorescence intensity. Since the upregulation of certain plasma molecules, like fibrinogen, are indicative of inflammation, it makes sense that the inflammatory disease samples produced more fluorescence than the control samples.

The project objectives have all been met. However, due to the novelty of the physiological research on which the project is based, as well as the multidisciplinary nature of the work that had to be done, there is much opportunity for further work and improvement. Recommendations for further work are discussed next.

5.2 Recommendations

Although the FID is able to detect and quantify the emission from fluorescing Amy630 molecules as required, the unexpected binding and fluorescence behaviour of the Amy630 molecules has brought the significance of the detected signal into question. In order to gain more insight into the significance of the detected signal, further tests with larger sample sizes have to be performed. Therefore, more control and inflammatory blood must be sourced and a well-structured database containing patient information and standardised test results pertaining to their inflammatory profile must be created.

The interaction between Amy630 and plasma molecules is uncertain. In further work, one could either attempt to characterize this interaction by doing affinity studies and using advanced techniques such as nuclear magnetic resonance, or one could explore alternative amyloid-specific fluorescence markers.

Since the FID is a rough prototype, there is much room for improvement and optimisation in terms of the structural and optical design. The following suggestions are made:

- The smartphone microscope can be replaced with a more custom optical design that reduces aberration and has better transmittance.
- The geometric tolerances for accurate optical systems are typically very small. Therefore, it is important to use high resolution 3D printing for prototyping. The MakerBot used to print the FID parts is an expensive 3D printer, but leaves much to be desired in terms of printing quality.
- Alternative methods of sample containment that do not cause sample meniscus variability can be explored.

Although the FID successfully measures and quantifies fluorescence intensity, additional image processing strategies should be explored. Recommendations for further work in terms of the FID software include:

- Although the unprocessed nature of RAW images is desirable, the large file sizes result in less than desirable processing times. Image processing methods that reduce file-size, while maintaining the relevant data-integrity must be explored.

- The use of machine learning techniques to analyse sample images and make diagnostic predictions based on structural and spectral information can be investigated.
- A user-interface that presents the test results as diagnostic information could be developed.

Appendices

Appendix A

Ethical Clearance

UNIVERSITEIT
STELLENBOSCH
UNIVERSITY

Approval Notice

New Application

25/04/2019

Project ID :9521

HREC Reference # N19/03/043

Title: Circulating inflammatory biomarkers and dysregulated coagulation in inflammatory conditions.

Dear Prof Etheresia Pretorius,

The **New Application** received on 15/04/2019 15:27 was reviewed by members of **Health Research Ethics Committee** via **expedited** review procedures on 25/04/2019 and was approved.

Please note the following information about your approved research protocol:

Protocol Approval Period: 25 April 2019 to 24 April 2020.

Please remember to use your project ID (9521)on any documents or correspondence with the HREC concerning your research protocol.

Please note that the HREC has the prerogative and authority to ask further questions, seek additional information, require further modifications, or monitor the conduct of your research and the consent process.

After Ethical Review

Translation of the informed consent document(s) to the language(s) applicable to your study participants should now be submitted to the HREC.

Please note you can submit your progress report through the online ethics application process, available at: Links Application Form Direct Link and the application should be submitted to the HREC before the year has expired. Please see *Forms and Instructions* on our HREC website (www.sun.ac.za/healthresearchethics) for guidance on how to submit a progress report.

The HREC will then consider the continuation of the project for a further year (if necessary). Annually a number of projects may be selected randomly for an external audit.

Provincial and City of Cape Town Approval

Please note that for research at a primary or secondary healthcare facility, permission must still be obtained from the relevant authorities (Western Cape Departement of Health and/or City Health) to conduct the research as stated in the protocol. Please consult the Western Cape Government website for access to the online Health Research Approval Process, see: https://www.westerncape.gov.za/general-publication/health-research-approval-process. Research that will be conducted at any tertiary academic institution requires approval from the relevant hospital manager. Ethics approval is required BEFORE approval can be obtained from these health authorities.

We wish you the best as you conduct your research.

For standard HREC forms and instructions, please visit: Forms and Instructions on our HREC website https://applyethics.sun.ac.za/ProjectView/Index/9521

If you have any questions or need further assistance, please contact the HREC office at 021 938 9677.

Yours sincerely,

Mrs. Melody Shana ,

Coordinator

HREC1.

National Health Research Ethics Council (NHREC) Registration Number:

REC-130408-012 (HREC1)•REC-230208-010 (HREC2)

Bibliography

[1] R. S. Gottfried, *Black death*. Simon and Schuster, 2010.

[2] D. Jordan, "The deadliest flu: The complete story of the discovery and reconstruction of the 1918 pandemic virus", *CDC: Centres for disease control and prevention*,

[3] W. H. Organization *et al.*, "Noncommunicable diseases progress monitor 2020", 2020.

[4] J. Camps and A. García-Heredia, "Introduction: Oxidation and inflammation, a molecular link between non-communicable diseases", in *Oxidative Stress and Inflammation in Non-communicable Diseases-Molecular Mechanisms and Perspectives in Therapeutics*, Springer, 2014, pp. 1–4.

[5] W. H. Organization *et al.*, *Global status report on noncommunicable diseases 2014*, WHO/NMH/NVI/15.1. World Health Organization, 2014.

[6] B. Ruiz-Núñez *et al.*, "Lifestyle and nutritional imbalances associated with western diseases: Causes and consequences of chronic systemic low-grade inflammation in an evolutionary context", *The Journal of nutritional biochemistry*, vol. 24, no. 7, pp. 1183–1201, 2013.

[7] E. Pretorius *et al.*, "Lipopolysaccharide-binding protein (lbp) reverses the amyloid state of fibrin seen in plasma of type 2 diabetics with cardiovascular co-morbidities", *Scientific reports*, vol. 7, no. 1, p. 9680, 2017.

[8] M. J. Page *et al.*, "Serum amyloid a binds to fibrin (ogen), promoting fibrin amyloid formation", *Scientific reports*, vol. 9, no. 1, pp. 1–14, 2019.

[9] L. Chen *et al.*, "Inflammatory responses and inflammation-associated diseases in organs", *Oncotarget*, vol. 9, no. 6, p. 7204, 2018.

[10] R. Pahwa and I. Jialal, "Chronic inflammation", 2018.

[11] S. Oshiro *et al.*, "Dysregulation of iron metabolism in alzheimer's disease, parkinson's disease, and amyotrophic lateral sclerosis", *Advances in pharmacological sciences*, vol. 2011, 2011.

[12] L. Rizzetto *et al.*, "Connecting the immune system, systemic chronic inflammation and the gut microbiome: The role of sex", *Journal of autoimmunity*, vol. 92, pp. 12–34, 2018.

[13] D. B. Kell and E. Pretorius, "On the translocation of bacteria and their lipopolysaccharides between blood and peripheral locations in chronic, inflammatory diseases: The central roles of lps and lps-induced cell death", *Integrative Biology*, vol. 7, no. 11, pp. 1339–1377, 2015.

[14] E. Pretorius, *Inflammation and the role of protein misfolding*, 2019.

[15] K. Strimbu and J. A. Tavel, "What are biomarkers?", *Current Opinion in HIV and AIDS*, vol. 5, no. 6, p. 463, 2010.

[16] Y.-y. Luan and Y.-m. Yao, "The clinical significance and potential role of c-reactive protein in chronic inflammatory and neurodegenerative diseases", *Frontiers in Immunology*, vol. 9, p. 1302, 2018.

[17] Pathcare. (). Fees lookup, [Online]. Available: `https://www.pathcare.co.za/fee-lookup-2/` (visited on 01/30/2019).

[18] S. Kattula *et al.*, "Fibrinogen and fibrin in hemostasis and thrombosis", *Arteriosclerosis, thrombosis, and vascular biology*, vol. 37, no. 3, e13–e21, 2017.

[19] E. Bień and A. Balcerska, "Clinical significance of erythrocyte sedimentation rate, c-reactive protein and serum lactate dehydrogenase levels in the diagnosis, prognosis and treatment monitoring of children suffering from cancer", *Medycyna wieku rozwojowego*, vol. 8, no. 4 Pt 2, pp. 1081–1089, 2004.

[20] Shaydakov ME, Blebea J. (). Thromboelastography (teg), [Online]. Available: `https://www.ncbi.nlm.nih.gov/books/NBK537061/`.

[21] C. Nickson. (). Thromboelastography (teg), [Online]. Available: `https://litfl.com/thromboelastogram-teg/` (visited on 10/21/2019).

[22] D. B. Kell and E. Pretorius, "The simultaneous occurrence of both hypercoagulability and hypofibrinolysis in blood and serum during systemic inflammation, and the roles of iron and fibrin (ogen)", *Integrative Biology*, vol. 7, no. 1, pp. 24–52, 2015.

[23] M. C. Leal *et al.*, "Interleukin-1β and tumor necrosis factor-α: Reliable targets for protective therapies in parkinson's disease?", *Frontiers in cellular neuroscience*, vol. 7, p. 53, 2013.

[24] S. Kany *et al.*, "Cytokines in inflammatory disease", *International Journal of Molecular Sciences*, vol. 20, no. 23, p. 6008, 2019.

[25] D. Eisenberg and M. Jucker, "The amyloid state of proteins in human diseases", *Cell*, vol. 148, no. 6, pp. 1188–1203, 2012.

[26] C. I. Branden and J. Tooze, *Introduction to protein structure*. Garland Science, 2012.

[27] C. M. O'Connor *et al.*, "Essentials of cell biology", *Cambridge, MA: NPG Education*, vol. 1, 2010.

[28] E. Pretorius *et al.*, "Both lipopolysaccharide and lipoteichoic acids potently induce anomalous fibrin amyloid formation: Assessment with novel amytracker™ stains", *Journal of The Royal Society Interface*, vol. 15, no. 139, p. 20 170 941, 2018.

[29] E. Pretorius *et al.*, "Lipopolysaccharide-binding protein (lbp) reverses the amyloid state of fibrin seen in plasma of type 2 diabetics with cardiovascular co-morbidities", *Scientific reports*, vol. 7, no. 1, pp. 1–16, 2017.

[30] E. Pretorius *et al.*, "The potential of lps-binding protein to reverse amyloid formation in plasma fibrin of individuals with alzheimer-type dementia", *Frontiers in aging neuroscience*, vol. 10, p. 257, 2018.

[31] M. J. Page *et al.*, "Serum amyloid a binds to fibrin (ogen), promoting fibrin amyloid formation", *Scientific reports*, vol. 9, no. 1, pp. 1–14, 2019.

[32] G. Keiser, *Biophotonics*. Springer, 2016.

[33] J. A. Soares, "Introduction to optical characterization of materials", in *Practical Materials Characterization*, Springer, 2014, pp. 43–92.

[34] *Light: Electromagnetic waves, the electromagnetic spectrum and photons*.

[35] H. Zimmermann, "Basics of optical emission and absorption", in *Integrated silicon optoelectronics*, Springer, 2000, pp. 1–10.

[36] W. Lauterborn and T. Kurz, *Coherent optics: fundamentals and applications*. Springer Science & Business Media, 2003.

[37] A. P. Demchenko, *Introduction to fluorescence sensing*. Springer Science & Business Media, 2008.

[38] J. Widengren and R. Rigler, "Mechanisms of photobleaching investigated by fluorescence correlation spectroscopy", *Bioimaging*, vol. 4, no. 3, pp. 149–157, 1996.

[39] T. F. Scientific. (). Fluorescence fundamentals, [Online]. Available: `https://www.thermofisher.com/za/en/home/references/molecular-probes-the-handbook/introduction-to-fluorescence-techniques.html`.

[40] C. A. Combs, "Fluorescence microscopy: A concise guide to current imaging methods", *Current protocols in neuroscience*, vol. 50, no. 1, pp. 2–1, 2010.

[41] B. Huang *et al.*, "Super-resolution fluorescence microscopy", *Annual review of biochemistry*, vol. 78, pp. 993–1016, 2009.

[42] W. G. Jerome and R. L. Price, *Basic confocal microscopy*. Springer, 2018.

[43] Y. Povrozin and B. Barbieri, "Fluorescence spectroscopy", *Handbook of Measurement in Science and Engineering*, vol. 3, pp. 2475–2498, 2016.

[44] J. R. Lakowicz, "Instrumentation for fluorescence spectroscopy", in *Principles of fluorescence spectroscopy*, Springer, 1999, pp. 25–61.

[45] F. T. Chan *et al.*, "Protein amyloids develop an intrinsic fluorescence signature during aggregation", *Analyst*, vol. 138, no. 7, pp. 2156–2162, 2013.

[46] J. R. Lakowicz, "Protein fluorescence", in *Principles of fluorescence spectroscopy*, Springer, 1983, pp. 341–381.

[47] P. Dey, "Amyloid staining", in *Basic and Advanced Laboratory Techniques in Histopathology and Cytology*, Springer, 2018, pp. 109–111.

[48] J. Sjöqvist *et al.*, "Toward a molecular understanding of the detection of amyloid proteins with flexible conjugated oligothiophenes", *The Journal of Physical Chemistry A*, vol. 118, no. 42, pp. 9820–9827, 2014.

[49] S. A. Hudson *et al.*, "The thioflavin t fluorescence assay for amyloid fibril detection can be biased by the presence of exogenous compounds", *The FEBS journal*, vol. 276, no. 20, pp. 5960–5972, 2009.

[50] A. A. Reinke and J. E. Gestwicki, "Insight into amyloid structure using chemical probes", *Chemical biology & drug design*, vol. 77, no. 6, pp. 399–411, 2011.

[51] M. Biancalana and S. Koide, "Molecular mechanism of thioflavin-t binding to amyloid fibrils", *Biochimica et Biophysica Acta (BBA)-Proteins and Proteomics*, vol. 1804, no. 7, pp. 1405–1412, 2010.

[52] D. J. Lindberg *et al.*, "Binding of thioflavin-t to amyloid fibrils leads to fluorescence self-quenching and fibril compaction", *Biochemistry*, vol. 56, no. 16, pp. 2170–2174, 2017.

[53] C. Wu *et al.*, "Binding of congo red to amyloid protofibrils of the alzheimer aβ9–40 peptide probed by molecular dynamics simulations", *Biophysical journal*, vol. 103, no. 3, pp. 550–557, 2012.

[54] E. I. Yakupova *et al.*, "Congo red and amyloids: History and relationship", *Bioscience reports*, vol. 39, no. 1, 2019.

[55] S. Nyström *et al.*, "Imaging amyloid tissues stained with luminescent conjugated oligothiophenes by hyperspectral confocal microscopy and fluorescence lifetime imaging", *JoVE (Journal of Visualized Experiments)*, no. 128, e56279, 2017.

[56] T. Klingstedt *et al.*, "The structural basis for optimal performance of oligothiophene-based fluorescent amyloid ligands: Conformational flexibility is essential for spectral assignment of a diversity of protein aggregates", *Chemistry–A European Journal*, vol. 19, no. 31, pp. 10 179–10 192, 2013.

[57] E. Biotech. (). Amytracker, [Online]. Available: `https://www.ebbabiotech.com/collections/amytracker` (visited on 01/30/2019).

[58] T. F. Scientific. (). Overview of filters and light sources, [Online]. Available: `https://www.thermofisher.com/za/en/home/life-science/cell-analysis/cell-analysis-learning-center/molecular-probes-school-of-fluorescence/fluorescence-basics/overview-filters-light-sources.html`.

[59] M. W. D. Christopher S. Murphy. (). Light source power levels, [Online]. Available: `http://zeiss-campus.magnet.fsu.edu/articles/lightsources/powertable.html`.

[60] M. Hébert *et al.*, "Fundamentals of optics and radiometry for color reproduction", *Handbook of Digital Imaging*, pp. 1–57, 2015.

[61] R. Rottenfusser *et al.*, "Education in microscopy and digital imaging", *ZEISS Microscopy*, 2014.

[62] M. W. Davidson. (). Fundamentals of mercury arc lamps, [Online]. Available: `http://zeiss-campus.magnet.fsu.edu/articles/lightsources/mercuryarc.html`.

[63] ——, (). Fundamentals of xenon arc lamps, [Online]. Available: `http://zeiss-campus.magnet.fsu.edu/articles/lightsources/xenonarc.html`.

[64] ——, (). Fundamentals of metal halide arc lamps, [Online]. Available: `http://zeiss-campus.magnet.fsu.edu/articles/lightsources/metalhalide.html`.

[65] ——, (). Fundamentals of light emitting diodes, [Online]. Available: `http://zeiss-campus.magnet.fsu.edu/articles/lightsources/leds.html`.

[66] E. Optics. (). Understanding microscope objectives, [Online]. Available: `https://www.edmundoptics.com/knowledge-center/application-notes/microscopy/understanding-microscopes-and-objectives/` (visited on 11/15/2019).

[67] M. Bass and V. N. Mahajan, *Handbook of Optics, ; Volume I: Geometrical and Physical Optics, Polarized Light, Components and Instruments*. McGraw-Hill, 2010.

[68] M. W. D. Joel S Silfies Stanley A. Schwartz. (). Understanding microscope objectives, [Online]. Available: `https://www.microscopyu.com/techniques/super-resolution/the-diffraction-barrier-in-optical-microscopy` (visited on 11/30/2019).

[69] E. Optics. (). Optical filters, [Online]. Available: `https://www.edmundoptics.com/knowledge-center/application-notes/optics/optical-filters/` (visited on 11/30/2019).

[70] A. Czajkowski *et al.*, "Optical filtering basics for life sciences", *LASER FOCUS WORLD*, vol. 51, no. 12, pp. 53–56, 2015.

[71] D. Durini, *High performance silicon imaging: fundamentals and applications of cmos and ccd sensors*. Woodhead Publishing, 2019.

[72] A. Orth *et al.*, "A dual-mode mobile phone microscope using the onboard camera flash and ambient light", *Scientific reports*, vol. 8, no. 1, pp. 1–8, 2018.

[73] M. Shakeri *et al.*, "Advanced cmos based image sensors", *Australian Journal of Basic and Applied Sciences*, vol. 6, no. 7, pp. 62–72, 2012.

[74] O. Burggraaff *et al.*, "Standardized spectral and radiometric calibration of consumer cameras", *Optics express*, vol. 27, no. 14, pp. 19 075–19 101, 2019.

[75] H. Guner *et al.*, "A smartphone based surface plasmon resonance imaging (spri) platform for on-site biodetection", *Sensors and Actuators B: Chemical*, vol. 239, pp. 571–577, 2017.

[76] I. Yedid, "The evolution of zoom camera technologies in smartphones", Corephotonics, Tech. Rep., 2017.

[77] R. Lukac and K. N. Plataniotis, "Color filter arrays: Design and performance analysis", *IEEE Transactions on Consumer electronics*, vol. 51, no. 4, pp. 1260–1267, 2005.

[78] P. Rojtberg, "Processing raw images in python", 2017.

[79] S. G. Solomon and P. Lennie, "The machinery of colour vision", *Nature Reviews Neuroscience*, vol. 8, no. 4, pp. 276–286, 2007.

[80] J. Best, *Colour design: theories and applications*. Woodhead Publishing, 2017.

[81] R. Lukac and K. N. Plataniotis, "Single-sensor camera image processing", *Color image processing: Methods and applications*, vol. 16, pp. 363–392, 2007.

[82] B. Fraser, "Understanding digital raw capture", *Digital camera raw file support, Adobe Systems Incorporated*, vol. 48, 2004.

[83] J. Mei *et al.*, "Aggregation-induced emission: The whole is more brilliant than the parts", *Advanced materials*, vol. 26, no. 31, pp. 5429–5479, 2014.

[84] Y. Hong *et al.*, "Aggregation-induced emission", *Chemical Society Reviews*, vol. 40, no. 11, pp. 5361–5388, 2011.